Neuron

Hypothalamic warm-sensitive neurons require TRPC4 channel for detecting internal warmth and regulating body temperature in mice

Graphical abstract

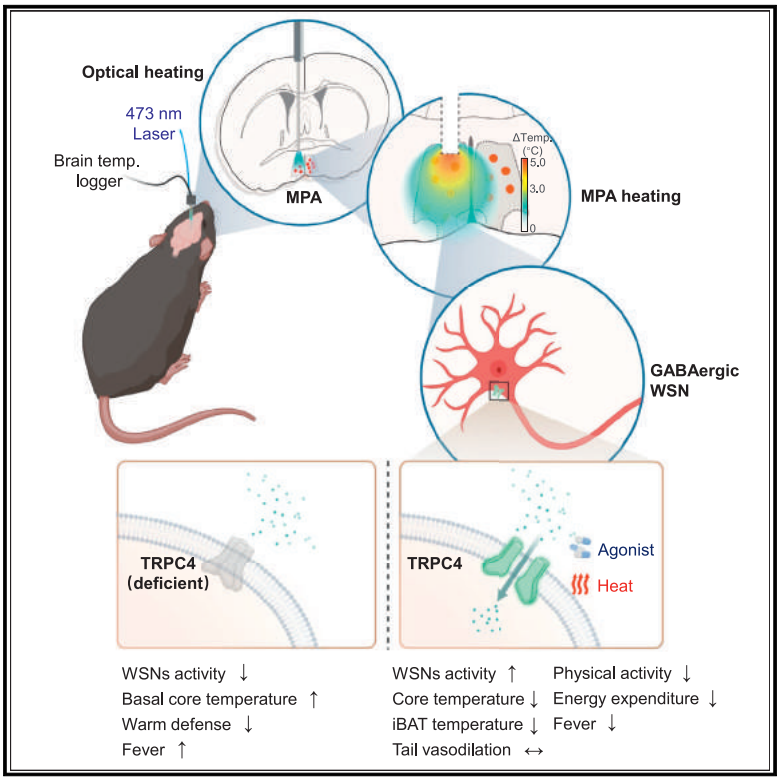

Highlights

- Precise evaluation of the optothermal effect under natural behaviors
- TRPC4 is essential for internal warm sensing in the preoptic area
- TRPC4^{+} GABAergic WSNs is a novel cellular warm sensor to regulate T_{core} and fever
- Pharmacological modulations of TRPC4 bidirectionally control body temperature

Authors

Qian Zhou, Xin Fu, Jianhui Xu, ..., Jie Zhang, Wen Z. Yang, Wei L. Shen

Correspondence

zhangjiefa8888@126.com (J.Z.), yangwen@shanghaitech.edu.cn (W.Z.Y.), shenwei@shanghaitech.edu.cn (W.L.S.)

In brief

Zhou et al. identified TRPC4 as an essential molecule for hypothalamic warm sensing and established TRPC4^{+} GABAergic WSNs as a novel cellular warm sensor to regulate body temperature and limit fever, providing a genetic entry for understanding thermal homeostasis and a molecular target for body temperature management.

Zhou et al., 2023, Neuron *111*, 387–404
February 1, 2023
https://doi.org/10.1016/j.neuron.2022.11.008

CellPress

Neuron

CellPress

Article

Hypothalamic warm-sensitive neurons require TRPC4 channel for detecting internal warmth and regulating body temperature in mice

Qian Zhou,[1,2,3,11] Xin Fu,[1,2,3,11] Jianhui Xu,[4,11] Shiming Dong,[3,5] Changhao Liu,[1] Dali Cheng,[6] Cuicui Gao,[1,2,3] Minhua Huang,[7] Zhiduo Liu,[3,8] Xinyan Ni,[1] Rong Hua,[9] Hongqing Tu,[1] Hongbin Sun,[1] Qiwei Shen,[9] Baoting Chen,[1,2,3] Jin Zhang,[10] Liye Zhang,[1] Haitao Yang,[1] Ji Hu,[1] Wei Yang,[7] Weihua Pei,[8] Qiyuan Yao,[9] Xing Sheng,[6] Jie Zhang,[4,*] Wen Z. Yang,[1,*] and Wei L. Shen[1,12,*]

[1]School of Life Science and Technology, Shanghai Clinical Research and Trial Center, Shanghai Institute for Advanced Immunochemical Studies, ShanghaiTech University, Shanghai 201210, China

[2]Institute of Neuroscience, State Key Laboratory of Neuroscience, CAS Center for Excellence in Brain Science and Intelligence Technology, Shanghai Institutes for Biological Sciences, Chinese Academy of Sciences, Shanghai 200031, China

[3]University of Chinese Academy of Sciences, Beijing 100049, China

[4]Thermoregulation and Inflammation Laboratory, Chengdu Medical College, Chengdu, Sichuan 610500, China

[5]Shanghai Institute of Biochemistry and Cell Biology, Chinese Academy of Sciences (CAS), Shanghai 200031, China

[6]Department of Electronic Engineering, Tsinghua University, Beijing 100084, China

[7]Department of Biophysics, NHC and CAMS Key Laboratory of Medical Neurobiology, Zhejiang University School of Medicine, Hangzhou 310058, China

[8]State Key Laboratory of Integrated Optoelectronics, Institute of Semiconductors, Chinese Academy of Sciences, Beijing 100083, China

[9]Department of General Surgery, Huashan Hospital, Fudan University, Shanghai 200433, China

[10]School of Basic Medical Sciences, Nanchang University, Nanchang 330031, China

[11]These authors contributed equally

[12]Lead contact

*Correspondence: zhangjiefa8888@126.com (J.Z.), yangwen@shanghaitech.edu.cn (W.Z.Y.), shenwei@shanghaitech.edu.cn (W.L.S.)

https://doi.org/10.1016/j.neuron.2022.11.008

SUMMARY

Precise monitoring of internal temperature is vital for thermal homeostasis in mammals. For decades, warm-sensitive neurons (WSNs) within the preoptic area (POA) were thought to sense internal warmth, using this information as feedback to regulate body temperature (T_{core}). However, the cellular and molecular mechanisms by which WSNs measure temperature remain largely undefined. Via a pilot genetic screen, we found that silencing the TRPC4 channel in mice substantially attenuated hypothermia induced by light-mediated heating of the POA. Loss-of-function studies of TRPC4 confirmed its role in warm sensing in GABAergic WSNs, causing additional defects in basal temperature setting, warm defense, and fever responses. Furthermore, TRPC4 antagonists and agonists bidirectionally regulated T_{core}. Thus, our data indicate that TRPC4 is essential for sensing internal warmth and that TRPC4-expressing GABAergic WSNs function as a novel cellular sensor for preventing T_{core} from exceeding set-point temperatures. TRPC4 may represent a potential therapeutic target for managing T_{core}.

INTRODUCTION

Warm-sensitive neurons (WSNs) have been found to account for 10%–30% of neurons within the preoptic area (POA).[1–7] For decades, it has been thought that WSNs function as internal cellular sensors for detecting brain warmth and triggering counteractive hypothermic responses.[1–6,8–14] Pioneer studies used large thermodes or water circulators to heat the hypothalamus of relatively large animals, including rats,[10–12,15,16] goats,[17] cats,[18] and dogs,[14] triggering hypothermic responses.[11,16,18] However, the function of WSNs in mice has not been thoroughly tested since the sizes of these early heaters were too large for mice brains. WSNs have also not been genetically characterized. For example, brain-derived neurotrophic factor (BDNF) neurons within the ventromedial preoptic area (VMPO), which were independently discovered by Tan et al.[8] and our group,[19] are weakly warm sensitive,[8] but whether these neurons function as WSNs has not been determined. It has been proposed that the warm-sensitive transient receptor potential melastatin 2 (TRPM2) channel functions as the warm sensor in WSNs.[6] However, genetic deletion of TRPM2 had only a small effect on thermoregulation, and the authors instead suggested that TRPM2 works as a synaptic sensor

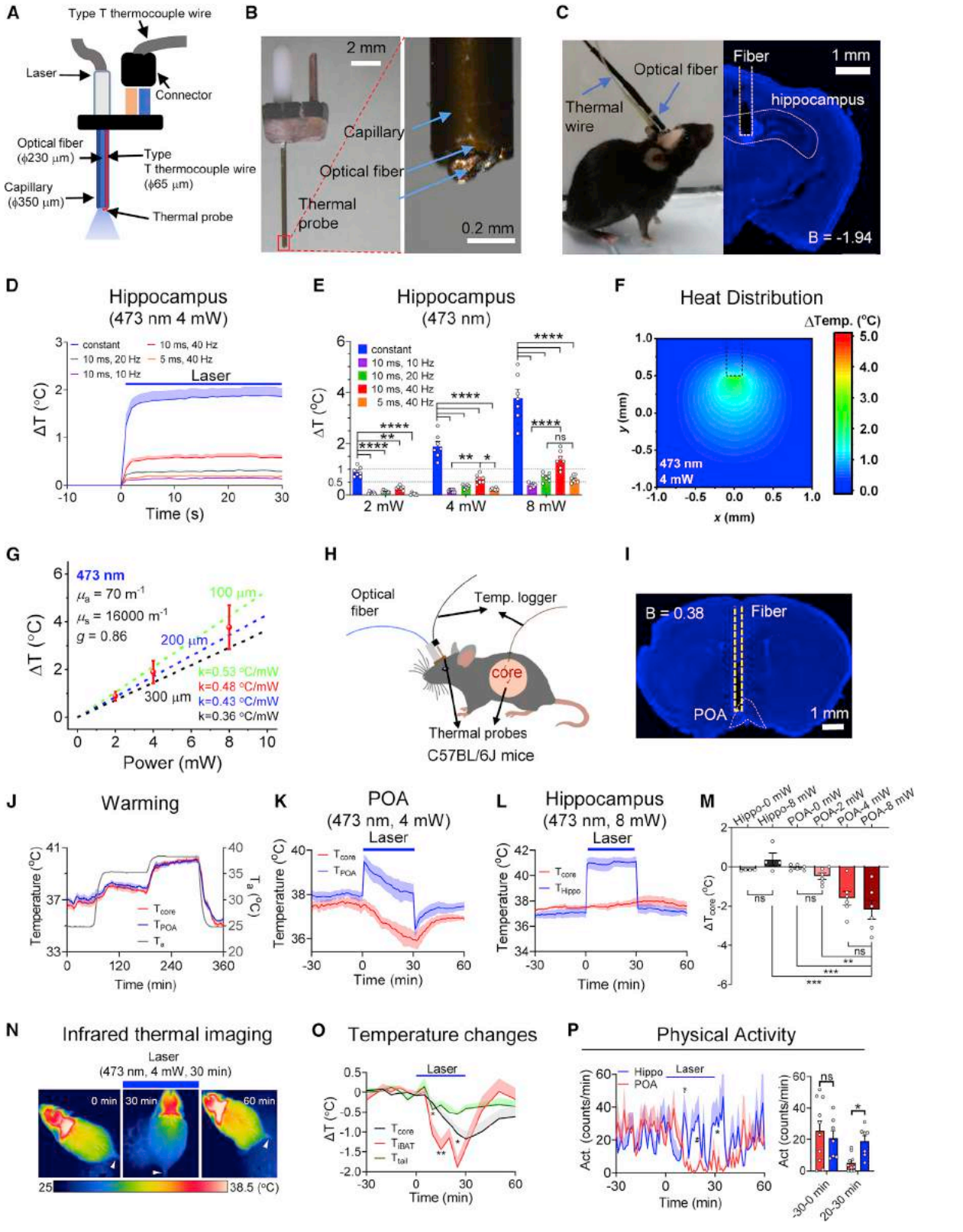

(legend on next page)

to modulate WSNs indirectly.[20] Therefore, the genetic properties of WSNs and their temperature sensors remain largely unknown.

The delivery of light to the brain inevitably results in an optothermal effect, with stimulations of 3–30 mW light power increasing temperature by 0.2°C–2°C.[21–25] This effect has been measured near the brain surface[22,24,26] and in brain slices,[21] anesthetized animals,[23] and head-fixed configurations.[21] However, direct measurement of this effect in freely behaving mice has not been possible, preventing the assessment of this effect under natural behaviors and limiting the utility of this system for studying WSN functions in mice.

In this study, we designed an implantable device for heating the brain in freely behaving mice. This device, along with genetic manipulation and pharmacological studies, was used to better understand the cellular and molecular mechanisms by which WSNs measure temperature. Our studies reveal that TRPC4 is essential for internal warm sensing and that TRPC4-expressing GABAergic WSNs is a novel warm cellular sensor for thermoregulation. Additionally, our studies provide a practical guide for accessing optothermal effects in neuroscience.[27–31]

RESULTS

Optothermal effects in the deep brain of freely behaving mice

To measure optothermal effects in the deep brain of mice, we designed a small, implantable device to simultaneously heat the brain optically and measure brain temperature in freely behaving animals (Figures 1A–1C). After testing the accuracy of our device (Figure S1A), we measured hippocampal temperature while applying either constant light or light pulses (Figures 1D, 1E, and S1B–S1G). We found that the delivery of blue light (473 nm) at 2–8 mW increased hippocampal temperature sharply, reaching a plateau within 3 s (Figures 1D, S1B, and S1C). Quantification of these changes revealed a power-dependent temperature increase (Figure 1E). As with blue light, induced temperature changes by green light (532 nm) were positively correlated with light powers (Figures S1D–S1G). Notably, following 1 s of blue light exposures (8 mW), a 2 s off interval is needed to recover the temperature (Figures S1I–S1K).

We next simulated the spatial distribution of heat in the brain in response to light stimuli using previously measured parameters[32,33] (Figures 1F and S2). We then plotted temperature changes against light powers at 100, 200, and 300 μm from the end of the fiber for both blue and green lights (Figures 1G and S2G). Temperature changes linearly correlated with light power, and the measured temperatures matched predicted values (Figures 1G and S2G). These results indicated that our model accurately predicts temperature changes.

As seen in the hippocampus, the optothermal effects measured in the POA had similar relationships between light patterns and heat (Figure S3). Finally, we compared optothermal effects elicited by optical fibers that were 200 (as above) or 300 μm in diameter. The 300-μm fibers had a slightly smaller optothermal effect due to reduced power density (Figure S4).

Heating the POA triggers counteractive body cooling

To begin to evaluate the functional significance of internal temperature sensors, we first used wired thermal probes to record brain temperature (measured in the POA, T_{POA}) and T_{core} (measured intraperitoneally) at high temporal resolution as we manipulated ambient temperature (T_a) (Figures 1H–1J). Strikingly, following warm exposure, T_{POA} quickly followed T_{core} changes without delay (Figure 1J). Following cold exposure, T_{core} tended to be lower than T_{POA} (statistically insignificant) but still varied in a similar way (Figure S5). These results suggest that brain temperature tightly follows T_{core} and that both are sensitive to T_a changes in mice.

Figure 1. Optical heating of the POA induced a counteractive hypothermic effect

(A and B) Diagram (A) and photo (B) of the device for delivering light to the brain and measuring brain temperature. The optical fiber and a T-type thermocouple were packed inside a capillary shown on the right panel of (B).Scale bar, 2 mm; scale bar for boxed ROI, 0.2 mm.

(C) Freely behaving mouse with the device implanted in the hippocampus (left) and representative image shows the track of the device capillary (right). Scale bar, 1 mm.

(D) Temperature changes of the hippocampus under constant and pulsed blue light (473 nm) stimulations (n = 7 mice).

(E) Summary distributions and statistics of hippocampal temperature changes induced by 2-, 4-, and 8-mW blue lights (n = 7 mice).

(F) Simulated heat distribution in brain tissues for blue light, assuming brain temperature was 37°C. The dashed line indicate the optical fiber position.

(G) Simulation of temperature increases from blue light illumination at the indicated depth from the fiber end (100, 200, and 300 μm), where μ_a is the absorption coefficient; μ_s is the scattering coefficient; g is the anisotropic parameter in the Henyey-Greenstein model (defined in STAR Methods); and k is the slope of the simulated lines as indicated. Solid red dots indicate the measured temperatures.

(H) Schematic showing simultaneous recording of T_{core} and brain temperature in the POA (T_{POA}) while optically heating the POA.

(I) Position of the device capillary implanted in the POA. Scale bar, 1 mm.

(J) Changes of T_{core} and T_{POA} with changes in ambient temperature (T_a) (n = 4 mice).

(K) Changes of T_{core} and T_{POA} after POA heating with a 4-mW blue laser (n = 6 mice).

(L) Changes of T_{core} and T_{hippo} (hippocampal temperature) after hippocampal optical heating with an 8-mW blue laser (0–30 min; n = 4 mice).

(M) Summary of ΔT_{core} changes after the optical heating under different powers (hippocampus, n = 4 mice; POA, n = 6 mice). ΔT_{core} was calculated as the temperature difference at t = 30 min subtracted by t = 1 min.

(N) Representative thermograph images showing the surface temperature of the interscapular brown adipose tissue (T_{iBAT}) and the tail skin temperature (T_{tail}) after heating the POA (fiber was inserted in the MPA) by blue laser (4 mW, 473 nm, 30 min) in WT mice. White arrows indicate the positions T_{tail} was measured.

(O) Dynamics of ΔT_{core}, ΔT_{iBAT}, and ΔT_{tail} after heating the POA (fiber was inserted in the MPA) by blue laser (4 mW, 473 nm, 30 min) in WT mice (n = 10 mice). Where ΔT_{core} and ΔT_{iBAT} differ significantly are indicated by *.

(P) Physical activity changes after heating POA (n = 10 mice) or hippocampus (n = 7 mice) as indicated. Laser pattern: 4 mW, 473 nm, 30 min. The physical activity changes before (−30–0 min) and after (20–30 min) heating of the POA or hippocampus are summarized in the right.

All data are shown as mean ± SEM and were analyzed by two-way RM ANOVA (E, J, O, and P), or one-way RM ANOVA (M). *p < 0.05, **p < 0.01, ***p < 0.001, ****p < 0.0001; ns, not significant.

See also Figures S1–S6.

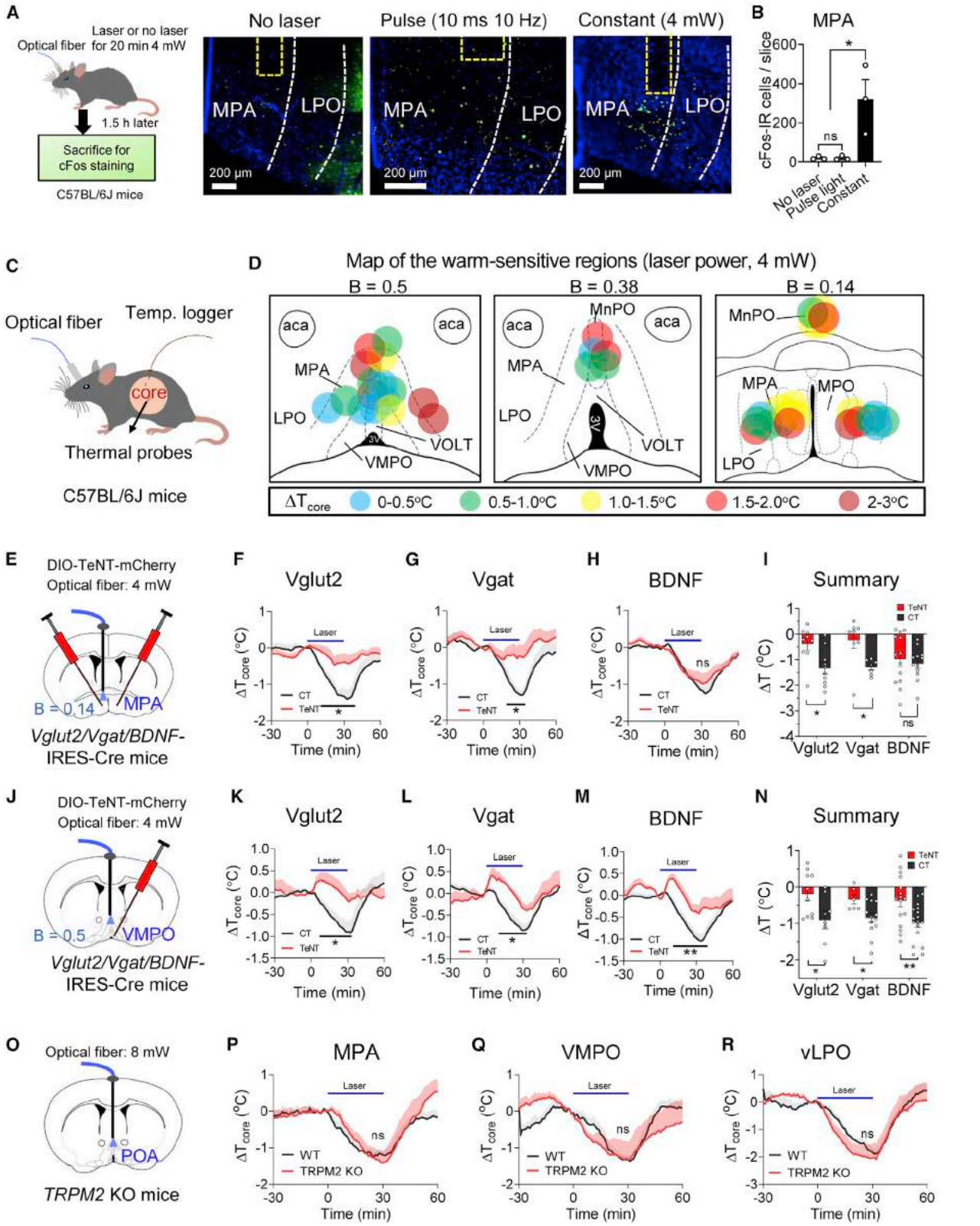

(legend on next page)

Next, we heated the POA using 4-mW blue light and measured a sharp increase in T_{POA} to 39.5°C (Figure 1K), which is within the temperature range of a fever. Remarkably, following the initial light-induced jump in T_{POA}, both T_{POA} and T_{core} gradually declined (~−2°C) while the laser was on (Figures 1K, S6A, and S6B). In contrast, heating the hippocampus with the same light pattern or heating the POA with pulses of light that did not affect brain temperature (Figure S3D) did not change T_{core} (Figures 1L, 1M, and S6C–S6F). These results suggest that this induced hypothermia is specific to heating the POA. Thus, we confirmed that the POA harbors functional WSNs that trigger hypothermic responses during brain heating.

POA heating is associated with changes in thermoeffector activities

To discern which thermoeffector activities underlie the hypothermic effect induced by POA heating, we measured the surface temperature of interscapular brown adipose tissue (T_{iBAT}) and tail skin temperature (T_{tail}) using infrared thermal imaging and measured physical activity by telemetry probes implanted intraperitoneally. Interestingly, after heating the POA (4 mW, 473 nm, 30 min) in the WT mice, where the fiber was inserted in the medial preoptic area (MPA), T_{iBAT} was sharply reduced prior to the T_{core} reduction (Figures 1N and 1O), suggesting the reduction in interscapular brown adipose tissue (iBAT) thermogenesis contributes to the decline of T_{core} as we observed previously.[34] However, T_{tail} did not increase but rather was slightly reduced by POA heating, suggesting that tail vasodilation is not activated (Figures 1N and 1O). The slight reduction in T_{tail} was probably a secondary effect of T_{core} reduction. Noticeably, physical activity was also sharply reduced (Figure 1P). Hence, these results suggest that the moderate hypothermia induced by POA heating is associated with reductions in iBAT thermogenesis and physical activity but not activation of tail vasodilation.

Mapping warm-sensitive nuclei within the POA

The POA is a complex area comprised of several small nuclei. To map the sensitivities of these nuclei to heating, we implanted heating optical fibers without the thermocouple (to minimize the size of the implant) and used pre-characterized light patterns to heat the POA. Heating the MPA, ventromedial preoptic nucleus (VMPO), ventral part of the lateral preoptic nucleus (vLPO), and median preoptic nucleus (MnPO) with 2-mW light stimuli induced modest reductions in T_{core} (Figure S7). When the light power was increased to 4–8 mW, stimulating the MPA and MnPO induced a more noticeable reduction of T_{core} compared with the VMPO and vLPO (Figure S7).

To estimate degrees of temperature that could effectively activate WSNs *in vivo*, we performed cFos staining after heating the MPA (4 mW, 20 min) (Figure 2A). Interestingly, the cFos was distributed underneath the fiber tip (Figures 2A and 2B), within areas with ≥1.5°C temperature increases predicted in Figure 1F. Hence, we defined the effective heating areas where temperature increased by ≥1.5°C, and we color coded the areas with ΔT_{core} (Figures 2C and 2D). We also plotted the effective heating areas together with their original fiber tip positions (Figure S8). These maps show that heating the MPA and MnPO elicited the most substantial hypothermic effects.

POA neuron types required for the heat-induced hypothermic effect

To identify the neuronal cell types necessary for the hypothermic effect of WSNs, we used Cre-dependent expression of tetanus neurotoxin (TeNT) to block different types of neurons in the POA. We injected adeno-associated viruses (AAVs) carrying DIO-TeNT into the MPA (bregma = 0.14 mm), the VMPO (bregma = 0.5 mm), and the vLPO (bregma = 0.14 mm). However, due to viral spreading, TeNT was expressed in multiple POA nuclei at each injected bregma site. Thus, we redefined the blocked areas as follows: the anterior POA (aPOA; bregma = 0.5 mm; Figure S9) and the central POA (cPOA; bregma = 0.0–0.38 mm; Figures S9 and S10). In the cPOA, blocking glutamatergic ($Vglut2^+$) or GABAergic ($Vgat^+$) but not BDNF neurons (labeled by BDNF-IRES-Cre[35]) nearly abolished the hypothermic effect induced by MPA heating (Figures 2E–2I and S9A–S9G). By

Figure 2. Several POA cell types were required for the heating-induced hypothermic effect

(A) Schematic for detecting cFos expression after POA heating (left panel). Representative cFos expressions after no light exposure, pulsed light, and constant light illuminations in the MPA (4-mW laser) (right three panels), the first two being used for control. Scale bars were 200 μm.

(B) Summary of cFos positive cells in the MPA following different light illuminations as indicated (n = 3 mice each).

(C) Schematic for testing the thermosensitivity of different POA nuclei in response to local heating. The optical fibers were implanted without the thermocouple to minimize the insert size.

(D) Anatomical map of the warm-sensitive regions as indicated by the areas with effective heating (≥1.5°C). Laser pattern: 4 mW, 473 nm, 30 min. The effective heating areas were defined as the areas with temperature increases ≥1.5°C as predicted in Figure 1F and are color coded using ΔT_{core}. aca, anterior commissure, anterior part; VOLT, vascular organ of the lamina terminalis.

(E) Schematic for blocking MPA heating-induced hypothermic effects by expressing TeNT in the $cPOA^{Vglut2/Vgat/BDNF}$ neurons as indicated. cPOA, central POA (bregma = 0.38–0 mm). The mCherry was the control (CT) for TeNT-mCherry.

(F–I) Changes of T_{core} induced by MPA heating (4 mW, 473 nm) after blocking $cPOA^{Vglut2}$ neurons (F; TeNT, n = 9 mice; CT, n = 10 mice), $cPOA^{Vgat}$ neurons (G; TeNT, n = 8 mice; CT, n = 7 mice), $cPOA^{BDNF}$ neurons (H; TeNT, n = 13 mice; CT, n = 12 mice), and a summary of ΔT_{core} (t = 30 min) is shown in (I).

(J) Schematic for blocking VMPO heating-induced hypothermic effects by TeNT in $aPOA^{Vglut2/Vgat/BDNF}$ neurons. aPOA, anterior POA (bregma = 0.5 mm).

(K–N) Changes of T_{core} by VMPO heating (4 mW, 473 nm) after blocking $aPOA^{Vglut2}$ neurons (K; TeNT, n = 10 mice; CT, n = 8 mice), $aPOA^{Vgat}$ neurons (L; TeNT, n = 6 mice; CT, n = 13 mice), $aPOA^{BDNF}$ neurons (M; TeNT, n = 16 mice; CT, n = 17 mice), and a summary of ΔT_{core} (t = 30 min) is shown in (N).

(O) Schematic for testing the requirement of TRPM2 channel in POA-heating induced hypothermic effect.

(P–R) POA heating-induced T_{core} changes after knocking out the TRPM2 channel. An 8-mW blue laser was used to heat the MPA (P; KO, n = 6 mice; WT, n = 5 mice), the VMPO (Q; n = 5 mice each), and the vLPO (R; KO, n = 6 mice; WT, n = 5 mice).

All data are shown as mean ± SEM and were analyzed by one-way RM ANOVA in (B), two-way RM ANOVA in (F)–(H), (K)–(M), and (P)–(R), or unpaired t test in (I) and (N). *p < 0.05, **p < 0.01, ns, not significant.

See also Figures S7–S11.

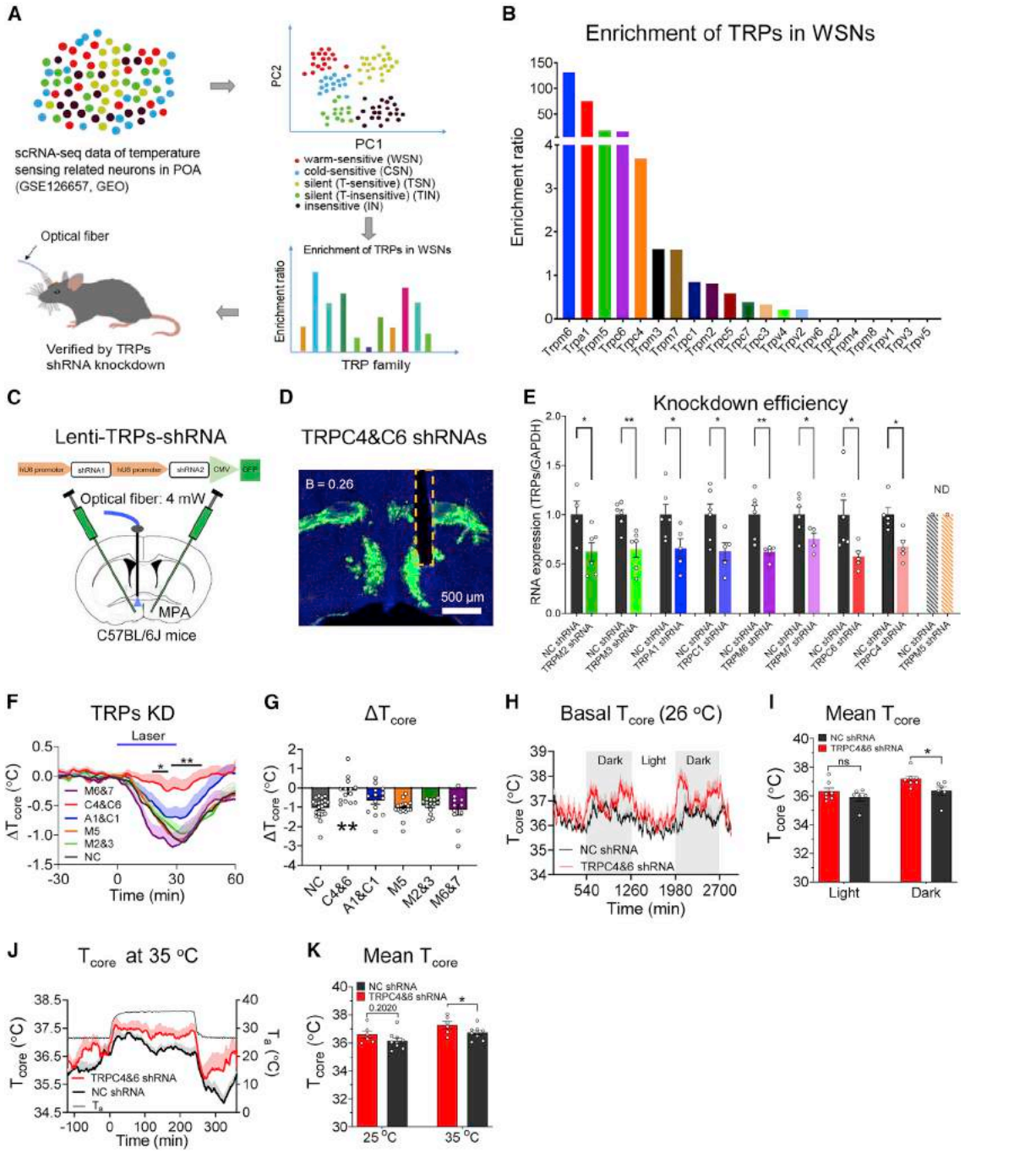

Figure 3. Identifying TRP channels that are required for internal warm sensing

(A) Schematic for screening TRP channels enriched in POA neurons. The single-cell RNA sequencing data (68 cells) were downloaded from databases online (GEO: GSE126657).

(B) Enrichment ratio of TRPs in WSNs calculated using the normalized expression counts in different clusters. Enrichment ratio = (counts in WSNs + silent-TSNs)/(counts in silent-TINs + CSNs + TINs). WSNs, warm-sensitive neurons; silent-TSNs, silent (temperature-sensitive neurons); TINs, temperature-insensitive neurons; silent-TINs, silent (temperature-insensitive neurons); CSNs, cold-sensitive neurons.

(C) Schematic illustration of shRNA mediated TRP knockdowns in the MPA. Two shRNAs were co-expressed in the same lentivirus vector except for TRPM5. The GFP was co-expressed with shRNAs.

(D) Representative expression of the lentivirus (green) carrying both TRPC4 and TRPC6 shRNAs in the MPA labeled by the GFP co-expressed. Scale bar, 500 μm.

(E) Validation of knockdown efficiency. The relative expression levels of TRPs mRNA from bulk POA tissues were determined by qPCR. NC shRNA, scramble RNA controls; ND, not detectable.

(legend continued on next page)

contrast, blocking these three neural types in the aPOA abolished the hypothermic effect of VMPO heating (Figures 2J–2N and S9H–S9M), which is consistent with previous findings that $VMPO^{Vglut2}$ neurons and $VMPO^{BDNF}$ neurons are hypothermic.[8,36] Unexpectedly, blocking Vglut2 neurons or Galanin-expressing neurons in the cPOA did not alter the hypothermic effect of vLPO heating (Figures S10A–S10E), although these neurons are hypothermic.[19,37,38] Blocking Vgat neurons in the cPOA suppressed hypothermic effects induced by the 8-mW laser but not those induced by the 4-mW laser (Figures S10F–S10H). These results suggest that vLPO WSNs are partly GABAergic. Since TeNT blocking did not abolish heating-induced hypothermic effects, vLPO WSNs may also use vesicle-independent mechanisms to control T_{core}, as exemplified by PGD_2.[5] Thus, these analyses reveal that several neural types within the POA are required for the hypothermic function of WSNs; however, determining whether they are actually WSNs or act downstream of WSNs require furthers tests.

To determine the temperature sensing mechanisms of WSNs, we knocked out *TRPM2*, a warm-sensitive channel proposed to be an internal warm sensor.[6,20] Surprisingly, *TRPM2* deletion did not affect basal T_{core} and hypothermia induced by heating the MPA, VMPO, or vLPO (Figures 2O–2R and S11), suggesting that TRPM2 does not function as a warm sensor.

Pilot screen to identify TRP channels required to detect hypothalamic warming

Several TRP channels function to detect temperature, either as direct sensors or acting downstream of a signaling cascade.[39–41] We, therefore, suspected that TRP channels other than TRPM2 might play roles in brain temperature detection. To identify TRPs enriched in WSNs, we downloaded single-cell RNA sequencing data (68 cells) that included WSNs in the MPA and classified cells into five groups as suggested previously:[5] (1) warm-sensitive, (2) cold-sensitive, (3) silent (T-sensitive), (4) silent (T-insensitive), and (5) insensitive. As the silent (T-sensitive) group was also warm-sensitive, we calculated the enrichment ratio of TRPs using the sum expression counts in warm-sensitive and silent (T-sensitive) groups divided by the sum counts of the other three groups (Figures 3A, 3B, and S12A). We then selected the top nine genes for further study, namely TRPM6, TRPA1, TRPM5, TRPC6, TRPC4, TRPM3, TRPM7, TRPC1, and TRPM2. We also analyzed the expression of TRPs in the POA using a larger dataset containing ~31,000 POA cells.[42] After data filtering, we obtained 23,476 cells and 18,553 neurons and confirmed that most WSN-enriched TRPs were expressed in POA neurons (Figure S12B).

To test the function of enriched TRPs, we knocked each down using shRNAs expressed by lentiviruses (two shRNAs were expressed by each vector; Figures 3C, 3D, and S13). We used qPCR to assess knockdown efficiency in POA bulk tissues and confirmed the reductions of TRP expressions except TRPM5 (Figure 3E). The TRPM5 expression was below the detection limit. In thermoregulatory behavior assays, knocking down TRPA1/TRPC1 (co-expressed), TRPM5, TRPM2/TRPM3 (co-expressed), or TRPM6/TRPM7 (co-expressed) in the MPA did not affect heating-induced hypothermic effects (Figures 3F and 3G). However, knocking down TRPC4/TRPC6 in the MPA significantly blocked the heating-induced hypothermic effect (Figures 3F and 3G). This knockdown also increased basal T_{core} during the dark phase (Figures 3H and 3I) and aggravated hyperthermia when mice were exposed to 35°C (Figures 3J and 3K). Therefore, we reveal that the co-knockdown of TRPC4 and TRPC6 impairs heating-induced hypothermic effects, basal temperature setting, and warm defense.

TRPC4 is required for warm sensing and thermoregulation

After using RNAi to demonstrate that TRPC4/C6 are critical in warm sensing, we sought to verify their function using knockouts (Figure 4A). Evidently, knocking out TRPC4 substantially blocked the hypothermia and hypoactivity phenotypes induced by MPA heating (Figures 4B and 4C). In contrast, TRPC4 heterozygotes (HEs) and TRPC5 KO mice exhibited strong hypothermic effect in response to MPA heating (Figure 4B). Similar to RNAi results, TRPC4 KO mice exhibited a higher basal T_{core} (Figures 4D and 4E) and more severe hyperthermia when exposed to 35°C compared with HE controls (Figures 4F and 4G). There was no significant difference in T_{core} when exposed to 10°C (Figure 4H). Notably, the fever temperature (induced by intra-MPA injection of prostaglandin E2 [PGE2]) was significantly increased in TRPC4 KO mice compared with HE controls (Figure 4I). In combination with our RNAi evidence that TRPC6 does not play a role in warm sensing (Figures 5I and 5J), our genetic evidence indicates that TRPC4 is required for warm sensing, basal temperature setting, warm defense, and fever responses.

TRPC4 neurons in the MPA are mainly GABAergic

As TRPC4 is essential for warm sensing, we sought to characterize the properties of TRPC4-expressing neurons. The mRNA *in situ* hybridization indicated that TRPC4 was expressed in 8.9% of cPOA cells (Figure 4J), which agreed with sequencing data (8.5% of POA cells and 12.7% of POA neurons; Figure S12).[42] TRPC4 was also expressed sparsely in other POA nuclei (Figure S14A). We then analyzed potential genetic markers co-expressed with TRPC4 using the sequencing dataset.[42] Interestingly, TRPC4 was co-expressed most often with the GABAergic markers, Slc32a1 (66%) and Gad2 (72%); only 15% of $TRPC4^+$ cells co-expressed the glutamatergic marker, Slc16a6 (Figure 4K). TRPC4 was co-expressed with other known hypothermic neural

(F and G) Changes of T_{core} induced by MPA heating after knockdown of TRPs in the MPA (TRPC4&6, n = 14 mice; TRPA1&TRPC1, n = 14 mice; TRPM2&3, n = 14 mice; TRPM5, n = 17 mice; TRPM6&7, n = 11 mice; negative control [NC], n = 21 mice). ΔT was the mean temperature at t = 30 min. Laser pattern: 4 mW, 473 nm, 30 min.
(H and I) Changes of basal T_{core} at 26°C after knockdown of MPA TRPC4 and TRPC6 (TRPC4&6, n = 7 mice; NC, n = 6 mice).
(J and K) Changes of T_{core} after warm exposure (35°C, TPRC4&6, n = 6 mice; NC, n = 9 mice).
All data are shown as mean ± SEM, and were analyzed by two-way RM ANOVA in (F), (H), and (J), ordinary one-way ANOVA in (G), or unpaired t test in (E), (I), and (K). *p < 0.05, **p < 0.01, ns, not significant.
See also Figures S12 and S13.

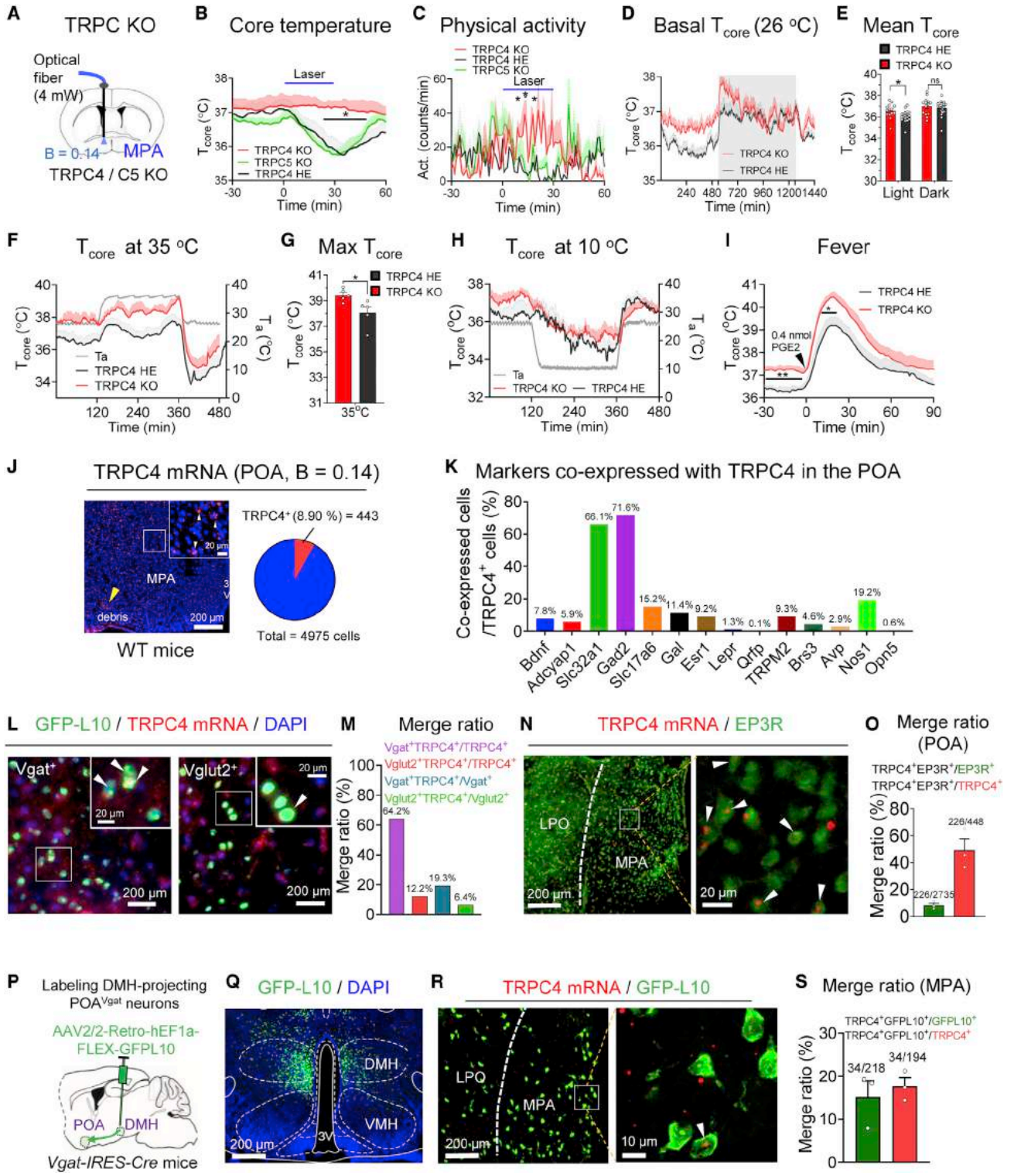

Figure 4. TRPC4 is required to regulate body temperature

(A) Schematic for testing the requirement of TRPC channels in POA heating-induced (4-mW blue laser) hypothermic effect.

(B and C) MPA heating-induced changes in T_{core} (B) and physical activity (C) after knocking out TRPC4 or TRPC5 (TRPC4 KO, n = 4 mice; TRPC5 KO, n = 8 mice; TRPC4 heterozygous [HE], n = 7 mice).

(D and E) Basal T_{core} of TRPC4 KO mice kept at 26°C (KO, n = 14 mice; HE, n = 19 mice). Summary statistics are shown in (E).

(legend continued on next page)

markers (Nos1, Gal, Esr1, Adcyap1, and BDNF[8,19,38,43–45]) but had low co-expression ratios (<5%) with other hypothermic (Lepr, Qrfp, and Opn5)[36,46,47] and hyperthermic (Avp and Brs3)[48,49] neural markers (Figure 4K). We confirmed the TRPC4 expression in GABAergic and glutamatergic neurons by analyzing the overlap between TRPC4 mRNA and Vgat^{GFPL10} or Vglut2^{GFPL10} neurons in the MPA. This was accomplished by injecting AAV2/8-DIO-GFPL10 into the MPA of Vgat-IRES-Cre or Vglut2-IRES-Cre mice to label Vgat^{GFPL10} or Vglut2^{GFPL10} neurons, respectively (Figure 4L). As expected, TRPC4 overlapped extensively with Vgat^{GFPL10} neurons but less so with Vglut2^{GFPL10} neurons (Figure 4M). TRPC4^{+} neurons accounted for 19.3% of MPA^{Vgat} neurons and 6.4% of MPA^{Vglut2} neurons (Figure 4M), which would account for 13% of total MPA neurons (assuming an equal number of GABAergic and glutamatergic neurons based on sequencing data[42] and our recordings shown in Figure 5). Thus, the prevalence of TRPC4 neurons matched the sequencing data, where TRPC4^{+} neurons accounted for 12.7% of POA neurons[42] (Figure S12) and half of the WSNs reported in the MPA (~26%).[5]

Furthermore, we analyzed the overlap between TRPC4 and EP3R. Interestingly, ~50% of TRPC4^{+} neurons in the MPA expressed EP3R, which accounted for 8.1% of EP3R neurons there (Figures 4N and 4O). This high overlap ratio suggests that TRPC4^{+} neurons may participate in fever development. Additionally, to evaluate whether TRPC4^{+} neurons could integrate with known thermoregulatory networks,[50–52] we checked whether GABAergic TRPC4^{+} neurons could innervate dorsomedial hypothalamic nucleus (DMH) neurons known to promote thermogenesis.[19,50] We injected the retrograde AAVs carrying Cre-dependent GFP (Retro-DIO-GFPL10) into the DMH of the Vgat-IRES-Cre mice and co-stained the TRPC4 mRNA with the GFPL10 in the MPA (Figures 4P and 4Q). Interestingly, 17.7% of TRPC4^{+} neurons in the MPA overlapped with DMH-projecting MPA GABAergic neurons, and 15.2% of DMH-projecting MPA GABAergic neurons co-expressed TRPC4 (Figures 4R and 4S), suggesting MPA TRPC4^{+} neurons could provide inhibitory tones to DMH thermogenic neurons. These data indicate that MPA TRPC4^{+} neurons are likely to integrate with the current thermoregulatory network.

TRPC4 functions in MPA GABAergic neurons to sense warmth

To determine whether TRPC4 affects the thermosensitivity of MPA GABAergic neurons, we analyzed intrinsic thermosensitivity by recording neural activity (blind to neural cell types and fluorescent markers; with synaptic blockers) (Figure 5A). After recording, we classified neurons according to their thermosensitivity, including WSNs (thermal coefficient $\geq$0.8 impulses/s/°C), temperature-insensitive neurons (TINs, thermal coefficient < 0.8 but >−0.6 impulses/s/°C), and cold-sensitive neurons (CSNs, thermal coefficient $\leq$ −0.6 impulses/s/°C).[53,54] Overall, WSN ratios were similar among MPA neurons recorded from Vgat^{NC} mice (Vgat-IRES-Cre injected with AAV-DIO-NC shRNA: 18.8%), Gad67-GFP mice (transgenic markers for GABAergic neurons: 21.1%), and Vglut2^{mCherry} mice (Vglut2-IRES-Cre injected with AAV-DIO-mCherry: 19.4%) (Figure 5B). We detected few CSNs since we blocked neural transmission.[55] However, knocking down TRPC4 in Vgat neurons substantially reduced the overall WSN ratio (10.8%; Figure 5B).

Noticeably, there were similar numbers of GABAergic and glutamatergic neurons within the MPA, as estimated from recordings of Gad67-GFP mice (GFP(+): GFP(−) = 56: 67) and Vglut2^{mCherry} mice (mCherry(+):mCherry(−) = 66:63) (Figures 5C–5F). WSNs were 25% (14/56) of Gad67-GFP(+) neurons, 18% (12/67) of Gad67-GFP(−) neurons, 20.6% (13/63) of Vglut2^{mCherry}(−) neurons, and 18.2% (12/66) of Vglut2^{mCherry}(+) neurons (Figures 5C–5F). Evidently, knocking down TRPC4 in Vgat(+) neurons reduced their overall warm sensitivity and WSN ratios when compared with the NC group (Figures 5C and 5D). In contrast, the warm sensitivity and WSN ratios were not significantly changed in Vgat(−) neurons that did not express shRNAs (Figures 5E and 5F). Taken together,

(F and G) T_{core} changes of TRPC4 KO mice in response to warm exposures (35°C; KO, n = 5 mice; HE, n = 5 mice) with summary statistics shown in (G). Max T_{core} is the maximum T_{core} at T_a = 35°C.

(H) T_{core} changes of TRPC4 KO mice in response to cold exposures (10°C; KO, n = 4 mice; HE, n = 5 mice).

(I) The impact of TRPC4 knockout on the fever induced by intra-POA PGE2 injection (TRPC4 KO, n = 4 mice; TRPC4 HE, n = 5 mice). PGE2 (0.4 nmol) was injected into the POA via a cannula.

(J) TRPC4 mRNA expression in the MPA of WT mice. White arrowheads indicate TRPC4 mRNA signals, and the yellow arrowhead indicates tissue debris with autofluorescence. Scale bar, 200 μm for main panels and 20 μm for close-up.

(K) Thermoregulation-related markers co-expressed with TRPC4 in the POA, which were reanalyzed from Single-cell RNA sequencing (scRNA-seq) data (GEO: GSE113576).

(L and M) Overlap between TRPC4 mRNA (red) and GABAergic or glutamatergic neurons labeled by GFP-L10 (green; L10 is a ribosomal resident protein) in the MPA. GABAergic or glutamatergic neurons were labeled by AAV8-DIO-GFPL10 injected into the MPA of Vgat-IRES-Cre or Vglut2-IRES-Cre mice, respectively. Arrowheads in the close up show the colocalization of neurons expressing TRPC4 and GFP. Scale bars, 200 μm for main panels and 20 μm for close-up. Merge ratios are shown in (M).

(N and O) Overlap between TRPC4 mRNA (red) and EP3R (green) in the POA. Merge ratios are shown in (O). Scale bar, 200 μm; scale bar for boxed ROI, 20 μm. The experiment was repeated 3 times independently.

(P) Schematic for labeling DMH-projecting POA^{Vgat} neurons. We injected retrograde tracing AAVs carrying Cre-dependent GFP-L10 (AAV2-Retro-hEF1a-FLEX-GFPL10) into the DMH of Vgat-IRES-Cre mice, driving the expression of GFP-L10 in Vgat^{+} neurons in the POA.

(Q) Representative image showing the expression of GFP-L10 (green) at the viral injection site in the DMH. AAV2-Retro-FLEX-GFPL10 was injected into the DMH of Vgat-IRES-Cre mice (n = 3 mice). 3V, dorsal 3rd ventricle; VMH, ventromedial hypothalamic nucleus; DMH, dorsomedial hypothalamic nucleus. Scale bar, 200 μm.

(R and S) Overlap between TRPC4 mRNA in the POA (red) and DMH-projecting POA^{Vgat} neurons (green). Merge ratios are shown in (S). Scale bar, 200 μm; scale bar for boxed ROI, 10 μm.

All data are shown as mean ± SEM and were analyzed by two-way RM ANOVA in (B), (C), and (I) or unpaired t test in (E) and (G). *p < 0.05, **p < 0.01, ns, not significant.

See also Figure S14.

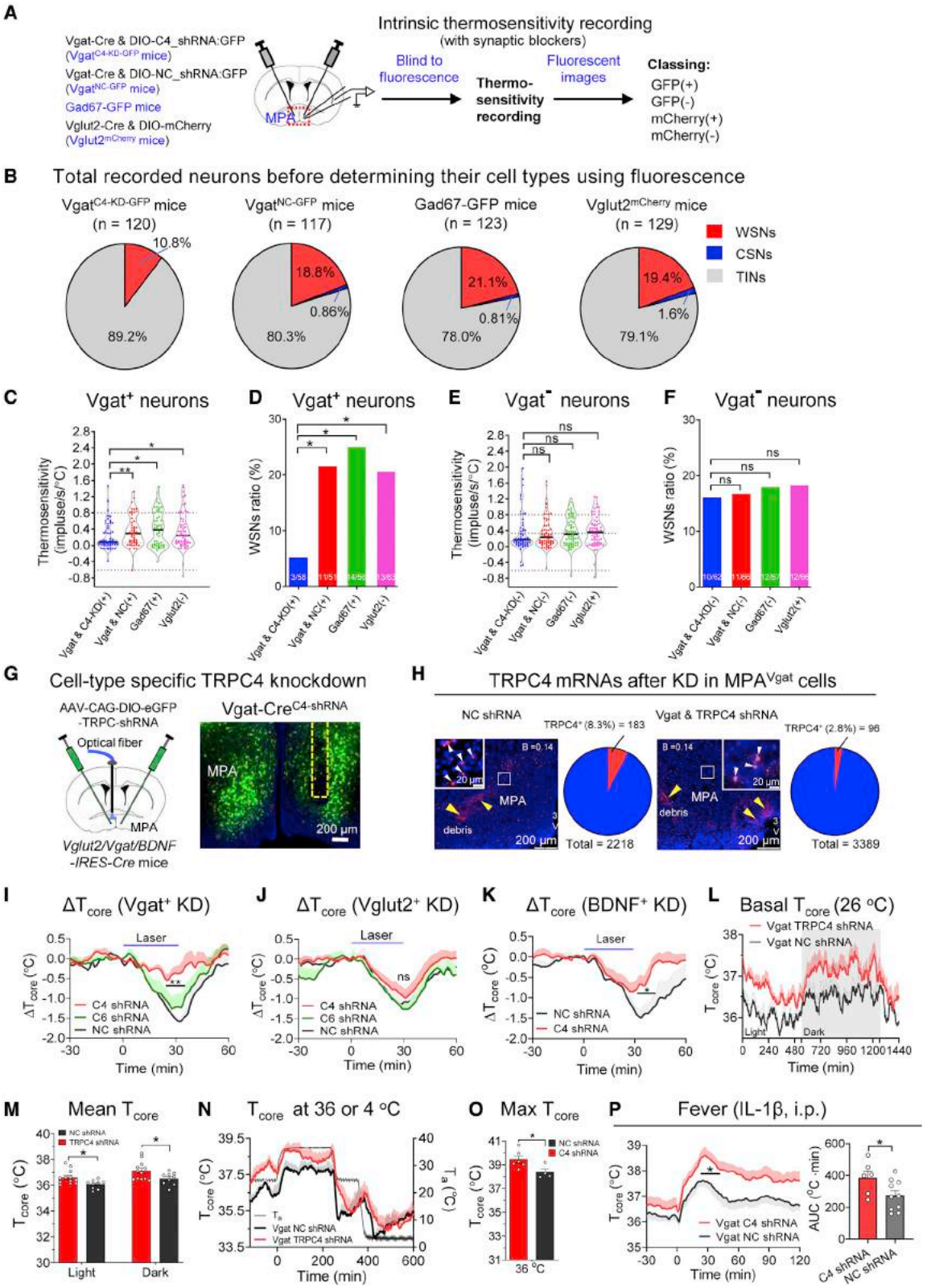

(legend on next page)

we conclude that TRPC4 is required in MPA GABAergic WSNs to sense brain warming.

TRPC4 functions in MPA GABAergic neurons to regulate T_{core}

To determine cell types required for TRPC4 function, we injected AAVs carrying Cre-dependent shRNA into the MPA of Vgat-IRES-Cre, Vglut2-IRES-Cre, and BDNF-IRES-Cre mice (Figures 5G and S15A–S15D). The expression of shRNA in MPA^{Vgat} neurons rendered 60% of MPA $TRPC4^{+}$ cells undetectable to TRPC4 RNAscope fluorescence (Figure 5H). As expected, TRPC4 knockdown in MPA^{Vgat} neurons, but not MPA^{Vglut2} neurons, reduced the hypothermic effect induced by MPA heating, compared with the NC (Figures 5I and 5J). TRPC4 knockdown in MPA^{BDNF} neurons also partially reduced heating-induced hypothermia (Figure 5K). This is consistent with the findings that BDNF and TRPC4 were co-expressed (Figure 4K) and that one-third of BDNF neurons are GABAergic.[19] In contrast, TRPC6 knockdown in MPA^{Vgat} or MPA^{Vglut2} neurons did not affect heating-induced hypothermia (Figures 5I and 5J). As seen with the knockouts, TRPC4 knockdown in MPA^{Vgat} neurons increased basal T_{core} and impaired warm defense (Figures 5L–5O). In addition, fever temperature was modestly but significantly increased by knocking down TRPC4 in Vgat neurons but not in Vglut2 or BDNF neurons (Figures 5P, S15E, and S15F). Together, these analyses reveal that TRPC4 is required in MPA GABAergic WSN neurons to set basal temperatures, prevent hyperthermia, and limit fever.

TRPC4 is not a warm thermoreceptor

To test whether TRPC4 functions as a direct thermoreceptor, we expressed it in HEK293T cells and used calcium imaging to measure its intrinsic thermal activity. We did not detect significant calcium activity in response to warming (Figure S16A). As a control, Englerin A, a selective agonist for TRPC4/TRPC5,[56–59] induced a strong calcium response (Figure S16B). Thus, TRPC4 is not a warm thermoreceptor. We further tested the PLCβ function since TRPC channels often function downstream of a PLCβ pathway.[39,40,60,61] First, we noticed that several PLCβ isoforms were co-expressed with TRPC4 in the POA (Figure S16C). Next, we blocked PLCβ using its blocker, U73122. U73122 did not affect the mean WSN thermosensitivity; however, it reduced thermosensitivity in 46% of WSNs (Figures S16D and S16E), implying that PLCβ might function only in a subset of WSNs. Behaviorally, U73122, but not its inactive analog, U73433, blocked the hypothermic effect induced by brain heating (Figures S16F and S16G). Therefore, our data suggest that TRPC4 is not a warm receptor but may function downstream of a PLCβ pathway to sense temperature.

TRPC4 antagonists and agonists bidirectionally control WSN activity and T_{core}

To evaluate whether TRPC4 could be targeted to manage T_{core}, we pharmacologically modulated TRPC4 activity and analyzed their effects on T_{core}. First, we analyzed the effects of these drugs on the WSN activity (Figure 6A). Perfusion of the TRPC4 blocker, ML204 (10 μM; IC_{50} = 1–3 μM[62,63]), but not the TRPC6 blocker, SAR7334 (100 nM; IC_{50} = 8–10 nM[64]), suppressed the intrinsic thermosensitivity of WSNs (Figures 6B–6D). Perfusion of the two blockers together did not cause a more noticeable suppression of the thermosensitivity than ML204 alone (Figure 6E). We also analyzed the effect of another TRPC4 blocker, HC-070. Similar to ML204, 20-nM of HC-070 (IC_{50} = 10–100 nM[65]) effectively suppressed the thermosensitivity of WSNs (Figures 6F and

Figure 5. TRPC4 is required in MPA GABAergic neurons to sense warmth and regulate body temperature

(A) Schematic for testing the thermosensitivity of MPA neurons from the indicated genotypes, including Vgat-Cre mice with the intra-MPA injection of AAV(2/9)-DIO-TRPC4-shRNA-GFP ($Vgat^{C4\text{-}KD\text{-}GFP}$), Vgat-Cre mice with the intra-MPA injection of AAV(2/9)-DIO-NC-shRNA ($Vgat^{NC\text{-}GFP}$), Gad67-GFP transgenic mice, and Vglut2-Cre mice with the intra-MPA injection of AAV(2/8)-DIO-mCherry ($Vglut2^{mCherry}$). The firing activity of neurons was continuously recorded during cyclic temperature changes (36°C–39°C–33°C–36°C) with synaptic transmission blockers (10 μM CNQX, 50 μM AP-5, and 25 μM bicuculline). Neurons were recorded blind to the fluorescence, and epifluorescent pictures were taken after the recordings to confirm the genotypes.

(B) Percentage of WSNs, CSNs, and TINs in the MPA from different mice. All recorded neurons were analyzed here before determining genotypes using epifluorescence.

(C and D) Summary of the thermosensitivity (C) and WSN percentage (D) of MPA $Vgat^{+}$ neurons, including GFP-positive neurons from $Vgat^{C4\text{-}KD\text{-}GFP}$ mice (Vgat & C4-KD(+)), GFP-positive neurons from $Vgat^{NC\text{-}GFP}$ mice (Vgat & NC(+)), GFP-positive neurons from Gad67-GFP mice (Gad67(+)), and mCherry-negative neurons in the $Vglut2^{mCherry}$ mice (Vglut2(−)).

(E and F) Summary of the thermosensitivity (E) and WSN percentage (F) of MPA $Vgat^{-}$ neurons, including GFP-negative neurons from $Vgat^{C4\text{-}KD\text{-}GFP}$ mice (Vgat & C4-KD(−)), GFP-negative neurons from $Vgat^{NC\text{-}GFP}$ mice (Vgat & NC(−)), GFP-negative neurons from Gad67-GFP mice (Gad67(−)), and mCherry-positive neurons in the $Vglut2^{mCherry}$ mice (Vglut2(+)).

(G) Schematic illustration of Cre-dependent TRPC4 knockdown in the MPA of Vglut2-IRES-Cre, Vgat-IRES-Cre, or BDNF-IRES-Cre mice. Representative shRNA expression labeled by GFP (co-expressed) is shown in the right. Scale bars, 200 μm.

(H) Knockdown efficiency of TRPC4 shRNA. Representative images of TRPC4 mRNA *in situ* from brain sections expressed the scramble sequence (NC shRNA) or TRPC4 shRNA (TRPC4 KD). TRPC4 mRNA signals are shown as small dots indicated by white arrowheads. Yellow arrowheads indicate tissue debris. Scale bar, 200 μm for main panels and 20 μm for boxed ROI.

(I–K) Changes of T_{core} by MPA heating after knockdown of TRPC4 or TRPC6 in MPA^{Vgat} neurons (I; C4, n = 6 mice; C6, n = 4 mice; NC, n = 4 mice), MPA^{Vglut2} neurons (J; C4, n = 10 mice; C6, n = 3 mice; NC, n = 5 mice) or MPA^{BDNF} neurons (K; C4, n = 6 mice; NC, n = 5 mice).

(L and M) Changes of basal T_{core} at 26°C after knockdown of TRPC4 in MPA^{Vgat} neurons (TRPC4, n = 12 mice; NC, n = 9 mice).

(N and O) Changes of T_{core} after knockdown of TRPC4 in MPA^{Vgat} neurons in response to warm and cold challenges (TRPC4, n = 6 mice; NC, n = 4 mice; 4–6 weeks post-viral injection). Max T_{core} in (O) is maximum T_{core} at T_a = 36°C.

(P) Impact of TRPC4 knockdown in MPA^{Vgat} neurons on the fever induced by IL-1β injection (i.p.) (TRPC4, n = 6 mice; NC, n = 10 mice).

All data are shown as mean ± SEM and were analyzed by two-way RM ANOVA (I–K and P), unpaired t test (M, O, and P), one-way ANOVA followed by Tukey's multiple comparison test (C and E), or chi-squared test (D and F). *p < 0.05, **p < 0.01, ns, not significant.

See also Figure S15.

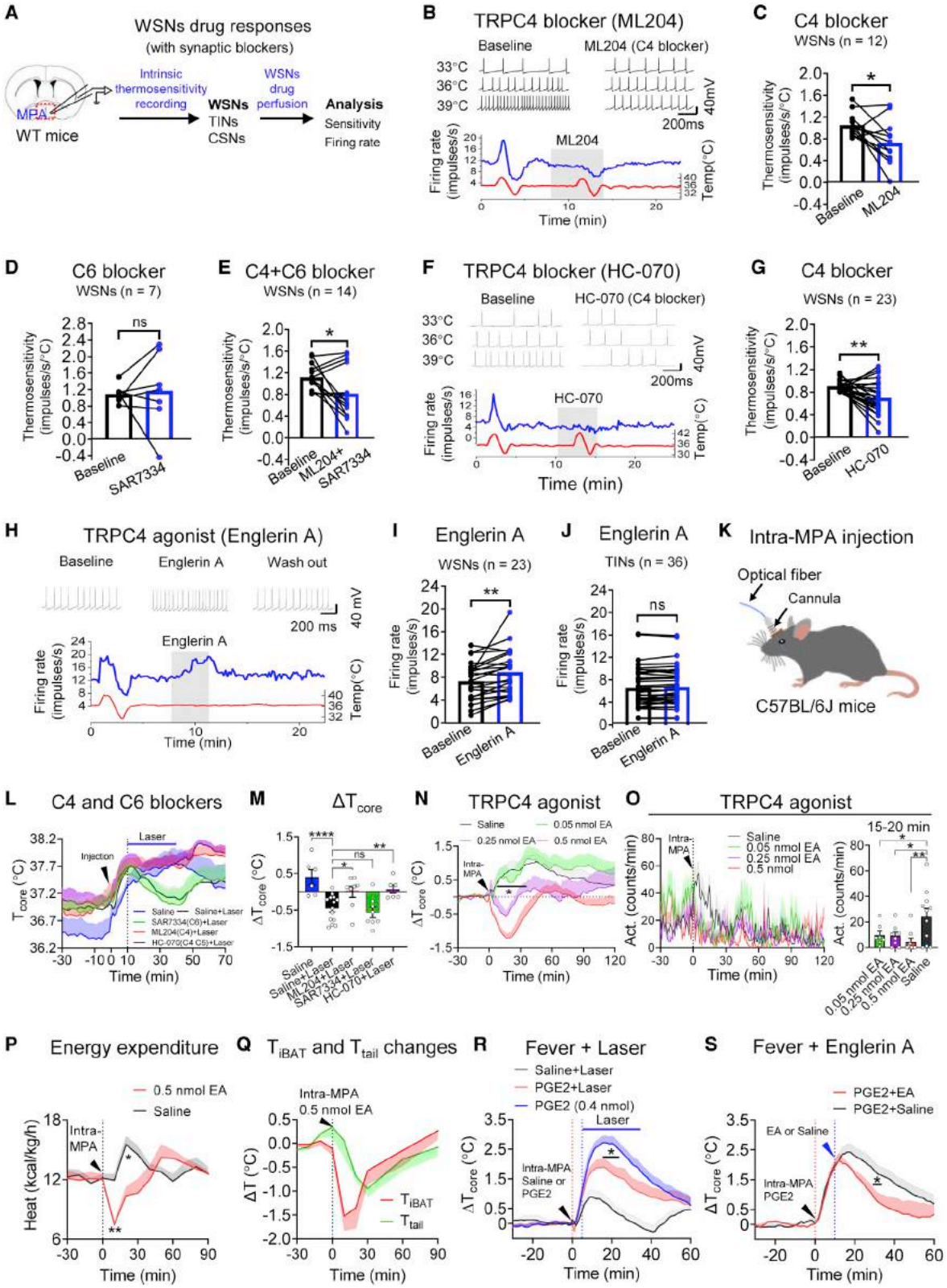

(legend on next page)

6G). As a control, these blockers did not affect the thermosensitivity of TINs (Figures S17A–S17D). Conversely, 10 nM of EA (EC_{50} = 11 nM[56]) increased firing rates of WSNs without affecting TINs (Figures 6H–6J). These data suggest that TRPC4 antagonists and agonists could bidirectionally regulate the activity of WSNs at low concentrations.

Next, we measured the effect of these blockers on the heating-induced hypothermic effect (Figure 6K). We estimated drug concentrations in the cerebrospinal fluid (CSF) by assuming the total CSF was 100 μL and injected ML204 (CSF concentration = ∼10 μM, 10-fold of IC_{50}), or SAR7334 (CSF concentration = ∼100 nM, 10-fold of IC_{50}), into the MPA 10-min before brain heating. The injection procedure itself induced mild hyperthermia, and the MPA heating could suppress it (Figure 6L). Interestingly, injection of ML204, but not SAR7334, blunted the suppression of injection-induced hyperthermia, suggesting that ML204 blocked the heating-induced hypothermic effect (Figures 6L and 6M). Similarly, HC-070 (CSF concentration = ∼1 μM, 10-fold of IC_{50}) also blocked the heating-induced hypothermic effect (Figures 6L and 6M). Next, we injected EA into the MPA and found it induced hypothermia in a concentration-dependent manner (Figure 6N). A concentration at 5-μM induced significant hypothermia (−1.2°C; Figure 6N), accompanied by reduced physical activity, energy expenditure, and T_{iBAT}, but not T_{tail} (Figures 6O–6Q). These data suggest that TRPC4 might be involved in the integration of the CNS control of body temperature and energy metabolism via regulating energy consumption. The relatively higher concentration used in behavioral analysis than that used in electrophysiology (Figure 6I) was probably due to the instability of this drug in vivo[66] and the need to suppress the injection-induced hyperthermia (Figure 6N). Finally, we tested whether MPA heating and EA could limit fever. As expected, heating the MPA lowered the fever temperature induced by PGE2 (Figure 6R). Interestingly, EA injection (∼5 μM) also significantly suppressed fever temperature (Figure 6S). Therefore, our results show that TRPC4 antagonists effectively block the hypothermic function of WSNs, whereas its agonist could induce hypothermia and limit fever, suggesting that TRPC4 may represent a molecular target for T_{core} management.

DISCUSSION

Feedback control of T_{core} by TRPC4-expressing GABAergic WSNs

WSNs have been proposed as an internal cellular sensor to detect brain warming and their artificial activation by brain heating triggers a counteractive body cooling response.[1,3–6,8–14] However, how WSNs contribute to physiological thermoregulation is unclear, and the genetic identity of WSNs remains undefined. Here, we first found that heating the POA (2°C–4°C) with a small-sized device induced a fast-cooling response in mice (Figure 1), suggesting the existence of functional WSNs. Next, we identified TRPC4 as an essential molecule in warm sensing

Figure 6. Pharmacological modulation of TRPC4 activity bidirectionally controlled WSN activity and body temperature

(A) Schematic illustration of testing drug responses of MPA WSNs in WT mice. The firing activity of neurons was recorded during cyclic temperature changes (36–39–33–36°C) with synaptic transmission blockers (10 μM CNQX, 50 μM AP-5, and 25 μM bicuculline). After characterizing the thermosensitivity, the response to drugs was recorded.

(B) Representative traces of a WSN in response to TRPC4 blocker ML204. Top: spontaneous firing activity of the WSN in response to ML204 (10 μM) treatment at 33°C, 36°C, and 39°C, where the thermosensitivity was decreased from 1.53 to 0.39 impulses/s/°C. Bottom: the spontaneous firing rate (blue) and tissue slice temperature (red) plotted over time. The perfusion period with ML204 is shaded in gray.

(C–E) Summary of the thermosensitivity of MPA WSNs before (black) and after (blue) perfusion with TRPC4 blocker ML204 (C; 10 μM), TRPC6 blocker SAR7334 (D; 100 nM; IC_{50} = 8–10 nM), or 10-μM ML204 plus 100-nM SAR7334 (E).

(F) Representative traces of a WSN in response to TRPC4 blocker HC-070. Top: spontaneous firing activity of the WSN in response to HC-070 (20 nM) treatment at 33°C, 36°C, and 39°C, where the thermosensitivity was decreased from 0.89 to 0.08 impulses/s/°C. Bottom: the spontaneous firing rate (blue) and tissue slice temperature (red) plotted over time. The HC-070 perfusion period is shaded in gray.

(G) Summary of the thermosensitivity of MPA WSNs before (black) and after (blue) perfusion with TRPC4 blocker HC-070 (20 nM).

(H) Representative traces of a WSN in response to TRPC4 agonist EA (10 nM), where the firing rate was increased from 11 to 19 impulses/s. Top: action potentials of the WSN at 36°C in response to EA perfusion. Bottom: experimental records of spontaneous firing rates (blue) and tissue slice temperature (red). The EA perfusion period is shaded in gray.

(I and J) Summary of firing rates of MPA WSNs (I) and TINs (J) before (black) and after (blue) perfusion with EA (10 nM).

(K) Schematic of the intra-MPA drug delivery and optical heating experiment. The same cannula placed in the MPA was used for both drug delivery and optical heating.

(L and M) Changes of T_{core} by heating the MPA after intra-POA delivery of ML204 (1 nmol; CSF concentration = ∼10 μM), SAR7334 (0.01 nmol; CSF concentration = ∼100 nM), or HC-070 (0.1 nmol; CSF concentration = ∼1 μM) as indicated. The saline injections were controls (Saline, n = 6 mice; Saline + Laser, n = 14 mice; ML204 + Laser, n = 8 mice; SAR7334 + Laser, n = 8 mice; HC-070 + Laser, n = 6 mice).

(N and O) Changes of T_{core} (N) and physical activity (O) after MPA injection of EA (0.05 nmol—CSF concentration = ∼0.5 μM, n = 7 mice; 0.25 nmol—CSF concentration = ∼2.5 μM, n = 8 mice; 0.5 nmol—CSF concentration = ∼5 μM, n = 9 mice; Saline, n = 11 mice). Changes in physical activity after EA injection (15–20 min) are summarized in the right panel of (O).

(P) Changes in energy expenditure after intra-MPA injection of EA (0.5 nmol) in WT mice (n = 9 mice).

(Q) Dynamics of ΔT_{iBAT} and ΔT_{tail} after intra-MPA injection of EA (0.5 nmol) in WT mice (n = 8 mice).

(R) Impact of optical heating (4 mW) on fever induced by intra-MPA PGE2 injection. PGE2 dose, 0.4 nmol. Saline + Laser, n = 6 mice; 0.4 nmol PGE2 + Laser, n = 7 mice; 0.4 nmol PGE2, n = 8 mice. Heating started 5-min after PGE2 injection.

(S) Impact of EA on the fever induced by intra-MPA PGE2 injection. 0.4 nmol PGE2 + Saline, n = 7 mice; 0.4 nmol PGE2 + 0.5 nmol EA, n = 5 mice. EA was injected 10-min after PGE2 injection.

All data are shown as mean ± SEM and were analyzed by paired t test (C–E, G, I, and J), ordinary one-way ANOVA (M and O), or two-way RM ANOVA (L, N, P, R, and S). *$p < 0.05$, **$p < 0.01$, ns, not significant.

See also Figures S16 and S17.

(Figures 4 and 5), allowing functional manipulation of TRPC4-expressing WSNs by targeting TRPC4. Indeed, TRPC4 deletion or its silencing in MPA GABAergic neurons increased basal core temperature, impaired warm defense, and aggravated fever. Therefore, our results establish that TRPC4-expressing GABAergic WSNs function as an essential warm cellular sensor to set body temperature, prevent hyperthermia, and limit fever. Furthermore, conditions such as fever, exercise, and heatstroke can also increase brain temperatures by 2°C–4°C[67–70] in humans. Hence, WSNs might also be activated in these conditions to control T_{core} as well.

Thermoreceptor for WSNs

Identifying the thermoreceptor that enables WSNs to detect temperature is crucial. Surprisingly, we found that the thermosensitive TRPM2 is not required for brain heating-induced hypothermia. Consistent with this, a recent study confirmed that TRPM2 does not function as an intrinsic warm receptor in WSNs, but instead acts as a synaptic warm sensor.[20] This study showed that TRPM2 deletion has a small effect on brain heating-induced hypothermia.[20] However, we could not replicate this effect, which might be due to different experimental settings (Figures 2P–2R and S11). Via a pilot RNAi screen, we found that TRPC4 is critical for warm sensing in WSNs and accounts for half of MPA WSNs[5] (Figures 3, 4, and 5). Genetic downregulation of TRPC4 suggests that TRPC4 is essential for intrinsic warm sensing in TRPC4-expressing GABAergic WSNs (Figures 3, 4, and 5). Noticeably, only 9.3% of $TRPC4^+$ cells co-expressed TRPM2 (Figure 4K), suggesting the two channels mainly function in different cells. Thus, if TPRM2 still plays a role in warm sensing, such as under more extreme heating, it may modulate the activity of $TRPC4^+$ WSNs via direct or indirect neural connections.

Notably, in vitro calcium imaging suggested that TRPC4 is not a direct thermoreceptor (Figure S16). It is known that TRPC channels can function downstream of the $G_{\alpha}q$-phospholipase Cβ (PLCβ) pathway,[60,61] and this pathway has been shown to mediate warm sensing in *Drosophila*.[39,40] Thus, we manipulated this pathway using a selective PLCβ blocker and found that it reduced the warmth sensitivity of 46% of WSNs and partially suppressed the hypothermic effect induced by brain warming (Figure S16). Thus, we propose that a TRPC4-mediated PLC pathway indirectly senses warmth in GABAergic WSNs. The sensing mechanism for glutamatergic WSNs remains unknown.

A molecular target for T_{core} management

Body temperature management is needed in thermoregulatory disorders such as fever, heatstroke, and malignant hyperthermia.[71–73] Also, the ability to therapeutically induce hypothermia helps reducing tissue damage during medical emergencies.[74,75] However, besides antipyretic drugs used to treat fever, few drugs are available to manage T_{core}, resulting in the use of physical methods.[75] Here, we showed that TRPC4 antagonists effectively alleviated the hypothermia induced by brain heating (Figure 6). Conversely, TRPC4 agonists effectively induced hypothermia and limited fever (Figure 6). These results indicate that TRPC4 might be a promising molecular target for body temperature management. Given that mice are torpid animals, which might use slightly different thermoregulatory mechanisms than non-torpid larger mammals, it would be exciting to know whether TRPC4 also regulates T_{core} in non-torpid mammals including humans. Interestingly, progesterone could inhibit TRPC4,[76] raising a question of whether this inhibition induces mild hyperthermia during menstrual cycles in women.[77]

Optothermal effects under natural behaviors

The delivery of light into the brain is vital for neuroscience research.[27,28,78,79] However, the optothermal effects associated with light may alter neuronal activity[2,4,21,25] and behavior,[10,21] which needs to be precisely evaluated in vivo. By designing a small, implantable device, we were able to precisely measure optothermal effects in the brain of freely behaving mice (Figure 1) and found that it was underestimated by up to 2-fold.[21,23,25] We further built mathematical models to accurately predict temperature changes (Figures 1 and S2). Therefore, we have provided a practical guide for neuroscientists to access the optothermal effect under natural behaviors.

STAR★METHODS

Detailed methods are provided in the online version of this paper and include the following:

- KEY RESOURCES TABLE
- RESOURCE AVAILABILITY
  - Lead contact
  - Materials availability
  - Data and code availability
- EXPERIMENTAL MODEL AND SUBJECT DETAILS
  - Animals
- METHOD DETAILS
  - Manufacture the device for intracranial temperature measurement
  - Manufacture the wired thermal probe for core body temperature measurement
  - T-type thermocouple calibration
  - Light stimulation patterns
  - In vivo temperature measurement in freely-behaving mice
  - Core body temperature and physical activity telemetry
  - Metabolic measurement
  - The iBAT and tail skin temperature measurement
  - Stereotaxic brain injection
  - cFos induction by brain warming
  - Immunohistochemistry and histological analysis
  - TRPC4 mRNA RNAscope (in-situ hybridization)
  - RNAi design
  - Quantitative (or real-time) PCR
  - Procedure to deliver drugs and laser simultaneously
  - Simulation of heat distribution in brain tissues
  - Brain slice electrophysiology
  - Bioinformatics for single-cell RNA sequencing data
  - Cell culture
  - Calcium imaging
- QUANTIFICATION AND STATISTICAL ANALYSIS

SUPPLEMENTAL INFORMATION

Supplemental information can be found online at https://doi.org/10.1016/j.neuron.2022.11.008.

ACKNOWLEDGMENTS

We thank Drs. Tian Xue and Zhenge Luo for sharing reagents; Dr. Tongfei Wang for valuable discussion; the MICF and Molecular Cellular Core of SLST, ShanghaiTech University for imaging and staining. This study was funded by MOST of China (2019YFA0801900), NSF of China (32122039, 91857104, 31900707, 32100825, 31771289, 32100926, and 61634006), Shenzhen-Hong Kong Program (NYKFKT20190017), Program of Shanghai Academic Research Leader (21XD1422700), China Postdoctoral Science Foundation (2019M651616), Shanghai Sailing Program (21YF1429800), MOST of China (2017YFA0205903), and Shanghai Frontiers Science Center for Biomacromolecules and Precision Medicine at ShanghaiTech University.

AUTHOR CONTRIBUTIONS

Experimental design, X.F., W.P., H.Y., X.S., J.H., Q.Y., W.Z.Y., J.Z., and W.L.S.; brain temperature measurement device, X.F., Z.L., and W.P.; data acquisition and analysis, Q.Z., X.F., J.X., C.L., C.G., M.H., W.Y., H.S., X.N., B.C., R.H., J.Z., and Q.S.; electrophysiology, J.X.; bioinformatic analysis, S.D. and L.Z.; modeling, D.C.; calcium imaging, C.L.; writing, X.F., Q.Z., W.Z.Y., J.Z., and W.L.S.; graphic abstract, H.T.

DECLARATION OF INTERESTS

The authors declare no competing interests.

INCLUSION AND DIVERSITY

We support inclusive, diverse, and equitable conduct of research.

Received: August 25, 2021
Revised: June 28, 2022
Accepted: November 7, 2022
Published: December 6, 2022

REFERENCES

1. Boulant, J.A. (2006). Neuronal basis of Hammel's model for set-point thermoregulation. J. Appl. Physiol. (1985) *100*, 1347–1354. https://doi.org/10.1152/japplphysiol.01064.2005.
2. Kelso, S.R., Perlmutter, M.N., and Boulant, J.A. (1982). Thermosensitive single-unit activity of in vitro hypothalamic slices. Am. J. Physiol. *242*, R77–R84. https://doi.org/10.1152/ajpregu.1982.242.1.R77.
3. Baldino, F., Jr., and Geller, H.M. (1982). Electrophysiological analysis of neuronal thermosensitivity in rat preoptic and hypothalamic tissue cultures. J. Physiol. *327*, 173–184.
4. Bligh, J. (1966). The thermosensitivity of the hypothalamus and thermoregulation in mammals. Biol. Rev. Camb. Philos. Soc. *41*, 317–368.
5. Wang, T.A., Teo, C.F., Åkerblom, M., Chen, C., Tynan-La Fontaine, M., Greiner, V.J., Diaz, A., McManus, M.T., Jan, Y.N., and Jan, L.Y. (2019). Thermoregulation via temperature-dependent PGD2 production in mouse preoptic area. Neuron *103*, 309–322.e7. https://doi.org/10.1016/j.neuron.2019.04.035.
6. Song, K., Wang, H., Kamm, G.B., Pohle, J., Reis, F.C., Heppenstall, P., Wende, H., and Siemens, J. (2016). The TRPM2 channel is a hypothalamic heat sensor that limits fever and can drive hypothermia. Science *353*, 1393–1398. https://doi.org/10.1126/science.aaf7537.
7. Eberwine, J., and Bartfai, T. (2011). Single cell transcriptomics of hypothalamic warm sensitive neurons that control core body temperature and fever response Signaling asymmetry and an extension of chemical neuroanatomy. Pharmacol. Ther. *129*, 241–259. https://doi.org/10.1016/j.pharmthera.2010.09.010.
8. Tan, C.L., Cooke, E.K., Leib, D.E., Lin, Y.C., Daly, G.E., Zimmerman, C.A., and Knight, Z.A. (2016). Warm-sensitive neurons that control body temperature. Cell *167*, 47–59.e15. https://doi.org/10.1016/j.cell.2016.08.028.
9. Griffin, J.D., Kaple, M.L., Chow, A.R., and Boulant, J.A. (1996). Cellular mechanisms for neuronal thermosensitivity in the rat hypothalamus. J. Physiol. *492*, 231–242.
10. Carlisle, H.J. (1966). Behavioural significance of hypothalamic temperature-sensitive cells. Nature *209*, 1324–1325.
11. Refinetti, R., and Carlisle, H.J. (1986). Effects of anterior and posterior hypothalamic temperature changes on thermoregulation in the rat. Physiol. Behav. *36*, 1099–1103. https://doi.org/10.1016/0031-9384(86)90486-5.
12. Dib, B. (1980). Continuous perfusion under pressure using several tubes in the freely behaving rat. Physiol. Behav. *24*, 177–178. https://doi.org/10.1016/0031-9384(80)90032-3.
13. Fusco, M.M., Hardy, J.D., and Hammel, H.T. (1961). Interaction of central and peripheral factors in physiological temperature regulation. Am. J. Physiol. *200*, 572–580.
14. Hammel, H.T., Hardy, J.D., and Fusco, M.M. (1960). Thermoregulatory responses to hypothalamic cooling in unanesthetized dogs. Am. J. Physiol. *198*, 481–486.
15. Boulant, J.A. (2000). Role of the preoptic-anterior hypothalamus in thermoregulation and fever. Clin. Infect. Dis. *31*, S157–S161. https://doi.org/10.1086/317521.
16. Carlisle, H.J., and Laudenslager, M.L. (1979). Observations on the thermoregulatory effects of preoptic warming in rats. Physiol. Behav. *23*, 723–732. https://doi.org/10.1016/0031-9384(79)90166-5.
17. Andersson, B., Grant, R., and Larsson, S. (1956). Central control of heat loss mechanisms in the goat. Acta Physiol. Scand. *37*, 261–280. https://doi.org/10.1111/j.1748-1716.1956.tb01362.x.
18. Magoun, H.W., Harrison, F., Brobeck, J.R., and Ranson, S.W. (1938). Activation of heat loss mechanisms by local heating of the brain. J. Neurophysiol. *1*, 101–114. https://doi.org/10.1152/jn.1938.1.2.101.
19. Zhao, Z.D., Yang, W.Z., Gao, C., Fu, X., Zhang, W., Zhou, Q., Chen, W., Ni, X., Lin, J.K., Yang, J., et al. (2017). A hypothalamic circuit that controls body temperature. Proc. Natl. Acad. Sci. USA *114*, 2042–2047. https://doi.org/10.1073/pnas.1616255114.
20. Kamm, G.B., Boffi, J.C., Zuza, K., Nencini, S., Campos, J., Schrenk-Siemens, K., Sonntag, I., Kabaoğlu, B., El Hay, M.Y.A., Schwarz, Y., et al. (2021). A synaptic temperature sensor for body cooling. Neuron *109*, 3283–3297.e11. https://doi.org/10.1016/j.neuron.2021.10.001.
21. Owen, S.F., Liu, M.H., and Kreitzer, A.C. (2019). Thermal constraints on in vivo optogenetic manipulations. Nat. Neurosci. *22*, 1061–1065. https://doi.org/10.1038/s41593-019-0422-3.
22. Picot, A., Dominguez, S., Liu, C., Chen, I.W., Tanese, D., Ronzitti, E., Berto, P., Papagiakoumou, E., Oron, D., Tessier, G., et al. (2018). Temperature rise under two-photon optogenetic brain stimulation. Cell Rep. *24*, 1243–1253.e5. https://doi.org/10.1016/j.celrep.2018.06.119.
23. Shin, Y., Yoo, M., Kim, H.S., Nam, S.K., Kim, H.I., Lee, S.K., Kim, S., and Kwon, H.S. (2016). Characterization of fiber-optic light delivery and light-induced temperature changes in a rodent brain for precise optogenetic neuromodulation. Biomed. Opt. Express *7*, 4450–4471. https://doi.org/10.1364/BOE.7.004450.
24. Arias-Gil, G., Ohl, F.W., Takagaki, K., and Lippert, M.T. (2016). Measurement, modeling, and prediction of temperature rise due to optogenetic brain stimulation. Neurophotonics *3*, 045007. https://doi.org/10.1117/1.NPh.3.4.045007.
25. Stujenske, J.M., Spellman, T., and Gordon, J.A. (2015). Modeling the spatiotemporal dynamics of light and heat propagation for in vivo optogenetics. Cell Rep. *12*, 525–534. https://doi.org/10.1016/j.celrep.2015.06.036.

26. Christie, I.N., Wells, J.A., Southern, P., Marina, N., Kasparov, S., Gourine, A.V., and Lythgoe, M.F. (2013). fMRI response to blue light delivery in the naive brain: implications for combined optogenetic fMRI studies. Neuroimage *66*, 634–641. https://doi.org/10.1016/j.neuroimage.2012.10.074.

27. Tye, K.M., and Deisseroth, K. (2012). Optogenetic investigation of neural circuits underlying brain disease in animal models. Nat. Rev. Neurosci. *13*, 251–266. https://doi.org/10.1038/nrn3171.

28. Zhao, Z.D., Chen, Z., Xiang, X., Hu, M., Xie, H., Jia, X., Cai, F., Cui, Y., Chen, Z., Qian, L., et al. (2019). Zona incerta GABAergic neurons integrate prey-related sensory signals and induce an appetitive drive to promote hunting. Nat. Neurosci. *22*, 921–932. https://doi.org/10.1038/s41593-019-0404-5.

29. Zheng, D., Fu, J.Y., Tang, M.Y., Yu, X.D., Zhu, Y., Shen, C.J., Li, C.Y., Xie, S.Z., Lin, S., Luo, M., and Li, X.M. (2022). A deep mesencephalic nucleus circuit regulates licking behavior. Neurosci. Bull. *38*, 565–575. https://doi.org/10.1007/s12264-021-00817-2.

30. Jiang, S., Wu, X., Rommelfanger, N.J., Ou, Z., and Hong, G. (2022). Shedding light on neurons: optical approaches for neuromodulation. Natl. Sci. Rev. *9*, nwac007. https://doi.org/10.1093/nsr/nwac007.

31. Parusel, S., Yi, M.H., Hunt, C.L., and Wu, L.J. (2022). Chemogenetic and optogenetic manipulations of microglia in chronic pain. Neurosci. Bull. https://doi.org/10.1007/s12264-022-00937-3.

32. Mcintosh, R.L., and Anderson, V. (2010). A comprehensive tissue properties database provided for the thermal assessment of a human at rest. Biophys. Rev. Lett. *05*, 129–151. https://doi.org/10.1142/S1793048010001184.

33. Duck, F. (1990). Physical Properties of Tissues: A Comprehensive Reference Book (Elsevier Science).

34. Yang, W.Z., Du, X., Zhang, W., Gao, C., Xie, H., Xiao, Y., Jia, X., Liu, J., Xu, J., Fu, X., et al. (2020). Parabrachial neuron types categorically encode thermoregulation variables during heat defense. Sci. Adv. *6*, eabb9414. https://doi.org/10.1126/sciadv.abb9414.

35. Luo, F., Mu, Y., Gao, C., Xiao, Y., Zhou, Q., Yang, Y., Ni, X., Shen, W.L., and Yang, J. (2019). Whole-brain patterns of the presynaptic inputs and axonal projections of BDNF neurons in the paraventricular nucleus. J. Genet. Genomics *46*, 31–40. https://doi.org/10.1016/j.jgg.2018.11.004.

36. Yu, S., Qualls-Creekmore, E., Rezai-Zadeh, K., Jiang, Y., Berthoud, H.R., Morrison, C.D., Derbenev, A.V., Zsombok, A., and Münzberg, H. (2016). Glutamatergic preoptic area neurons that express leptin receptors drive temperature-dependent body weight homeostasis. J. Neurosci. *36*, 5034–5046. https://doi.org/10.1523/JNEUROSCI.0213-16.2016.

37. Ma, Y., Miracca, G., Yu, X., Harding, E.C., Miao, A., Yustos, R., Vyssotski, A.L., Franks, N.P., and Wisden, W. (2019). Galanin neurons unite sleep homeostasis and α2-adrenergic sedation. Curr. Biol. *29*, 3315–3322.e3. https://doi.org/10.1016/j.cub.2019.07.087.

38. Kroeger, D., Absi, G., Gagliardi, C., Bandaru, S.S., Madara, J.C., Ferrari, L.L., Arrigoni, E., Münzberg, H., Scammell, T.E., Saper, C.B., and Vetrivelan, R. (2018). Galanin neurons in the ventrolateral preoptic area promote sleep and heat loss in mice. Nat. Commun. *9*, 4129. https://doi.org/10.1038/s41467-018-06590-7.

39. Shen, W.L., Kwon, Y., Adegbola, A.A., Luo, J., Chess, A., and Montell, C. (2011). Function of rhodopsin in temperature discrimination in Drosophila. Science *331*, 1333–1336. https://doi.org/10.1126/science.1198904.

40. Kwon, Y., Shim, H.S., Wang, X., and Montell, C. (2008). Control of thermotactic behavior via coupling of a TRP channel to a phospholipase C signaling cascade. Nat. Neurosci. *11*, 871–873. https://doi.org/10.1038/nn.2170.

41. Vriens, J., Nilius, B., and Voets, T. (2014). Peripheral thermosensation in mammals. Nat. Rev. Neurosci. *15*, 573–589. https://doi.org/10.1038/nrn3784.

42. Moffitt, J.R., Bambah-Mukku, D., Eichhorn, S.W., Vaughn, E., Shekhar, K., Perez, J.D., Rubinstein, N.D., Hao, J., Regev, A., Dulac, C., and Zhuang, X. (2018). Molecular, spatial, and functional single-cell profiling of the hypothalamic preoptic region. Science *362*. eaau5324. https://doi.org/10.1126/science.aau5324.

43. Harding, E.C., Yu, X., Miao, A., Andrews, N., Ma, Y., Ye, Z., Lignos, L., Miracca, G., Ba, W., Yustos, R., et al. (2018). A neuronal hub binding sleep initiation and body cooling in response to a warm external stimulus. Curr. Biol. *28*, 2263–2273.e4. https://doi.org/10.1016/j.cub.2018.05.054.

44. Hrvatin, S., Sun, S., Wilcox, O.F., Yao, H., Lavin-Peter, A.J., Cicconet, M., Assad, E.G., Palmer, M.E., Aronson, S., Banks, A.S., et al. (2020). Neurons that regulate mouse torpor. Nature *583*, 115–121. https://doi.org/10.1038/s41586-020-2387-5.

45. Zhang, Z., Reis, F.M.C.V., He, Y., Park, J.W., DiVittorio, J.R., Sivakumar, N., van Veen, J.E., Maesta-Pereira, S., Shum, M., Nichols, I., et al. (2020). Estrogen-sensitive medial preoptic area neurons coordinate torpor in mice. Nat. Commun. *11*, 6378. https://doi.org/10.1038/s41467-020-20050-1.

46. Takahashi, T.M., Sunagawa, G.A., Soya, S., Abe, M., Sakurai, K., Ishikawa, K., Yanagisawa, M., Hama, H., Hasegawa, E., Miyawaki, A., et al. (2020). A discrete neuronal circuit induces a hibernation-like state in rodents. Nature *583*, 109–114. https://doi.org/10.1038/s41586-020-2163-6.

47. Zhang, K.X., D'Souza, S., Upton, B.A., Kernodle, S., Vemaraju, S., Nayak, G., Gaitonde, K.D., Holt, A.L., Linne, C.D., Smith, A.N., et al. (2020). Violet-light suppression of thermogenesis by opsin 5 hypothalamic neurons. Nature *585*, 420–425. https://doi.org/10.1038/s41586-020-2683-0.

48. Tabarean, I.V. (2021). Activation of preoptic arginine vasopressin neurons induces hyperthermia in male mice. Endocrinology *162*. bqaa217. https://doi.org/10.1210/endocr/bqaa217.

49. Piñol, R.A., Mogul, A.S., Hadley, C.K., Saha, A., Li, C., Škop, V., Province, H.S., Xiao, C., Gavrilova, O., Krashes, M.J., and Reitman, M.L. (2021). Preoptic BRS3 neurons increase body temperature and heart rate via multiple pathways. Cell Metab. *33*, 1389–1403.e6. https://doi.org/10.1016/j.cmet.2021.05.001.

50. Morrison, S.F., and Nakamura, K. (2019). Central mechanisms for thermoregulation. Annu. Rev. Physiol. *81*, 285–308. https://doi.org/10.1146/annurev-physiol-020518-114546.

51. da Conceição, E.P.S., Morrison, S.F., Cano, G., Chiavetta, P., and Tupone, D. (2020). Median preoptic area neurons are required for the cooling and febrile activations of brown adipose tissue thermogenesis in rat. Sci. Rep. *10*, 18072. https://doi.org/10.1038/s41598-020-74272-w.

52. Nakamura, Y., Yahiro, T., Kataoka, N., Hioki, H., and Nakamura, K. (2022). Prostaglandin EP3 receptor-expressing preoptic neurons bidirectionally control body temperature via tonic GABAergic signaling. Preprint at bioRxiv. https://doi.org/10.1101/2022.04.15.488488.

53. Griffin, J.D., and Boulant, J.A. (1995). Temperature effects on membrane potential and input resistance in rat hypothalamic neurones. J. Physiol. *488*, 407–418. https://doi.org/10.1113/jphysiol.1995.sp020975.

54. Ranels, H.J., and Griffin, J.D. (2003). The effects of prostaglandin E2 on the firing rate activity of thermosensitive and temperature insensitive neurons in the ventromedial preoptic area of the rat hypothalamus. Brain Res. *964*, 42–50. https://doi.org/10.1016/s0006-8993(02)04063-5.

55. Kelso, S.R., and Boulant, J.A. (1982). Effect of synaptic blockade on thermosensitive neurons in hypothalamic tissue slices. Am. J. Physiol. *243*, R480–R490. https://doi.org/10.1152/ajpregu.1982.243.5.R480.

56. Akbulut, Y., Gaunt, H.J., Muraki, K., Ludlow, M.J., Amer, M.S., Bruns, A., Vasudev, N.S., Radtke, L., Willot, M., Hahn, S., et al. (2015). (-)-Englerin A is a potent and selective activator of TRPC4 and TRPC5 calcium channels. Angew. Chem. Int. Ed. Engl. *54*, 3787–3791. https://doi.org/10.1002/anie.201411511.

57. Carson, C., Raman, P., Tullai, J., Xu, L., Henault, M., Thomas, E., Yeola, S., Lao, J., McPate, M., Verkuyl, J.M., et al. (2015). Englerin A agonizes the TRPC4/C5 cation channels to inhibit tumor cell line proliferation. PLoS One *10*. e0127498. https://doi.org/10.1371/journal.pone.0127498.

58. Sourbier, C., Scroggins, B.T., Ratnayake, R., Prince, T.L., Lee, S., Lee, M.J., Nagy, P.L., Lee, Y.H., Trepel, J.B., Beutler, J.A., et al. (2013). Englerin A stimulates PKCθ to inhibit insulin signaling and to simultaneously activate HSF1: pharmacologically induced synthetic lethality. Cancer Cell *23*, 228–237. https://doi.org/10.1016/j.ccr.2012.12.007.

59. Ludlow, M.J., Gaunt, H.J., Rubaiy, H.N., Musialowski, K.E., Blythe, N.M., Vasudev, N.S., Muraki, K., and Beech, D.J. (2017). (-)-Englerin A-evoked Cytotoxicity Is Mediated by Na+ Influx and Counteracted by Na+/K+-ATPase. J. Biol. Chem. *292*, 723–731. https://doi.org/10.1074/jbc.M116.755678.

60. Montell, C. (2012). Drosophila visual transduction. Trends Neurosci. *35*, 356–363. https://doi.org/10.1016/j.tins.2012.03.004.

61. Xue, T., Do, M.T., Riccio, A., Jiang, Z., Hsieh, J., Wang, H.C., Merbs, S.L., Welsbie, D.S., Yoshioka, T., Weissgerber, P., et al. (2011). Melanopsin signalling in mammalian iris and retina. Nature *479*, 67–73. https://doi.org/10.1038/nature10567.

62. Duan, J., Li, J., Zeng, B., Chen, G.L., Peng, X., Zhang, Y., Wang, J., Clapham, D.E., Li, Z., and Zhang, J. (2018). Structure of the mouse TRPC4 ion channel. Nat. Commun. *9*, 3102. https://doi.org/10.1038/s41467-018-05247-9.

63. Miller, M., Shi, J., Zhu, Y., Kustov, M., Tian, J.B., Stevens, A., Wu, M., Xu, J., Long, S., Yang, P., et al. (2011). Identification of ML204, a novel potent antagonist that selectively modulates native TRPC4/C5 ion channels. J. Biol. Chem. *286*, 33436–33446. https://doi.org/10.1074/jbc.M111.274167.

64. Maier, T., Follmann, M., Hessler, G., Kleemann, H.W., Hachtel, S., Fuchs, B., Weissmann, N., Linz, W., Schmidt, T., Löhn, M., et al. (2015). Discovery and pharmacological characterization of a novel potent inhibitor of diacylglycerol-sensitive TRPC cation channels. Br. J. Pharmacol. *172*, 3650–3660. https://doi.org/10.1111/bph.13151.

65. Just, S., Chenard, B.L., Ceci, A., Strassmaier, T., Chong, J.A., Blair, N.T., Gallaschun, R.J., Del Camino, D., Cantin, S., D'Amours, M., et al. (2018). Treatment with HC-070, a potent inhibitor of TRPC4 and TRPC5, leads to anxiolytic and antidepressant effects in mice. PLoS One *13*. e0191225. https://doi.org/10.1371/journal.pone.0191225.

66. Minard, A., Bauer, C.C., Wright, D.J., Rubaiy, H.N., Muraki, K., Beech, D.J., and Bon, R.S. (2018). Remarkable progress with small-molecule modulation of TRPC1/4/5 channels: implications for understanding the channels in health and disease. Cells *7*, 52. https://doi.org/10.3390/cells7060052.

67. Fuller, A., Carter, R.N., and Mitchell, D. (1998). Brain and abdominal temperatures at fatigue in rats exercising in the heat. J. Appl. Physiol. (1985) *84*, 877–883.

68. Walters, T.J., Ryan, K.L., Tate, L.M., and Mason, P.A. (2000). Exercise in the heat is limited by a critical internal temperature. J. Appl. Physiol. (1985) *89*, 799–806.

69. Bain, A.R., Nybo, L., and Ainslie, P.N. (2015). Cerebral vascular control and metabolism in heat stress. Compr. Physiol. *5*, 1345–1380. https://doi.org/10.1002/cphy.c140066.

70. Bain, A.R., Morrison, S.A., and Ainslie, P.N. (2014). Cerebral oxygenation and hyperthermia. Front. Physiol. *5*, 92. https://doi.org/10.3389/fphys.2014.00092.

71. Nakamura, K., and Morrison, S.F. (2011). Central efferent pathways for cold-defensive and febrile shivering. J. Physiol. *589*, 3641–3658. https://doi.org/10.1113/jphysiol.2011.210047.

72. Cheshire, W.P., Jr. (2016). Thermoregulatory disorders and illness related to heat and cold stress. Auton. Neurosci. *196*, 91–104. https://doi.org/10.1016/j.autneu.2016.01.001.

73. Hemmelgarn, C., and Gannon, K. (2013). Heatstroke: thermoregulation, pathophysiology, and predisposing factors. Compend. Contin. Educ. Vet. *35*, E4.

74. Karnatovskaia, L.V., Wartenberg, K.E., and Freeman, W.D. (2014). Therapeutic hypothermia for neuroprotection: history, mechanisms, risks, and clinical applications. Neurohospitalist *4*, 153–163. https://doi.org/10.1177/1941874413519802.

75. Galinsky, R., Dean, J.M., Lear, C.A., Davidson, J.O., Dhillon, S., Wassink, G., Bennet, L., and Gunn, A.J. (2016). In the era of therapeutic hypothermia, how well do studies of perinatal neuroprotection control temperature? Dev. Neurosci. *39*. 37–22. https://doi.org/10.1159/000452859.

76. Miehe, S., Crause, P., Schmidt, T., Löhn, M., Kleemann, H.W., Licher, T., Dittrich, W., Rütten, H., and Strübing, C. (2012). Inhibition of diacylglycerol-sensitive TRPC channels by synthetic and natural steroids. PLoS One *7*, e35393. https://doi.org/10.1371/journal.pone.0035393.

77. Charkoudian, N., Hart, E.C.J., Barnes, J.N., and Joyner, M.J. (2017). Autonomic control of body temperature and blood pressure: influences of female sex hormones. Clin. Auton. Res. *27*, 149–155. https://doi.org/10.1007/s10286-017-0420-z.

78. Wang, W., Wildes, C.P., Pattarabanjird, T., Sanchez, M.I., Glober, G.F., Matthews, G.A., Tye, K.M., and Ting, A.Y. (2017). A light- and calcium-gated transcription factor for imaging and manipulating activated neurons. Nat. Biotechnol. *35*, 864–871. https://doi.org/10.1038/nbt.3909.

79. Lee, D., Hyun, J.H., Jung, K., Hannan, P., and Kwon, H.B. (2017). A calcium- and light-gated switch to induce gene expression in activated neurons. Nat. Biotechnol. *35*, 858–863. https://doi.org/10.1038/nbt.3902.

80. Ye, M., Yang, W., Ainscough, J.F., Hu, X.P., Li, X., Sedo, A., Zhang, X.H., Zhang, X., Chen, Z., Li, X.M., et al. (2014). TRPM2 channel deficiency prevents delayed cytosolic Zn2+ accumulation and CA1 pyramidal neuronal death after transient global ischemia. Cell Death Dis. *5*. e1541. https://doi.org/10.1038/cddis.2014.494.

81. Oh, S.-J., Lee, J.M., Kim, H.-B., Lee, J., Han, S., Bae, J.Y., Hong, G.-S., Koh, W., Kwon, J., Hwang, E.-S., et al. (2019). Ultrasonic neuromodulation via astrocytic TRPA1. Curr. Biol. *29*, 3386–3401.e8. https://doi.org/10.1016/j.cub.2019.08.021.

82. Staaf, S., Maxvall, I., Lind, U., Husmark, J., Mattsson, J.P., Ernfors, P., and Pierrou, S. (2009). Down regulation of TRPC1 by shRNA reduces mechanosensitivity in mouse dorsal root ganglion neurons in vitro. Neurosci. Lett. *457*, 3–7. https://doi.org/10.1016/j.neulet.2009.03.082.

83. Riccio, A., Li, Y., Tsvetkov, E., Gapon, S., Yao, G.L., Smith, K.S., Engin, E., Rudolph, U., Bolshakov, V.Y., and Clapham, D.E. (2014). Decreased anxiety-like behavior and Gαq/11-dependent responses in the amygdala of mice lacking TRPC4 channels. J. Neurosci. *34*, 3653–3667. https://doi.org/10.1523/JNEUROSCI.2274-13.2014.

84. Shen, B., He, Y., Zhou, S., Zhao, H., Mei, M., and Wu, X. (2016). TRPC6 may protect renal ischemia-reperfusion injury through inhibiting necroptosis of renal tubular epithelial cells. Med. Sci. Monit. *22*, 633–641. https://doi.org/10.12659/msm.897353.

85. Jia, J., Verma, S., Nakayama, S., Quillinan, N., Grafe, M.R., Hurn, P.D., and Herson, P.S. (2011). Sex differences in neuroprotection provided by inhibition of TRPM2 channels following experimental stroke. J. Cereb. Blood Flow Metab. *31*, 2160–2168. https://doi.org/10.1038/jcbfm.2011.77.

86. Wagner, T.F.J., Loch, S., Lambert, S., Straub, I., Mannebach, S., Mathar, I., Düfer, M., Lis, A., Flockerzi, V., Philipp, S.E., and Oberwinkler, J. (2008). Transient receptor potential M3 channels are ionotropic steroid receptors in pancreatic β cells. Nat. Cell Biol. *10*, 1421–1430. https://doi.org/10.1038/ncb1801.

87. Maeda, T., Suzuki, A., Koga, K., Miyamoto, C., Maehata, Y., Ozawa, S., Hata, R.I., Nagashima, Y., Nabeshima, K., Miyazaki, K., and Kato, Y. (2017). TRPM5 mediates acidic extracellular pH signaling and TRPM5 inhibition reduces spontaneous metastasis in mouse B16-BL6 melanoma cells. Oncotarget *8*, 78312–78326. https://doi.org/10.18632/oncotarget.20826.

88. Geng, Y., and Feng, B. (2015). Mesendogen, a novel inhibitor of TRPM6, promotes mesoderm and definitive endoderm differentiation of human embryonic stem cells through alteration of magnesium homeostasis. Heliyon *1*, e00046. https://doi.org/10.1016/j.heliyon.2015.e00046.

89. Binding, J., Ben Arous, J., Léger, J.-F., Gigan, S., Boccara, C., and Bourdieu, L. (2011). Brain refractive index measured in vivo with high-NA defocus-corrected full-field OCT and consequences for two-photon microscopy. Opt. Express *19*, 4833–4847. https://doi.org/10.1364/OE.19.004833.

90. Aravanis, A.M., Wang, L.-P., Zhang, F., Meltzer, L.A., Mogri, M.Z., Schneider, M.B., and Deisseroth, K. (2007). An optical neural interface:in vivocontrol of rodent motor cortex with integrated fiberoptic and optogenetic technology. J. Neural Eng. *4*, S143–S156. https://doi.org/10.1088/1741-2560/4/3/S02.

91. Yaroslavsky, A.N., Schulze, P.C., Yaroslavsky, I.V., Schober, R., Ulrich, F., and Schwarzmaier, H.J. (2002). Optical properties of selected native and coagulated human brain tissues in vitro in the visible and near infrared spectral range. Phys. Med. Biol. *47*, 2059–2073. https://doi.org/10.1088/0031-9155/47/12/305.

92. Satija, R., Farrell, J.A., Gennert, D., Schier, A.F., and Regev, A. (2015). Spatial reconstruction of single-cell gene expression data. Nat. Biotechnol. *33*, 495–502. https://doi.org/10.1038/nbt.3192.

93. Zhu, Y., Wang, S., Chu, Y., Zhang, K., Wen, X., Feng, L., Yu, F., and Ma, X. (2022). TRPC5 is essential in endothelium-dependent contraction of aorta from diet-induced obese mice. Fundam. Res. *2*, 429–436. https://doi.org/10.1016/j.fmre.2022.01.017.

STAR★METHODS

KEY RESOURCES TABLE

REAGENT or RESOURCE	SOURCE	IDENTIFIER
Antibodies		
Chicken anti-GFP	Abcam	Cat# ab13970; RRID: AB_300798
DyLight 488 conjugated goat anti-chicken	Invitrogen	Cat# SA5-10070; RRID: AB_2556650
Rabbit anti-EP3R antibody	Cayman Chemical	Cat# 101760; AB_10077931
Alexa Fluor 488 conjugated goat anti-rabbit IgG	Jackson	Cat# 111-545-003; RRID: AB_2338046
Guinea pig anti-cfos	Synaptic systems	Cat# 226004; RRID: AB_2619946
Alexa Fluor 488 conjugated goat anti-Guinea pig IgG(H+L)	Jackson	Cat# 106-545-003; RRID: AB_2337438
Chemicals, peptides, and recombinant proteins		
DAPI Fluoromount-G mounting medium	SouthernBiotech	Cat#0100-20
PGE2	Tocris	2296
CNQX	Sigma-Aldrich	C127
AP-5	Sigma-Aldrich	A8054
Bicuculline	Alomone	B-135
ML204	Tocris Bioscience	Cat. No. 4732
HC-070	Chengdu Ji'ante Pharmaceutical Technology Co., Ltd.	CAS#1628291-95-1
SAR7334	Tocris Bioscience	Cat. No. 5831
U 73122	Tocris Bioscience	Cat. No.1268
(−)-Englerin A	Sigma	PHL82530
IL-1β	Sigma	SPR8033
U 73433	Tocris	Cat No. 4133
RNAscope® Probe- Mm-TRPC4-ex4	acdbio	Cat No. 312271
RNAscope™ 2.5 HD Assay - RED	acdbio	Cat No. 322360
RNA-Protein Co-detection Ancillary Kit	acdbio	Cat No. 323180
Experimental models: Organisms/strains		
Vgat-IRES-Cre	Jackson Laboratory (USA)	JAX: 028862
Vglut2-IRES-Cre	Jackson Laboratory (USA)	JAX: 028863
BDNF-IRES-Cre	The core facility of Peking Union Medicine College	Reference: Luo et al.[35]
Galanin-Cre	MMCCR	031060-UCD
TRPM2 KO	From Ye et al.[80]	N/A
C57BL/6J	Shanghai Silaike Experiment Animal Co., Ltd.	N/A
GAD67-GFP	Jackson Laboratory (USA)	JAX: #007677
TRPC4 KO	From Xue et al.[61]	N/A
TRPC5 KO	From Xue et al.[61]	N/A
Oligonucleotides		
shRNA targeting sequence: TRPA1: gcaagcttccttttctgcatat	From Oh et al.[81]	N/A
shRNA targeting sequence: TRPC1:gggtgactattatatggtt	From Staaf et al.[82]	N/A

(*Continued on next page*)

Continued

REAGENT or RESOURCE	SOURCE	IDENTIFIER
shRNA targeting sequence: TRPC4: ggtggaatctaatggact	From Riccio et al.[83]	N/A
shRNA targeting sequence: TRPC6: ggaccagcatacatgttta	From Shen et al.[84]	N/A
shRNA targeting sequence: TRPM2:gctcatggattcccgagaatac	From Jia et al.[85]	N/A
shRNA targeting sequence: TRPM3: agagaatgtgttcacatcata	From Wagner et al.[86]	N/A
shRNA targeting sequence: TRPM5: attgatgaggctcgtgtgaac	From Maeda et al.[87]	N/A
shRNA targeting sequence: TRPM6: ccaaattctaatggagtg	From Geng and Feng [88]	N/A
shRNA targeting sequence: TRPM7: ccttatcaaaccctattgaatc	This paper	N/A
Recombinant DNA		
AAV2/8-hEF1a-FLEX-GFPL10-WPRE-hGHpA	Shanghai Taitool Bioscience Co.	N/A
AAV2/9-hEF1a-DIO-mCherry-2A-TetTox	Shanghai Taitool Bioscience Co.	N/A
AAV2/9-hSyn-FLEX-tdTomato	Shanghai Taitool Bioscience Co.	N/A
AAV2/9-hSyn-DIO-mCherry	Shanghai Taitool Bioscience	N/A
AAV2-Retro-hEF1a-FLEX-GFPL10-WPRE-hGHpA	Shanghai Taitool Bioscience	N/A
Lenti-TRPM5-shRNA-CMV-EGFP	OBiO Technology (Shanghai) Corp, Ltd.	N/A
Lenti-TRPC4&C6-shRNA-CMV-EGFP	OBiO Technology (Shanghai) Corp, Ltd.	N/A
Lenti-TRPM2&M3-shRNA-CMV-EGFP	OBiO Technology (Shanghai) Corp, Ltd.	N/A
Lenti-TRPA1&C1-shRNA-CMV-EGFP	OBiO Technology (Shanghai) Corp, Ltd.	N/A
Lenti-TRPM6&M7-shRNA-CMV-EGFP	OBiO Technology (Shanghai) Corp, Ltd.	N/A
AAV2/9-DIO-EGFP-TRPC4-shRNA	Shanghai Sunbio Medical Biotechnology Co., Ltd.	N/A
AAV2/9-DIO-EGFP-TRPC6-shRNA	Shanghai Sunbio Medical Biotechnology Co., Ltd.	N/A
AAV2/9-DIO-EGFP-NC-shRNA	Shanghai Sunbio Medical Biotechnology Co., Ltd.	N/A
pCS2-TRPC4-mcherry	GENEWIZ Biotechnology Co.	N/A
pGP-CMV-GCaMP6s	Shanghai Taitool Bioscience Co.	N/A
Software and algorithms		
GraphPad Prism 8	GraphPad	https://www.graphpad.com/scientific-software/prism/
Excel	Microsoft	https://www.microsoft.com/zh-cn/microsoft-365/excel
Labview 2017 software	National Instruments Co.	https://www.ni.com/en-us/support/downloads/software-products/download.labview.html
ImageJ bundled with Java 1.8.0_172	NIH ImageJ	https://imagej.nih.gov/ij/
FLIR Tools software	Teledyne FLIR	https://www.flir.com
CLAMS	Columbus, USA	http://www.colinst.com/
COMSOL Multiphysics® software	COMSOL	https://www.comsol.com/comsol-multiphysics
R package version 1.11.2.	Free Software Foundation's GNU General Public License in source code form	https://www.r-project.org

(*Continued on next page*)

Continued

REAGENT or RESOURCE	SOURCE	IDENTIFIER
Other		
T-type thermocouple 44 Gauge	Physitemp instruments	T466D
T-type thermocouple 40 Gauge	Xinghua suma electric instrument	QX-0.08mm*2
T-type thermocouple 36 Gauge	Suzhou ETA	TT-T36-SLE
T-type thermocouple 24 Gauge	Suzhou ETA	TT-T24-SLE
A high-density thermocouple module for Compact DAQ and Compact RIO chassis	National Instruments Corporation	NI-9213
Optical inserts	Inper Ltd, Hangzhou, China.	FOC-C-200-1.25-0.37-5.5 FOC-C-200-1.25-0.37-5.0 FOC-C-200-1.25-0.37-3.0 FOC-C-200-1.25-0.37-13.0
Polyimide tube	Shanghai Gukai New Materials Technology Corporation	300 μm-350 μm
Guide cannnula	RWD Life Science Co.,Ltd	62003
Dummy cannula	RWD Life Science Co.,Ltd	62102
Internal cannula	RWD Life Science Co.,Ltd	62203
Fixing screw	RWD Life Science Co.,Ltd	62502
Micro injector	Shanghai Gaoge industrial and trading Co.,LTd	2 μL
Regular Chow Diet	SLAC	Cat# M03

RESOURCE AVAILABILITY

Lead contact

Further information and requests for reagents may be directed to and will be fulfilled by the corresponding author Wei L. Shen (shenwei@shanghaitech.edu.cn).

Materials availability

This study did not generate new unique reagents or mouse lines.

Data and code availability

Any raw data supporting the current study is available from the lead contact upon request. The paper does not report original code. Any additional information required to reanalyze the data reported in this paper is available from the lead contact upon request.

EXPERIMENTAL MODEL AND SUBJECT DETAILS

Animals

Animal care and use conformed to institutional guidelines of ShanghaiTech University, Shanghai Biomodel Organism Co., and governmental regulations. All experiments were performed on male adult mice (8–16 weeks old). Mice were housed with a reversed 12-h light-dark cycle (9 am–9 pm, dark phase), and allowed to receive food and water ad libitum. All behaviors were tested during the dark phase. The mice strains were listed in the key resources table.

METHOD DETAILS

Manufacture the device for intracranial temperature measurement

1.5-cm long thermocouple wire (44 Gauge, Physitemp instruments) with the T-type thermal probe on one tip and the optical fiber (200 μm, NA 0.37, Inper Ltd, Hangzhou, China) were encapsulated by a polyimide tube with an inner diameter of 300 μm and an outer diameter of 350 μm (Shanghai Gukai New Materials Technology Corporation). The thermocouple wire end was bent 90 degrees so that the thermal probe was 100 μm beneath the optical fiber tip. The ceramic cannula of the optical fiber was glued on a plastic base, and the two endings of the thermocouple wire (copper and constantan) were co-assembled with copper and constantan pins into the holes on the base, respectively, without introducing a third type of metal. The device weighted approximately 0.1 grams. The custom-made device was implanted on the mouse skull seven days before the experiment. During the

experiment, a standard T-type female connector with extension wire (SMPW-T-M, OMEGA) was used to connect the copper and constantan pins to a temperature logger (USB-TC01, National Instruments Co.), and the fiber cannula was connected with standard optical fiber to deliver laser lights.

Manufacture the wired thermal probe for core body temperature measurement

We cut out a 5-cm long T-type thermocouple wire (40 Gauge, Xinghua suma electric instrument), left 5-mm naked overhangs in one end, and welded together the overhangs to form a T-type thermocouple probe. The probe can be implanted intraperitoneally to measure the core body temperature. The other wire endings were co-assembled with the copper and constant pins into holes on the pin base and fixed with glue. The pin base could be implanted on the back of mice during the experiment.

T-type thermocouple calibration

We inserted a standard T-type thermocouple (used as the reference), together with our custom-made T-type thermocouples, into a warm water bath. Then, we recorded both temperatures while the water was cooled down gradually from 45 to 25 °C, and plotted our probe temperatures against the reference temperatures. We calculated the correlation coefficients by linear regression.

Light stimulation patterns

For optical stimulation, lights were generated by the 473-nm laser (Inper, China) or 532-nm laser (Anilab, China). The light intensity from the fiber tip was measured by using a power meter (PM20A, Thorlabs). The laser powers and patterns were indicated directly in the figures.

In vivo temperature measurement in freely-behaving mice

The intracranial temperature of freely-behaving mice was performed by implanting the custom-made device on the skull seven days before the experiment. During the experiment, a standard T-type male connector with wire (SMPW-T-M, OMEGA) was used to connect the copper and constantan pins on the device to a temperature logger (USB-TC01, National Instruments Co.). The recording frequency was 1 Hz. The temperature changes in response to laser illumination were recorded for the indicated time, and each laser power was repeated twice.

For wired core body temperature measurement, a custom-made T-type thermocouple probe was implanted in the abdomen cavity, and the base was left on the back skin. 3∼5 days after the surgery, we connected the base with the temperature logger (NI-9213, National Instruments Co.). The supporting Labview 2017 software (National Instruments Co.) was used for data collection, with a sampling rate of 1 Hz.

Core body temperature and physical activity telemetry

The core temperature and physical activity were recorded at a 1-min interval by VitalView Data Acquisition System Series 4000 (Starr Life Sciences Corp., Oakmont, USA) unless specified. To record core temperature and physical activity, we used G2 E-Mitter transponders (Mini-Mitter, Oregon, USA) implanted intraperitoneally[34]. At least three days before experiments, mice were housed in a temperature-controlled chamber in their home cages on ER4000 energizer/receivers (Mini-Mitter, Oregon, USA). All measurements were conducted during the dark phase. Experiments were performed at 22 ∼ 25 °C unless indicated otherwise.

Metabolic measurement

Energy expenditure was monitored by the Comprehensive Lab Animal Monitoring System (CLAMS; Columbus Instruments). The data was acquired at a 10-min interval, as shown in the figures. Mice were adapted in the chambers for 2 days before giving saline (intra-MPA) and Englerin A (5 μM in the CSF, intra-MPA). Stimuli (Englerin A or saline) were delivered in the dark phase.

The iBAT and tail skin temperature measurement

The interscapular brown adipose tissue (iBAT) surface temperature (T_{iBAT}) and the tail skin temperature (T_{tail}) were measured using a thermal infrared camera (A655sc, FLIR). We analyzed the infrared images using the FLIR Tools software (Teledyne FLIR). To measure the iBAT surface temperature, the hair on top of the iBAT was shaved 3-5 days before measurement. The T_{iBAT} was defined as the average temperature in the interscapular region. The T_{tail} referred to the temperature at the tail base, which also indicated by white arrow heads in the Figures 1N and 6P. We used the factory settings to convert raw pixel counts to units of temperature and analyzed the pictures taken from the same angle.

Stereotaxic brain injection

Mice were anesthetized and placed in a stereotaxic frame (David Kopf Instruments, #PF-3983; RWD Life Science, #68030; Thinker Tech Nanjing Biotech, #SH01A). A feedback heater was used to keep mice warm during surgeries. We delivered ∼0.15 μl (unless specified) of AAV virus through a pulled-glass pipette at a slow rate (20 nl min^{-1}). We delivered ∼1 μl Lenti-Trp-shRNA at a faster rate (100 nl min^{-1}). Following infusion, the needle was kept at the injection site for 10 min and then slowly withdrawn.

Virus preparations were injected at the following coordinates. VMPO: (AP +0.5 mm, ML ±0.1 mm, DV -4.8 mm), MPA: (AP +0.14 mm, ML ±0.4 mm, DV -5.25 mm), vLPO: (AP +0.14 mm, ML ±0.7 mm, DV -5.25 mm). The optogenetic fiber was inserted

into the following coordinates. VMPO: (AP +0.5 mm, ML ±0.1 mm, DV -4.6 mm), MPA: (AP +0.14 mm, ML ±0.4 mm, DV -5.0 mm), vLPO: (AP +0.14 mm, ML ±0.7 mm, DV -5.0 mm), MnPO (AP +0.14 mm, ML 0 mm, DV -3.9 mm), hippocampus: (AP -2.0 mm, ML ±1.5 mm, DV -2.0 mm), DMH: (AP -1.67 mm, ML ±0.35 mm, DV -5.10 mm). The drug delivery cannula was inserted at the following coordinates. MPA: (AP +0.14 mm, ML ±0.4 mm, DV -5.0 mm),

The fiber cannulas or drug delivery cannula were chronically implanted and secured with dental cement (C&B Metabond® Quick Adhesive Cement System, Parkell, Japan). The mice were allowed to recover for at least one week before experimental procedures.

cFos induction by brain warming

After implantation of optical inserts for five days, mice were transferred to the climatic chamber and maintained at a T_a of 25 °C. To acclimate the mice, the animals were handled for 10 min and then attached optical fiber for 6 h. Seven days after acclimation, the mice were divided into two groups. All the mice were attached to optical fiber for 2 h. Then the POA of the experimental groups was heated for 20 min by 473 nm laser (4 mW). No operation was performed on the control groups that have also been implanted with optical inserts. After the laser off for 1.5 h, mice were anesthetized with isoflurane and perfused transcardially with PBS followed by 50-mL 4% paraformaldehyde (PFA) in PBS without post-fixation. Brains were dissected and immersed in 30% sucrose for 2 days at 4 °C before sectioning and immunohistochemistry.

Immunohistochemistry and histological analysis

Mice were deeply anesthetized and then fixed by transcardial perfusion with 4% paraformaldehyde, then brain tissues were dehydrated in 20% sucrose for 1 day and 30% sucrose for 2 days at 4°C. Mouse brains were sectioned at 45 μm thicknesses using cryostat microtome (Leica, CM3050s). Brain slices were collected and washed three times in PBS to remove embedding agent. For cFos staining, brain slices were collected and blocked with blocking solution containing 10% Normal goat serum (v/v), 1.5% Bovine serum albumin (w/v), 0.7% Triton X-100 (v/v) in PBS for 1 h at room temperature, and subsequently incubated with primary antibodies (anti-cFos, 1:1000, listed in the key resources table) for 24 h at 4 °C. Then, the samples were washed three times in PBST (PBS with 0.7% Triton X-100, v/v) before incubation in secondary antibodies (Alexa Fluor 488 conjugated goat anti-Guinea pig IgG(H+L), 1:1000, listed in the key resources table) for 2 h at room temperature. Subsequently, brain sections were mounted on slides and then cover-slipped with DAPI Fluoromount-G mounting medium (SouthernBiotech, #0100-20). Images were captured on a Leica SP8 confocal microscope or Olympus VS120 Virtual Microscopy Slide Scanning System. Antibodies for immunolabeling were listed in the key resources table.

TRPC4 mRNA RNAscope (in-situ hybridization)

To detect TRPC4 expression, mRNA in situ hybridization was performed on PFA-fixed (10%) brain sections using the RNAscope 2.5 HD-Red Assay (ACD, Inc., Newark, NJ, USA) with probes against murine TRPC4-ex4 (Cat No. 312271). Briefly, mice were deeply anesthetized and followed by transcardial perfusion with 4% paraformaldehyde, and then brains were dissected. Brains were dehydrated in 20% sucrose for one day and 30% sucrose for one day at 4 °C, then cryosectioned at 18 μm and placed onto SuperFrost Plus slides, which were then dried at −20 °C for 1 hr and transferred to −80 °C for storage. Before probes incubation, pretreated first with hydrogen peroxide for 10 min at room temperature, then with Protease for 30 min at 40 °C. After the pretreatment steps, brain sections were incubated with individual probes for 2 hours, and the standard RNAscope protocol was followed. Lastly, an RNAscope® 2.5 Fast-RED kit was used for chromogenic labeling. After the rinse, the slides were then cover-slipped with DAPI Fluoromount-G mounting medium (SouthernBiotech, #0100-20). To co-detect the TRPC4 mRNA with GFPL10-labeled neurons or EP3R-expressing neurons, a RNA-Protein Co-detection Ancillary Kit (ACD, Inc., Newark, NJ, USA; cat #323180) was used and followed its standard protocol, where TRPC4 was stained for mRNA, and GFP or EP3R was stained for their antibodies (anti-GFP, 1:250; anti-EP3R, 1:200; secondary antibodies, 1:500) listed in the key resources table. Images were acquired on a Nikon CSU Sora 2 Camera microscope using 20 x objective (Nikon, CSU-W1) or Olympus VS120 Virtual Microscopy Slide Scanning System. Cell numbers were counted by ImageJ software (NIH ImageJ).

RNAi design

Short-hairpin (sh) oligonucleotides designed to target TRP-mRNAs were cloned into the pCLenti-U6-shRNA-CMV-EGFP-WPRE vector in which EGFP was under the pCMV promoter and anti-TRP shRNAs were under the pU6 promoter. The targeting sequence was listed in the table oligonucleotides. TRPA1 shRNA & TRPC1 shRNA, TRPC4 shRNA & TRPC6 shRNA, TRPM5 shRNA, TRPM3 shRNA & TRPM2 shRNA, or TRPM7 shRNA & TRPM6 shRNA were packaged into lentivirus as indicated in the following table. Titers of Lenti-NC-shRNA-CMV-EGFP, Lenti-TRPM5-shRNA-CMV-EGFP, Lenti-TRPC4&C6-shRNA-CMV-EGFP, Lenti-TRPM2&M3-shRNA-CMV-EGFP, Lenti-TRPA1&C1-shRNA-CMV-EGFP, Lenti-TRPM6&M7-shRNA-CMV-EGFP were 5.80E+08 TU ml^{-1}, 6.16E+08 TU ml^{-1}, 6.22E+08 TU ml^{-1}, 7.11E+08 TU ml^{-1}, 7.69E+08 TU ml^{-1}, 5.51E+08 TU ml^{-1}, respectively. For Cre-dependent RNAi, short-hairpin (sh) oligonucleotides designed to target TRPC4-mRNA or TRPC6-mRNA were cloned into the pAAV2/9-CAG-DIO-eGFP-shRNA vector. Titers of pAAV2/9-CAG-DIO-eGFP-NC shRNA, pAAV2/9-CAG-DIO-eGFP-TRPC4 shRNA and pAAV2/9-CAG-DIO-eGFP- TRPC6 shRNA were 8.43 E+12 vg ml^{-1}, 8.85 E+12 vg ml^{-1} and 10.91 E+12 vg ml^{-1}, respectively.

Lentivirus	Trp Channels	Gene accesion number	shRNA sequence
virus 1	TRPA1	NM_001348288	5-GCAAGCTTCCTTTCTGCATATTTCCAAGTTA ATATGCAGAAAGGAAGCTTGC TTTTG-3
	TRPC1	NM_011643	5-GATCCGGGTGACTATTATATGGTTTTCAAGAGAAACCATATAATAGTCACCCTTTTTG-3
Virus 2	TRPC4	NM_016984	5-GGTGGAATCTAATGGACTTTCCAAGTTAACCAAAGTCCATTAGATTCCACCCTTTTTG-3
	TRPC6	NM_001282087	5-GGACCAGCATACATGTTTATTCCAAGTTATAAACATGTATGCTGGTCC TTTTG-3
Virus 3	TRPM2	NM_138301	5-TTTGGCTCATGGATTCCCGAGAATACTCGAGTATTCTCG GGAATCCATGAGCTTTTTG-3
	TRPM3	JF706722	5-AGAGAATGTGTTCACATCATATTCCAAGTTATATGATGTGAACACATTCTCT TTTTG-3
Virus 4	TRPM5	NM_020277	5-ATTGATGAGGCTCGTGTGAACTTCCAAGTTAGTTCACACGAGCCTCATCAATTTTTTG-3
Virus 5	TRPM6	NM_153417	5-CCGGCCAAATTCTAATGGAGTGTATCTCGAGATACACTCCATTAGAATTTGGTTTTT-3
	TRPM7	NM_021450	5-CCGGCCTTATCAAACCCTATTGAATCTCGAGATTCAATAGGGTTTGATAAGGTTTTTG-3

Quantitative (or real-time) PCR

Total RNA was isolated from brain tissue (the POA region) using trizol (Sangon, #B511311-0100). Total RNAs (1.0 μg) were reverse-transcribed with PrimerScript™ RT Master Mix (Takara, #RR047A) after DNase I treatment (Takara, #RR047A). qPCR was performed in triplicate using an SYBR Green PCR kit (Takara, #RR820A) in a 10 μl volume. Mouse *GAPDH* was used as endogenous control to which sample values were normalized. Expression levels were calculated based on the $2^{-\Delta\Delta Cq}$ method. The primers used were listed below.

Gene	Primer	Sequence
TRPM2	Forward	5'-CTTTGGGGTGCAGTCAAGGAG-3'
	Reverse	5'-TCCATGAGCTAAGGTTTTCTTGC-3'
TRPM3	Forward	5'-CAAGATGCCTGCCGTTTTTCT-3'
	Reverse	5'-GTCTAATTGGCAACTACCCCAAA-3'
TRPA1	Forward	5'-GTCCAGGGCGTTGTCTATCG-3'
	Reverse	5'-CGTGATGCAGAGGACAGAGAT-3'
TRPC1	Forward	5'-TACGGTTGTCAGTCCGCAGA-3'
	Reverse	5'-TCGTTTTGGCCGATGATTAAGTA-3'
TRPM5	Forward	5'-CCAGCATAAGCGACAACATCT-3'
	Reverse	5'-GAGCATACAGTAGTTGGCCTG-3'
TRPM6	Forward	5'-TCTGCCACAATTTAGTCAGGTG3'
	Reverse	5'-TGGTGCCGAAGGTATCTGTAG-3'
TRPM7	Forward	5'-AGGATGTCAGATTTGTCAGCAAC-3'
	Reverse	5'-CCTGGTTAAAGTGTTCACCCAA-3'
TRPC4	Forward	5'-GTGTGCTACCTGATAGCTCCC-3'
	Reverse	5'-GGCAGAGACACGTTCGTTATT-3'
TRPC6	Forward	5'-AGCCAGGACTATTTGCTGATGG-3'
	Reverse	5'-AACCTTCTTCCCTTCTCACGA-3'
GAPDH	Forward	5'-TGGATTTGGACGCATTGGTC-3'
	Reverse	5'-TTTGCACTGGTACGTGTTGAT-3'

Procedure to deliver drugs and laser simultaneously

When the core body temperature of mice fluctuated less than 0.5 °C for half an hour, the pre-implanted dummy cannula was unscrewed, and the internal cannula was inserted into the guide cannula. The drug injection was done by a microinjector at slow speed until the drug was fully injected into the brain. Then, the internal cannula was left for 1 min. After pulling out of the internal cannula, a modified optic fiber with a fixing screw was re-inserted into the guide cannula and locked there. The tip of the optical fiber was at the same position as the drug delivery location. Mice were gently returned to the home cage after connecting the optical fiber with the 473 nm laser. The time of grasping the mouse was recorded as the zero points. 10 min later, the brain nucleus was heated by a 4-mW laser for 30 min. The dosages of the drugs were listed as the following: TRPC4 antagonist ML204 (1 nmol, 1 μl) and HC-070 (0.1 nmol, 1 μl), TRPC6 antagonist SAR7334 (0.01 nmol, 1 μl), TRPC4/C5 agonist Englerin A (0.05 nmol, 0.25, nmol, or 0.5 nmol, 1 μl), PLCβ inhibitor U73122 (1 nmol, 1 μl), and U73122 inactive analog U73433 (1 nmol, 1 μl), PGE2 (0.4 nmol, 1 μl).

Simulation of heat distribution in brain tissues

The simulation of temperature changes in brain tissues after continuous optical heating was performed by finite element methods in COMSOL Multiphysics® software, using the module of *Heat Transfer with Radiation in Absorbing-Scattering Media*. The brain tissue was modeled by a cylinder with a 2-mm diameter and 2-mm height, and the end of the fiber was placed along the axes of the tissue cylinder as an ideal circle plane. For light transport simulations, the total optical incident power was distributed uniformly on the surface of the fiber end, and incident into the tissue within the shape of a cone, whose semi-angle θ_{accept} was calculated by

$$\varphi(\mu_0) = (1 - g^2)(1 + g^2 - 2g\mu_0)^{-3/2}$$

where g was the anisotropy parameter (value between -1 and 1, indicating the extent to which the scattering was backward or forward). The solid angle was discretized using the discrete ordinates method with 80 space directions in total. Optical parameters of brain tissue were determined from previous experiments.[89]

For heat transfer studies, heat sources in brain tissue (designated as Q in the following equation, W/m^3) were defined as the absorbed optical radiation energy, which was automatically implemented by the COMSOL Multiphysics® coupling feature. Absorbing boundary conditions with a constant temperature of 37°C (310.15 K) were applied to all surfaces of the brain tissue cylinder to simulate a semi-infinite tissue block, and the temperature distribution T was calculated by solving the following heat transfer equation:

$$\rho C_p \mathbf{u}\cdot\nabla T + \nabla\cdot\mathbf{q} = Q$$

$$\theta_{accept} = \sin^{-1}(NA/n)$$

where NA was the numerical aperture of the fiber (0.37) and n was the refractive index (n = 1.36) of brain tissue.[90,91] In other words, the fiber output radiation intensity (I, W/m^2/sr) can be expressed as

$$I = P / (\pi r^2) / (2\pi(1 - \cos\theta_{accept}))$$

where P denotes the total optical power and r was the radius of the fiber. The absorbing-scattering light transport within the tissue was modeled by the Henyey-Greenstein phase function as follows:

$$q = -K\nabla T$$

where ρ was the density of brain tissue, C_p was the heat capacity at constant pressure and κ was the thermal conductivity. The values of these parameters were determined from previous experimental measurement results.[32,33]

A self-adaptive mesh setup was applied to the geometric model with a minimum element size of 0.05 mm, and three temperature probes were located along the axes of the cylinder in the simulation at distances to the fiber end of 0.1, 0.2, and 0.3 mm, respectively. Solutions of temperature distribution and radiation distribution were acquired by a stationary segregated solver within the convergence tolerance of 10^{-7}. The final results of temperature changes were plotted on the section plane crossing the axes of the tissue cylinder, as illustrated in Figures 1G and S2G.

Brain slice electrophysiology

Brain slice electrophysiology recording was performed on male C57BL/6 mice (Chengdu Dossy Experimental Animals Co., Ltd), Gad67-GFP mice, Vgat-IRES-Cre mice received intra-MPA microinjection of AAV2/9 vectors expressing Cre-dependent GFP, and Vglut2-IRES-Cre mice received intra-MPA microinjection of AAV2/9 vectors expressing Cre-dependent mCherry. The mice were anesthetized with isoflurane and perfused transcardially with ice-cold oxygenated (95% O_2/5% CO_2) cutting solution containing (in mM) 213 sucrose, 0.5 $CaCl_2$, 1.25 NaH_2PO_4, 10 $MgSO_4$, 2.5 KCl, 26 $NaHCO_3$, and 10 glucose (pH: 7.4, 300 mOsm), and decapitated to remove the brain. The tissue block containing the POA was then cut and sectioned into 300-μm thick coronal slices in the buffer using a vibrating blade microtome (VT1200; Leica, Germany). The slices were incubated in oxygenated artificial cerebrospinal fluid (ACSF) containing (in mM) 124 NaCl, 5 KCl, 2.4 $CaCl_2$, 1.3 $MgSO_4$, 1.24 KH_2PO_4, 26 $NaHCO_3$, and 10 glucose (pH: 7.4, 300 mOsm) for at least 1 h at 32°C. Subsequently, slices containing the POA were transferred to a recording chamber and were constantly perfused at 1.2 ml/min with oxygenated ACSF, which was warmed to 35–37°C using a Peltier thermoelectric device (SC-20, Warner Instruments Inc., USA). Patch pipettes (4–7 MΩ) were pulled from borosilicate glass and filled with an internal solution containing (in mM) 130 potassium gluconate, 10 EGTA, 10 HEPES, 2 MgATP, 2 Na_2GTP, 1 $CaCl_2$ (pH: 7.2, 295 mOsm). Whole-cell recordings were made from the somata of POA neurons in current-clamp mode and monitored by infrared differential interference contrast (ID-DIC) video microscopy using an upright microscope (Nikon, Tokyo, Japan) and an infrared camera (IR-1000, DAGE-MTI, USA). The spontaneous firing activity of the POA neurons was amplified with an EPC-10 patch-clamp amplifier (HEKA, Germany), filtered at 2 kHz, and digitized at 10 kHz. All voltage measurements were corrected for the liquid junction potential (approximately –12 mV).[53]

The thermoelectric assembly allowed the tissue slice temperature to be periodically varied 3–5 °C above and below the neutral temperature (35–37 °C) to characterize the thermosensitivity of each recorded neuron. The firing activity of neurons was continuously recorded during cyclic temperature changes. To test the intrinsic neural thermosensitivity, synaptic transmission blockers of AMPA-receptors (CNQX, 10 μM), NMDA-receptors (AP-5, 50 μM), $GABA_A$-receptors (bicuculline, 25 μM) were added into the chamber throughout the whole recording. Thermosensitivity (impulses/s/°C) was defined by the slope of the linear regression line (thermal

coefficient) plotted by the firing rate as a function of temperature. This plot was determined over a temperature range (minimal 3°C). Based on the thermal coefficient, neurons were classified as warm-sensitive neurons (WSNs, thermal coefficient $\geq$ 0.8 impulses/s/°C), cold-sensitive neurons (CSNs, thermal coefficient $\leq$ -0.6 impulses/s/°C) and temperature-insensitive neurons (TINs, thermal coefficient < 0.8 but > -0.6 impulses/s/°C).[53,54] After determining the intrinsic thermosensitivity of each neuron, we tested its response to ML204 (10 μM, TRPC4/TRPC5 channel blocker), SAR7334 (100 nM, TRPC6 inhibitor), ML204 (10 μM) & SAR7334 (100 nM), HC-070 (20 nM, TRPC4/TRPC5 channel blocker), U73122 (10 μM, PLCβ inhibitor), or Englerin A (10 nM, TRPC4/C5 agonist). The neuron was exposed to these drugs for a period from 3 to 5 min. The criteria for a change in the thermosensitivity were an increase or decrease of > 0.1 impulses/s/°C in thermal coefficient after treatment. The criteria for a change in the firing rates was $\geq$10% change in frequency after drug perfusion, and the frequency number should be no less than $\geq$ 1 impulses/s and could recover after wash. When patch-clamp recordings were made from POA neurons from Gad67-GFP, Vgat-IRES-Cre, or Vglut2-IRES-Cre mice shown in Figure 5, neurons were visualized with epifluorescence to determine whether they were labeled by GFP or mCherry after the recordings.

Bioinformatics for single-cell RNA sequencing data

Single-cell RNA seq data of 96 neurons (GEO: GSE126657) obtained from whole-cell patch-clamp recordings[5] was used for analyzing expression profiling of temperature-sensitive neurons. Using the SingleCellExperiment method (SingleCellExperiment: S4 Classes for Single Cell Data, R package version 1.11.2.) and KNN clustering, we got similar clustering results after LogNormalization. Then we manually quality-checked the clustering results by marker genes obtained in the original report.[5] The expression levels (in counts) of Transient Receptor Potential (TRP) channels in each cluster were calculated after CPM normalization across these five different clusters, including warm-sensitive, cold-sensitive, silent (T-sensitive), silent (T-insensitive), and insensitive. Next, as the silent (T-sensitive) group was also sensitive to warmth, we calculated the warm-sensing enrichment ratio using TRPs expression counts in different clusters by this formula: [warm-sensitve + silent (T-insensitive)]/[cold-sensitive + insensitive + silent (T-insensitive) + 0.1], where 0.1 was added to avoid zero of the denominator.

To analyze TRPs expression in the POA in a larger dataset, we used a more comprehensive dataset (GEO: GSE113576) where ~3,1000 POA cells were sequenced[42] by using Seurat suite version 3.0.0 implemented in R (version 3.6.1).[92] Cells with < 200 or > 6500 unique genes expressed or > 6% of reads mapping to mitochondria were filtered out to obtain a total of 23476 cells. The expression levels (in counts) were also CPM normalized. We defined a gene as "expressed" when its expression counts were larger than the mean counts of the total 23476 cells. The expression ratio in neurons was calculated as the following: number of expression cells / 18553 (number of neurons defined in the original publication[42]), as shown in Figure S12A. The "co-expression" of two genes was defined when both two genes of interest were "expressed" in one single cell (Figures 4K and S16C).

Cell culture

For ex vivo imaging, HEK 293t cells were plated onto Nunc™ EasyDish™ (Thermo Scientific™) and were cultured in DMEM containing 10% fetal bovine serum, 1% glutamax (Invitrogen), 1% penicillin/streptomycin at 37 °C in a humidity-controlled incubator with 5% CO_2. Cells were then transfected with TRPC4-mCherry and GCaMP6s using Lipo2000 (Invitrogen Lipofectamine 2000, Thermo Scientific™). Following transfection, cells were cultured at 37 °C for an additional 24 – 48 h before they were used for experiments.

Calcium imaging

Cells bathed in the bath solution were recorded for one minute at 33 °C to establish a base line. Then the solution temperature were changed to 36 °C or 39 °C by a heating equipment, or the bath solution changed to Englerin A (100 nM, TRPC4/C5 agonist). Solutions in the perfusion chamber were controlled by a valve commander (Scientific Instruments). After, samples were washed out again with bath solution. The bath solution contained (in mM): 150 NaCl, 4 KCl, 2 CaCl2, 2 MgCl2, 10 glucose, and 10 HEPES, pH 7.4 with NaOH, as reported previously.[93] All calcium imaging were performed on Olympus TH4-200. Image analyses were performed in ImageJ and plotted in Excel (Microsoft) or Matlab (MathWorks). The ratio changes were calculated using the following formula: $\Delta F/F=[F - F_0] / F_0$, where F is the mean florescence of cell body, F_0 is the average base line (1-min interval before stimulation).

QUANTIFICATION AND STATISTICAL ANALYSIS

Statistical analyses were conducted using Excel or Graphpad (GraphPad Software Inc.). No specific test for normality or outliers was performed. We used parametric statistics including paired and unpaired Student's t-tests, one-way ANOVA or two-way ANOVA. Two-tailed tests and an alpha cutoff of <0.05 were employed. Statistical tests used for analyses were also described in the respective figure legends and detailed statistical analysis data can be found in Table S1.

Neuron, Volume *111*

Supplemental information

Hypothalamic warm-sensitive neurons require TRPC4 channel for detecting internal warmth and regulating body temperature in mice

Qian Zhou, Xin Fu, Jianhui Xu, Shiming Dong, Changhao Liu, Dali Cheng, Cuicui Gao, Minhua Huang, Zhiduo Liu, Xinyan Ni, Rong Hua, Hongqing Tu, Hongbin Sun, Qiwei Shen, Baoting Chen, Jin Zhang, Liye Zhang, Haitao Yang, Ji Hu, Wei Yang, Weihua Pei, Qiyuan Yao, Xing Sheng, Jie Zhang, Wen Z. Yang, and Wei L. Shen

Figure S1. Optothermal effects in the hippocampus, Related to Figure 1.

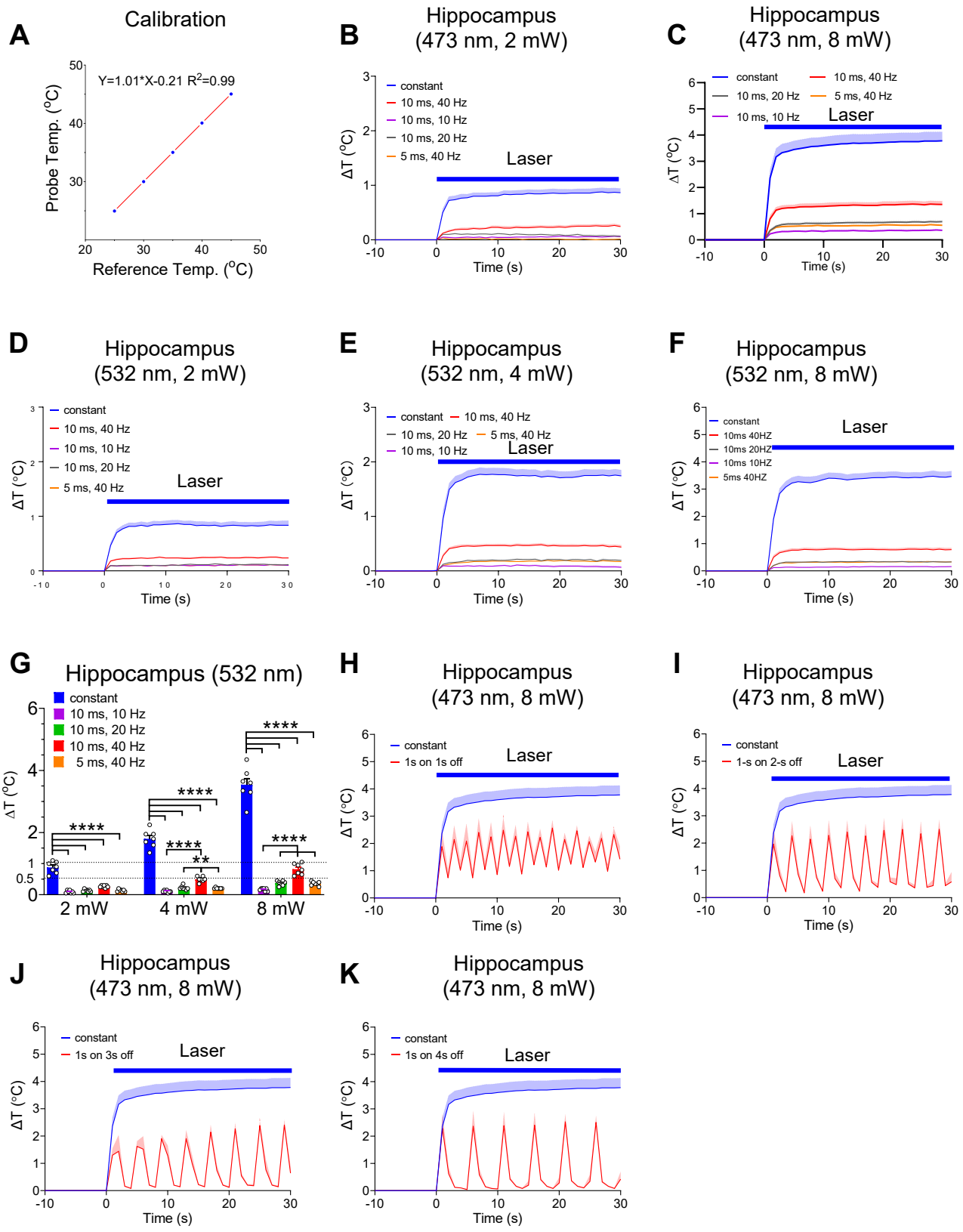

Figure S1. Optothermal effects measured in the hippocampus in freely behaving mice, Related to Figure 1.

(A) Calibration of the temperature probe. The water bath temperature was measured simultaneously by a device thermocouple probe (probe temperature) and a standard T-type thermometer (reference temperature) (n = 4 probes). The probe temperature was plotted against the reference temperature to calibrate the probe.

(B-C) Temperature changes of the hippocampus under constant or pulsed blue lasers as indicated (n = 7 mice for each group).

(D-F) Temperature changes of the hippocampus under constant or pulsed green lasers as indicated (n = 7 mice for each group).

(G) Summary of hippocampal temperature changes induced by different green light patterns (n = 7 mice).

(H-K) Temperature changes of the hippocampus under light patterns (different on-off intervals) used for optogenetic inhibition. For comparison, the data for constant blue light are repotted from (**Figure. S1C**)(n = 5 mice for each group).

All data are shown as mean ± SEM. Data in (**G**) were analyzed by Two-way RM ANOVA followed by Tukey's multiple comparison test. *p < 0.05, **p < 0.01, ****p < 0.0001.

Figure S2. Modelling heat distribution, Related to Figure 1.

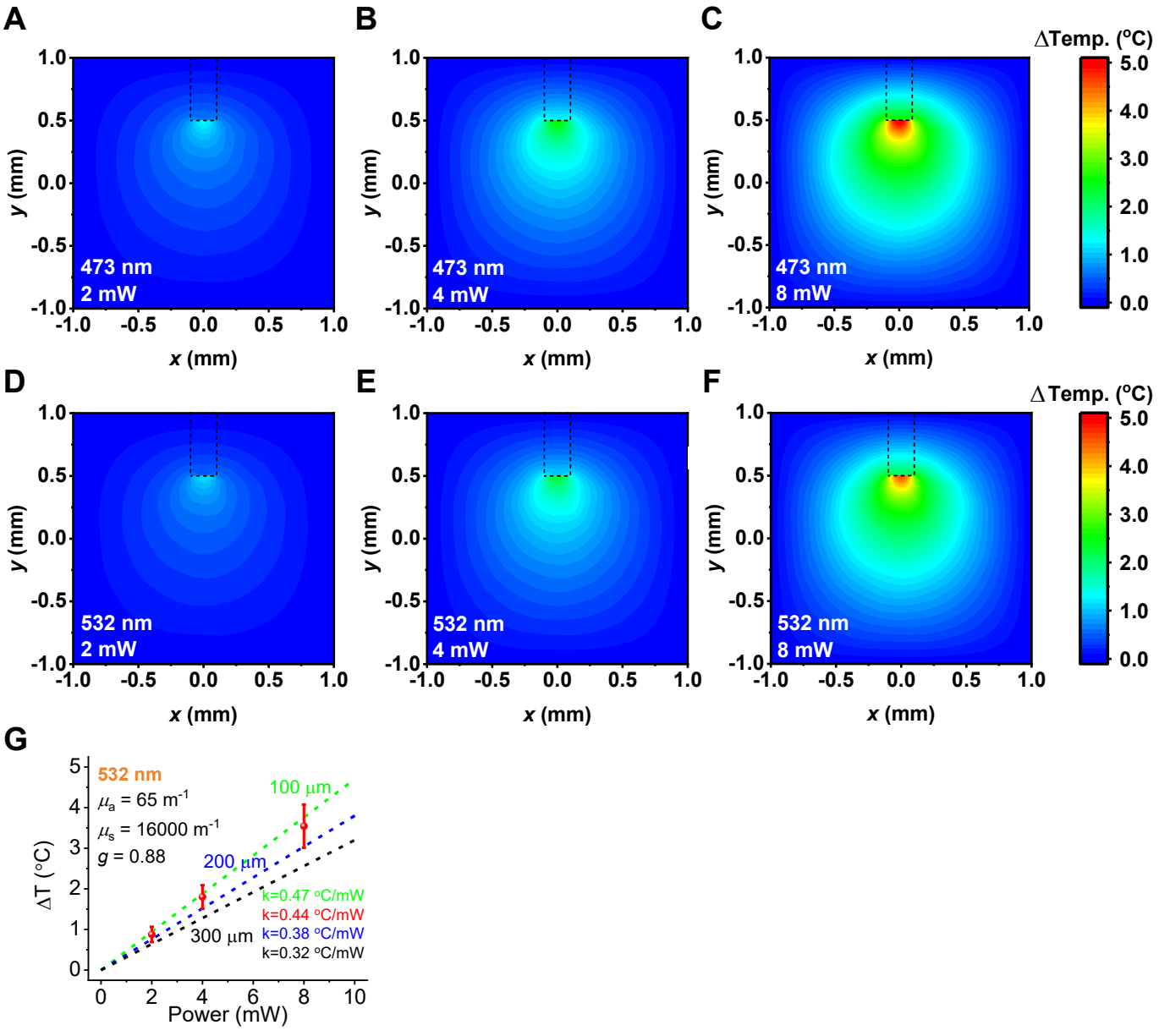

Figure S2. Modelling heat distribution in the mouse brain after optical heating, Related to Figure 1.

(A-C) Simulated heat distribution in brain tissues for blue (473-nm) laser, assuming average brain temperature was 37 ^{o}C. The optical fiber position is indicated by the dashed line.

(D-F) Simulated heat distribution in brain tissues for green (532-nm) laser, assuming the average brain temperature was 37 ^{o}C. The optical fiber position is indicated by the dashed line.

(G) Simulation of temperature increases from the 532-nm laser at the indicated depth from the fiber end. Where μ_a is the absorption coefficient; μ_s is the scattering coefficient; g is the anisotropic parameter in the Henyey-Greenstein model defined in methods; k is the slope of the simulated lines as indicated. The solid red dots were the measured temperatures (mean ± SEM). 100 μm, 200 μm, and 300 μm were depths from the fiber end. As in **Figure 1G** but for 532-nm laser.

Figure S3. Optothermal effects measured in the POA, Related to Figure 1.

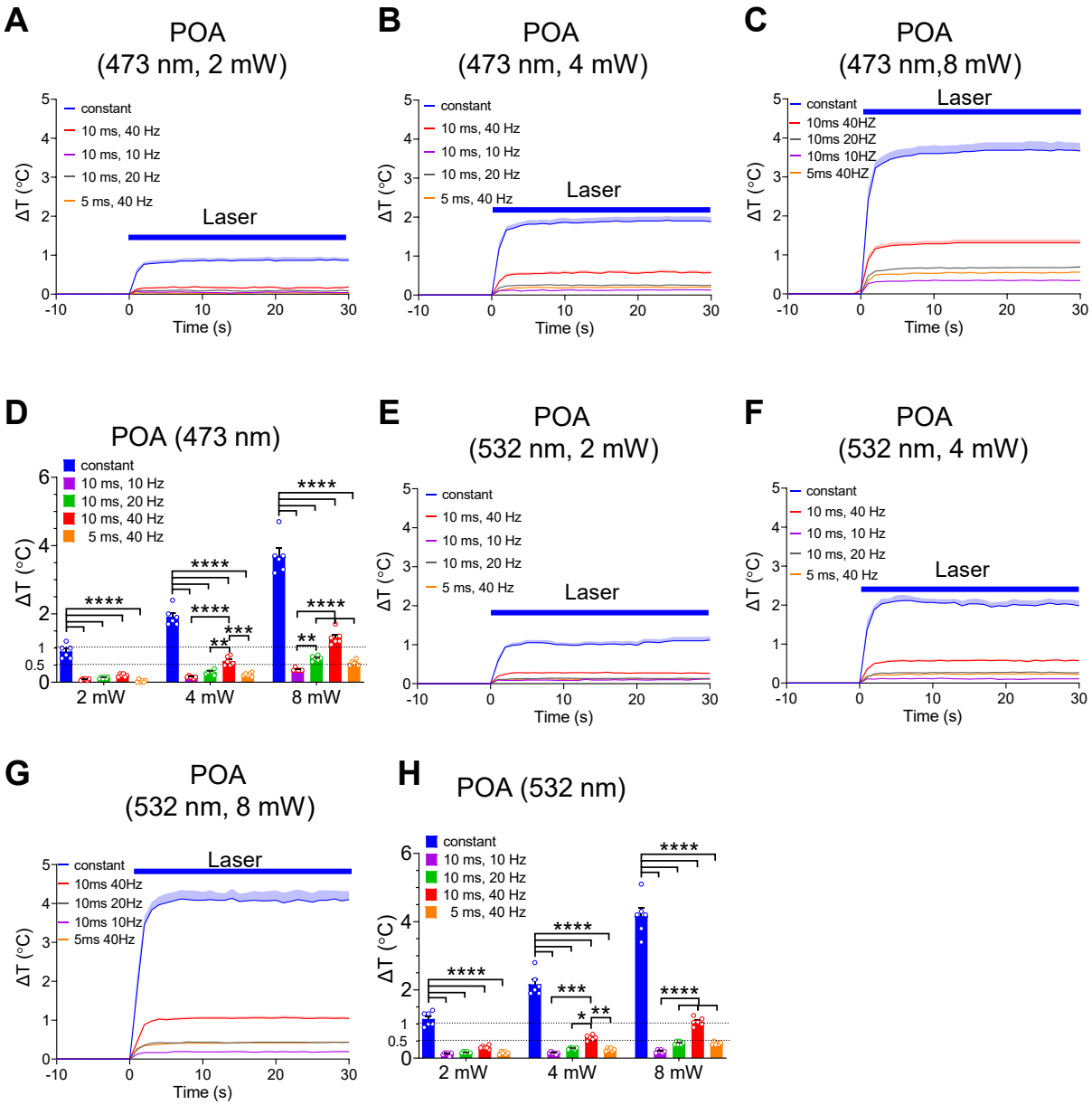

Figure S3. Optothermal effects measured in the POA in freely-behaving mice, Related to Figure 1.

(A-C) Temperature changes of the POA under constant or pulsed blue lights as indicated (n = 6 mice for each group).

(D) Summary of POA temperature changes induced by blue lights (n = 6 mice).

(E-G) Temperature changes of the POA under constant or pulsed green lasers as indicated (n = 6 mice for each group).

(H) Summary of POA temperature changes induced by green lights (n = 6 mice).

All data are shown as mean ± SEM. (**D**) and (**H**) were analyzed by two-way RM ANOVA followed by Tukey's multiple comparison test. *p < 0.05, **p < 0.01, ***p < 0.001, ****p < 0.0001.

Figure S4. Optothermal effects using 300-μm optical fibers, Related to Figure 1.

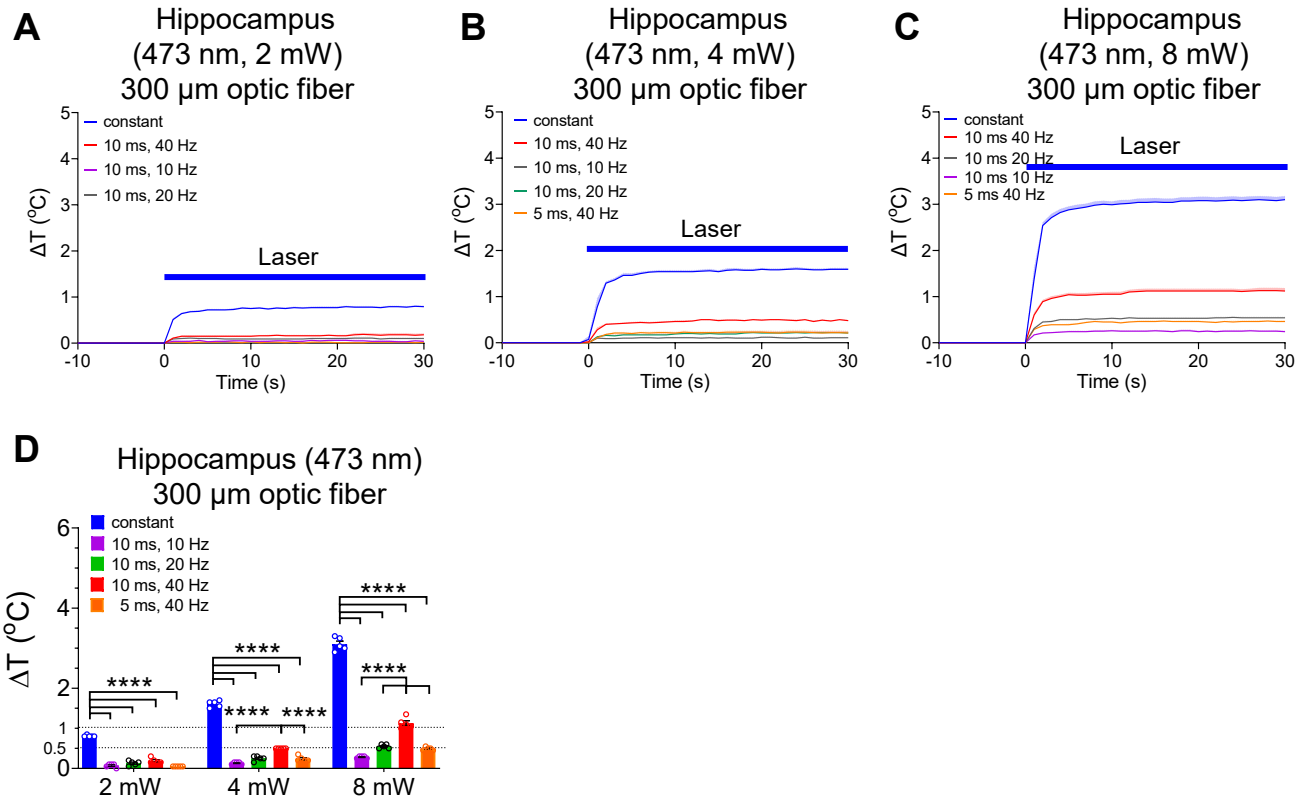

Figure S4. Optothermal effects measured using 300-μm optical fibers in freely-behaving mice, Related to Figure 1.

(A-C) Temperature changes of the hippocampus under constant or pulsed blue lasers by using 300-μm (in diameter) optic fibers.

(D) Summary of hippocampal temperature changes induced by using 300-μm optic fibers under blue lights (n = 6 mice for each group).

All data are shown as mean ± SEM. (**D**) were analyzed by Two-way RM ANOVA followed by Tukey's multiple comparison test. *p < 0.05, **p < 0.01, ***p < 0.001, ****p < 0.0001.

Figure S5. Changes of T_{core} and T_{POA} after cold exposure, Related to Figure 1J.

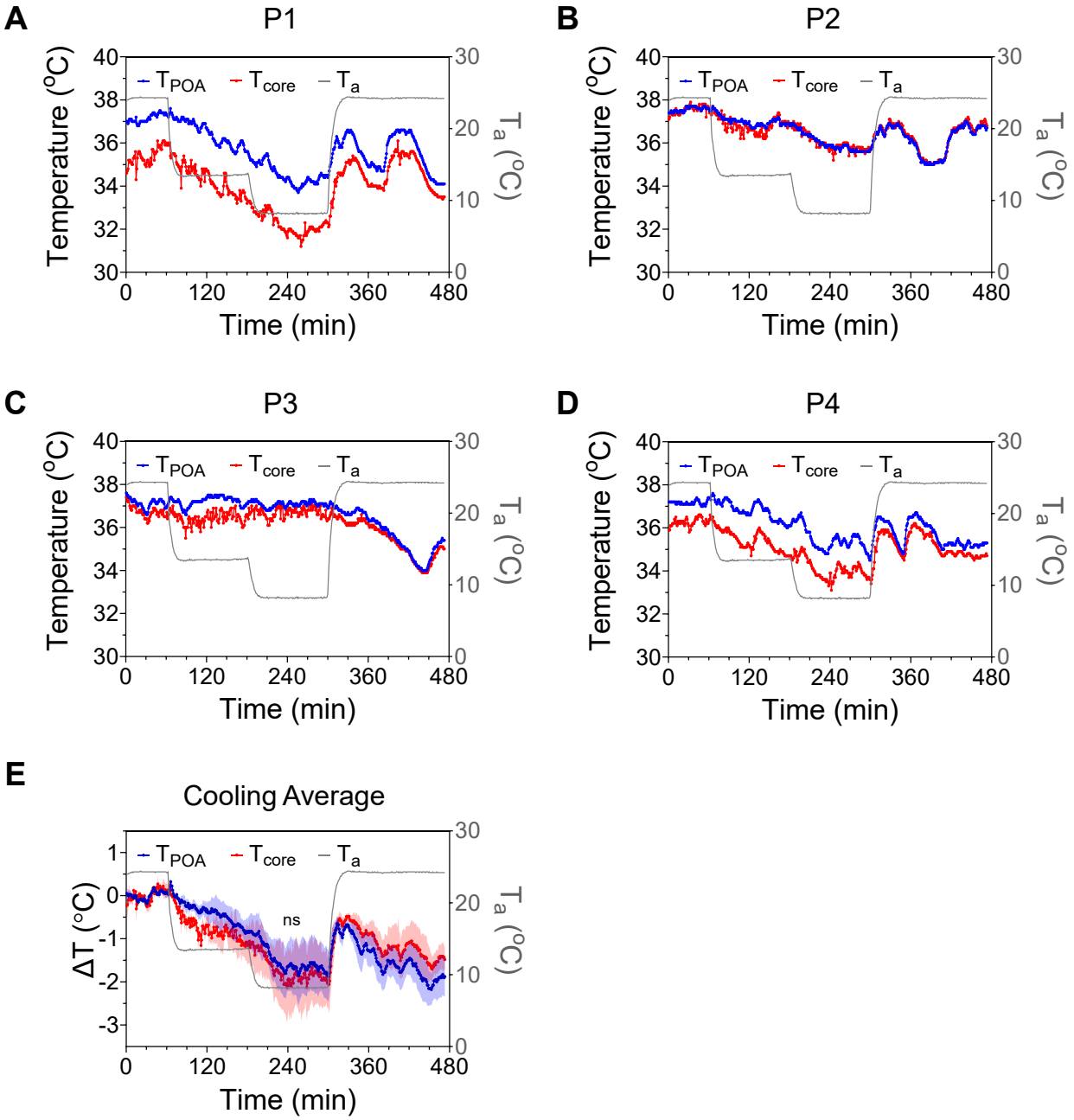

Figure S5. Changes of T_{core} and T_{POA} after cold exposure, Related to Figure 1J.

(A-E) Changes of T_{core} and T_{POA} after cold exposure with T_a giving the ambient temperature. Each graph in (**A-D**) showed the temperature change from an individual mouse with mean changes shown in (**E**; n = 4). The p-value in (**E**) was determined by two-way RM ANOVA. ns, not significant.

Figure S6. Heating of the POA triggered body cooling, Related to Figure 1J.

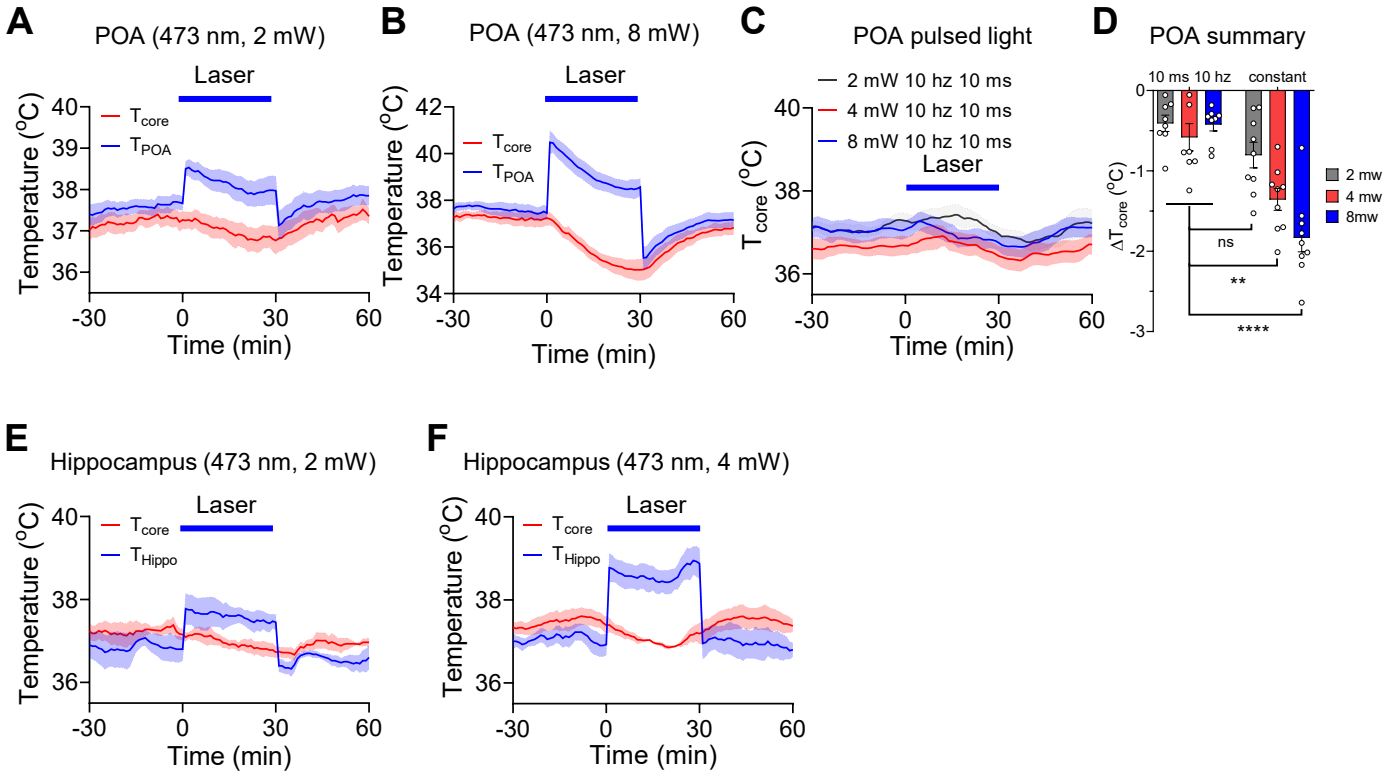

Figure S6. Heating of the POA, but not the hippocampus, triggered a counteractive body cooling effect, Related to Figure 1.

(A-B) Changes of T_{core} and T_{POA} after the optical heating of the POA with different laser powers (0 - 30 min; n = 6 mice).

(C) Changes of T_{core} after the optical heating of the POA with pulsed light as indicated (n = 8 mice).

(D) Summary of ΔT_{core} during heating by constant or pulsed lights as indicated. ΔT_{core} are the difference of temperature values at t = 30 min subtracted by t = 1 min.

(E-F) Changes of T_{core} and T_{Hippo} after the optical heating of the hippocampus with different laser powers (0 - 30 min; n = 6 mice).

All data are shown as mean ± SEM, and data in (**D**) were analyzed by two-way RM ANOVA. *p < 0.05, **p < 0.01, ****p < 0.0001, ns, not significant.

Figure S7. Warm-sensitive regions, Related to Figure 2.

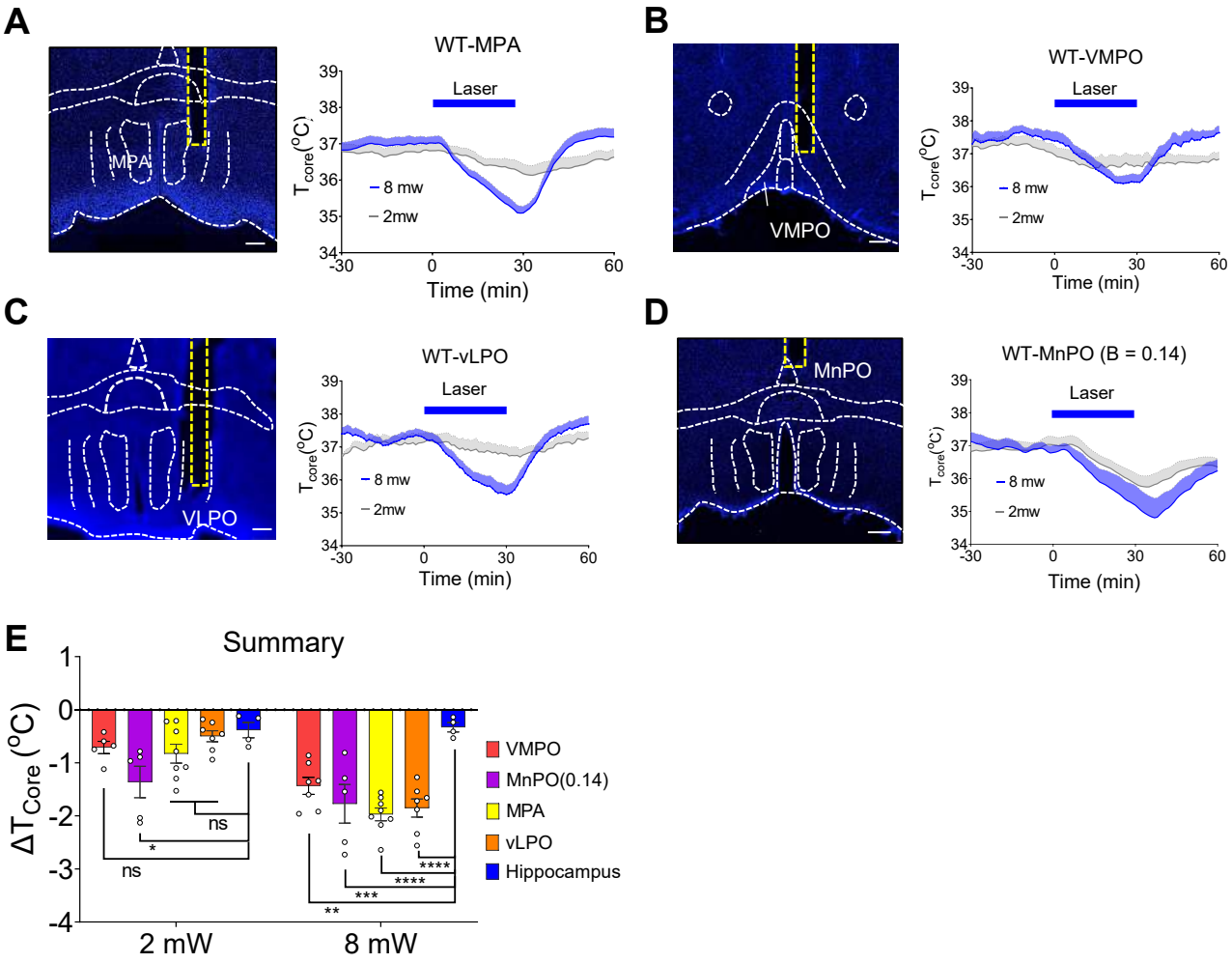

Figure S7. Anatomical map of the warm-sensitive regions, Related to Figure 2.

(A-D) T_{core} changes after heating of the MPA (**A**, n = 8 mice), VMPO (**B**, n = 7 mice), vLPO (**C**, n = 7 mice), and MnPO (**D**, n = 5 mice) with different laser powers as indicated (right). The position of the optical fiber is outlined in yellow (left). Scale bar, 0.2 mm.

(E) Summary of the ΔT_{core} after heating at different POA nuclei as indicated.

All data are shown as mean ± SEM, and were analyzed by two-way RM ANOVA in (**E**). *p < 0.05, **p < 0.01, ns, not significant.

Figure S8. Map of the warm-sensitive regions, Related to Figure 2.

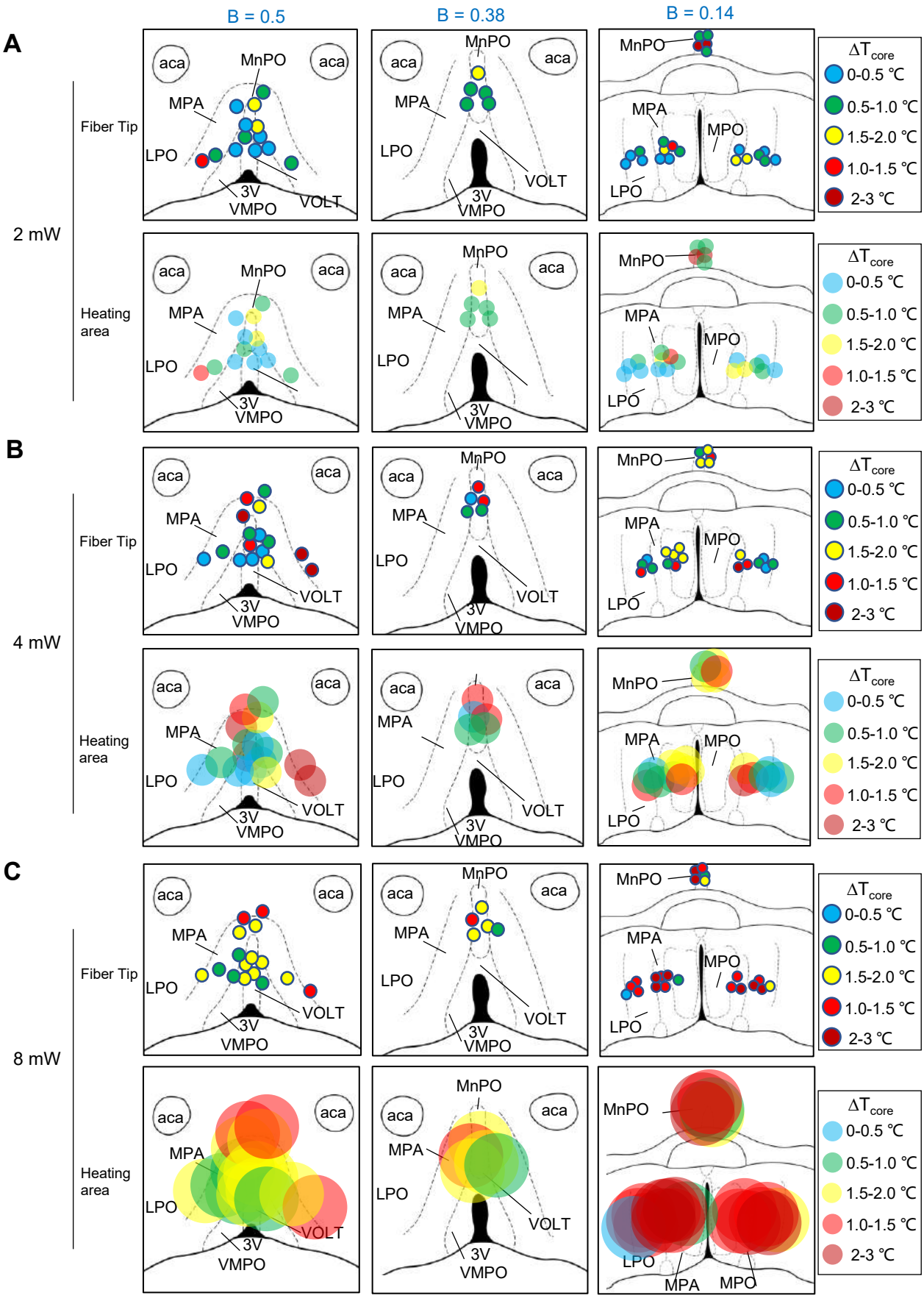

Figure S8. Anatomical map of the warm-sensitive regions, Related to Figure 2D.

(A-C) Anatomical map of the warm-sensitive regions heated by 473-nm blue laser with powers at 2 mW (**A**), 4 mW (**B**), and 8 mW (**C**). Upper panels, each circle represents the position of an optical fiber tip used for heating (473 nm, 30 min, powers indicated). Of note, the areas underneath the fiber tips were illuminated. Lower panels, each circle represents the position of a heating area (≥ 1.5^{o}C). The heating areas were defined as in **Figure 2D**, where temperature increased by ≥ 1.5^{o}C after POA heating as predicted in **Figure 1F**, and are color-coded by the amplitudes of ΔT_{core} (right).

B, Bregma; aca, anterior commissure, anterior part; VMPO, ventromedial preoptic nucleus; MPA, medial preoptic area; MnPO, median preoptic nucleus; LPO, lateral preoptic area; VOLT, vascular organ of the lamina terminalis.

Figure S9. Roles of POA neural types in the hypothermic effect induced by MPA/VMPO heating, Related to Figure 2.

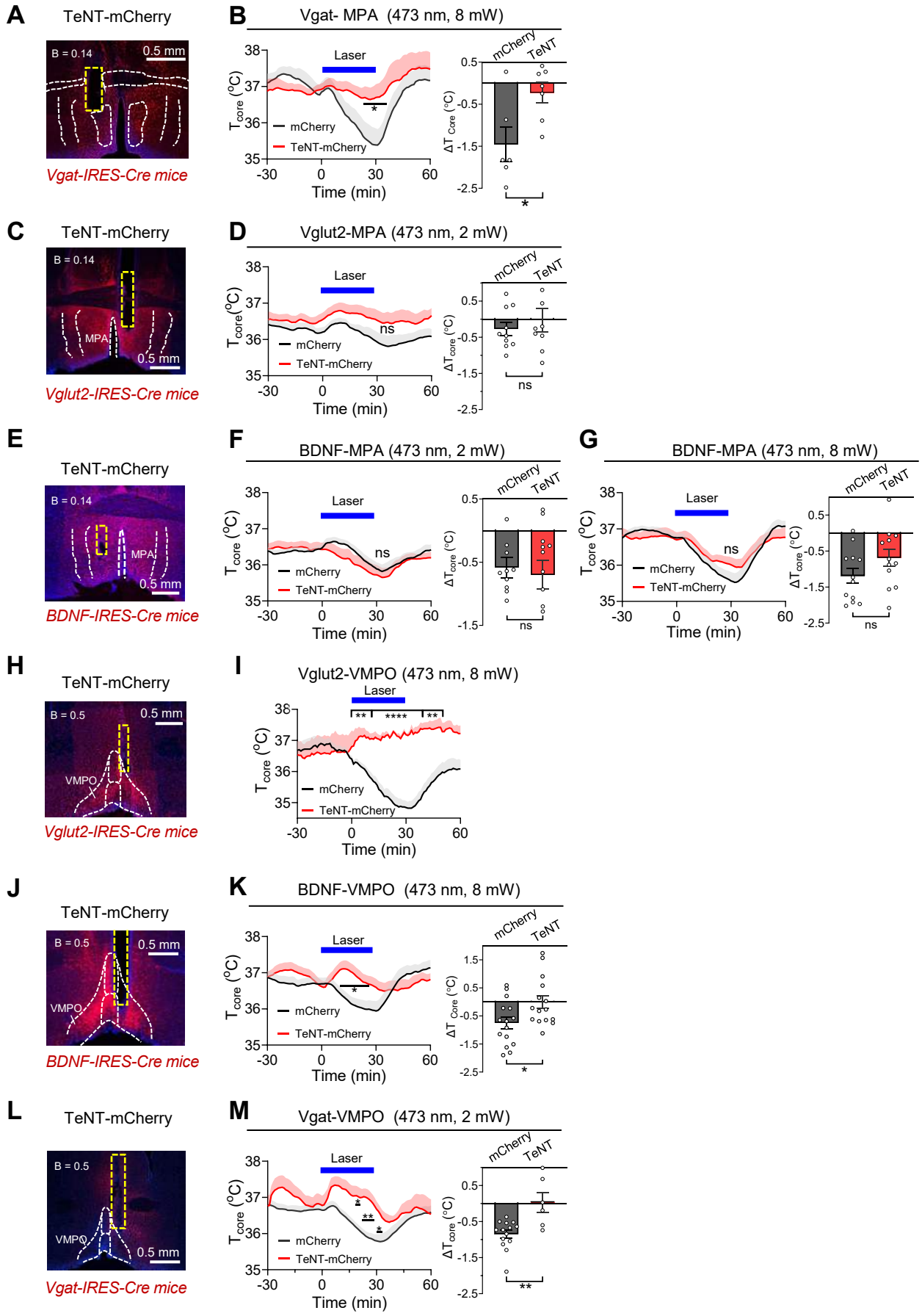

Figure S9. Roles of POA neural types in the hypothermic effect induced by MPA/VMPO heating, Related to Figure 2.

(A, C, E) Expression (red) of TeNT in $cPOA^{Vgat}$ (**A**), $cPOA^{Vglut2}$ (**C**), and $cPOA^{BDNF}$ (**E**) neurons, respectively. cPOA, central POA (Bregma = 0.38~0 mm). Scale bar, 0.5 mm.

(B, **D**, **F**, **G)** Changes of T_{core} induced by MPA heating after TeNT blocking $cPOA^{Vgat}$ (**B**, TeNT, n = 7; mCherry control, n = 6), $cPOA^{Vglut2}$ (**D**, TeNT, n = 8; mCherry control, n = 10), and $cPOA^{BDNF}$ (**F**, 2-mW laser, n = 10 each group; **G**, 8-mW laser, n = 12 each group) neurons, respectively.

(H, J, L) Expression (red) of TeNT in $aPOA^{Vglut2}$ (**H**), $aPOA^{BDNF}$ (**J**), and $aPOA^{Vgat}$ (**L**) neurons, respectively. aPOA, anterior POA (Bregma = 0.5 mm). Scale bar, 0.5 mm.

(I, **K**, **M)** Changes of T_{core} induced by VMPO heating after TeNT blocking $aPOA^{Vglut2}$ (**I**, n = 5 each group), $aPOA^{BDNF}$ (**K**, n = 15 each group), and $aPOA^{Vgat}$ (**M**, TeNT, n = 6; mCherry control, n = 14) neurons, respectively.

All data are shown as mean ± SEM, and were analyzed by unpaired t-test in bar graphs (**B**, **D**, **F-G**, **K**, and **M**) or two-way RM ANOVA in (**B**, **D**, **F-G**, **I**, **K**, and **M**). *$p < 0.05$, **$p < 0.01$, ns, not significant.

Figure S10. Roles of vLPO neural types, Related to Figure 2.

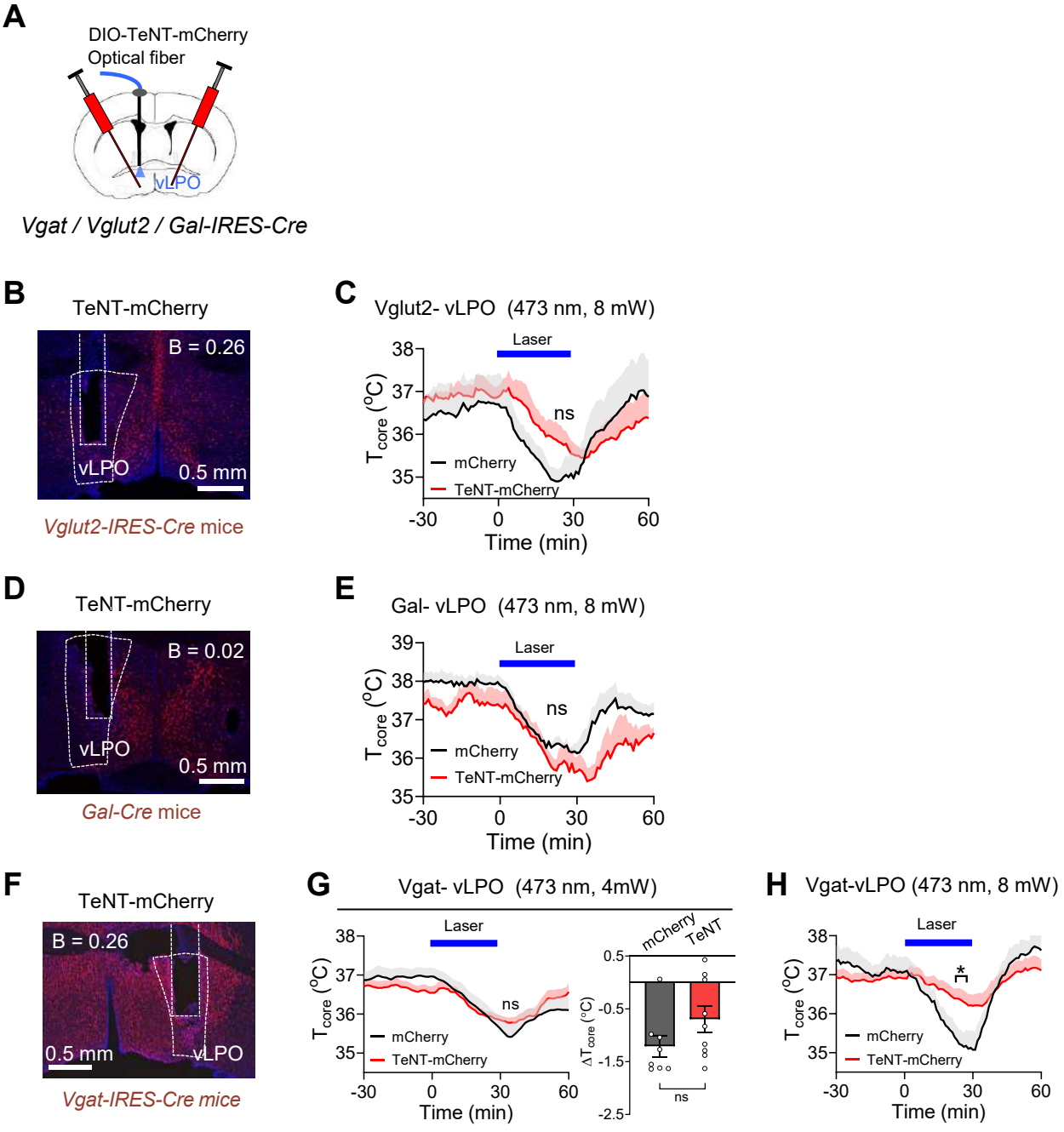

Figure S10. Roles of POA neural types in the hypothermic effect induced by vLPO heating, Related to Figure 2.

(A) Schematic for blocking vLPO heating-induced hypothermic effects by TeNT expression in $POA^{Vglut2\ /\ Vgat\ /\ Gal}$ neurons. vLPO, lateral preoptic area, ventral part.

(B, D, F) Expression (red) of TeNT in in $vLPO^{Vglut2}$ (**B**), $vLPO^{Gal}$ (**D**), $vLPO^{Vgat}$ (**F**) neurons, respectively. Scale bar, 0.5 mm.

(C, E, G, H) Changes of T_{core} induced by vLPO heating after TeNT blocking $cPOA^{Vglut2}$ (**C**, n = 4 mice each group), $cPOA^{Gal}$ (**E**, n = 4 mice each group), and $cPOA^{Vgat}$ (**G,** 4-mW laser TeNT, n = 9 mice, mCherry control, n = 8 mice; **H**, 8-mW laser, TeNT, n = 13 mice, mCherry control, n = 4 mice) neurons, respectively. cPOA, central POA (Bregma = 0.38~0 mm).

All data are shown as mean ± SEM, and were analyzed by two-way RM ANOVA in (**C**, **E**, and **G-H**) or unpaired t-test for bar graph in (**G**). *$p < 0.05$, **$p < 0.01$, ns, not significant.

Figure S11. Phenotypes associated with TRPM2 KO, Related to Figure 2.

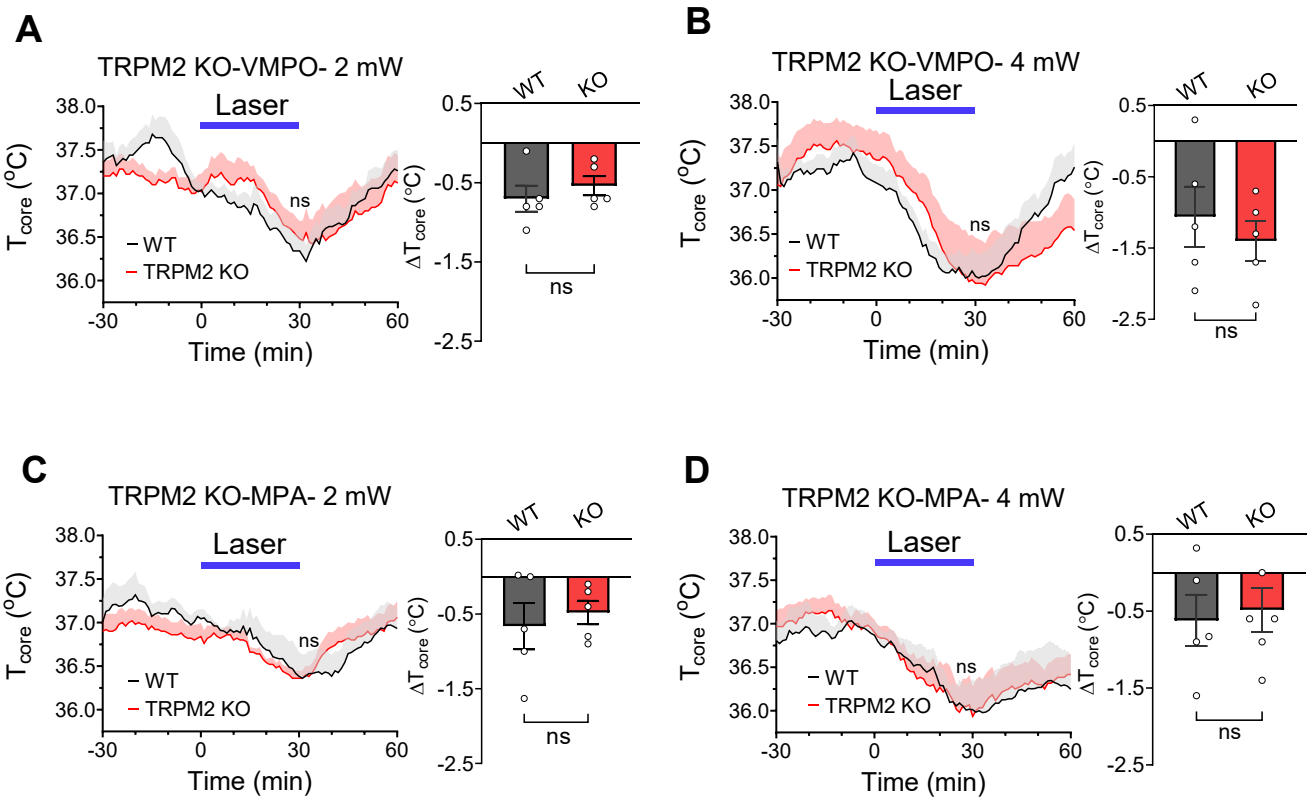

Figure S11. Phenotypes associated with knocking out of TRPM2, Related to Figure 2.

(A-B) T_{core} changes in TRPM2 knock-out mice after heating with a 2-mW (**A**) or 4-mw (**B**) blue laser in the VMPO (n = 5 mice each).

(C-D) T_{core} changes in TRPM2 knock-out mice after heating with a 2-mW (**C**) or 4-mw (**D**) blue laser in the MPA (n = 5 mice each).

All data are shown as mean ± SEM, and were analyzed by two-way RM ANOVA in (**A-D**) or by unpaired t-test for all bar graphs. ns, not significant.

Figure S12. TRP family genes in the POA, Related to Figure 3.

A

Symbol	silent,t-sensitive	silent,t-insensitive	cold-sensitive	warm-sensitive	insensitive	average counts in 23476 cells	cell number over average counts	percentage in 23476 POA cells (%)	percentage in 18553 neurons (%)	(warm+silenct(t-sensitive))/(cold+ins+silent(t-insensitive)+0.1)	(warm)/(cold+ins+0.1)
Trpm6	13.04448936	0	0	0.034129991	0	1.4007197	263	1.120293065	1.27203148	130.7861936	0.34129991
Trpa1	7.52928813	0	0	0.024738857	0	0.06476516	14	0.059635372	0.10240931	75.54026986	0.247388566
Trpm5	0	0	0	1.849067916	0	0.02767926	4	0.017038678	0.01077993	18.49067916	18.49067916
Trpc6	7.549006209	0.080766128	0.28185253	0.031308327	0	1.38879436	282	1.201226785	1.66010888	16.38566538	0.067676318
Trpc4	24.5249767	8.070843638	0	5.611502379	0	12.40125306	1987	8.463963196	12.75804452	3.688294675	0.68677148
Trpm3	16.56602354	6.021401239	2.206892111	3.819796791	4.397406341	8.43487617	1262	5.375702845	6.12299898	1.601941019	0.30016399
Trpm7	22.12847384	24.07741142	20.64344366	52.50951464	2.216961515	43.86108393	5994	25.53245868	28.59914839	1.586765583	1.116325511
Trpc1	7.209945981	0.375162972	7.227468426	1.304860239	2.280339679	38.98489926	5703	24.29289487	27.26243734	0.852933075	0.130708607
Trpm2	6.601107444	2.662553409	5.356745854	0.043718622	0.130014885	5.92763261	1121	4.775089453	8.13884547	0.805500427	0.005299667
Trpc5	11.30614766	16.14483332	0	0.076916179	3.015480478	25.89036838	3725	15.8672687	21.55985555	0.591011339	0.003993506
Trpc7	14.79747208	24.36109113	16.82839859	1.074706292	0.455052099	10.34237546	1968	8.383029477	12.12741875	0.380221645	0.025744834
Trpc3	0.729731203	2.18791772	0.053115749	0.063661594	0.065007443	4.44306083	766	3.262906798	5.06656605	0.329750335	0.026459066
Trpv4	0.623700624	2.870591254	0.053115749	0	0	1.36630235	178	0.758221162	0.38268744	0.206270192	0
Trpv2	8.292226431	20.51897724	33.68704215	3.205748989	1.436243637	13.1896407	2270	9.669449651	12.82272409	0.206270338	0.057510205
Trpv6	0.039381955	0	8.825250844	0	0	0.01384162	3	0.012779008	0.02694982	0.00441242	0
Trpc2	0	0	0	0	0	NA	0	0	0	0	0
Trpm4	0	0	0	0	1.048200011	6.65586934	1254	5.34162549	6.67816526	0	0
Trpm8	0	0.325887202	0	0	0	0.03493363	8	0.034077356	0.03772975	0	0
Trpv1	0	0	0	0	0	0.0472538	7	0.029817686	0.02155986	0	0
Trpv3	0	0	0	0	0.131539139	0.64510174	89	0.379110581	0.08623942	0	0
Trpv5	0	0	0	0	0	NA	0	0	0	0	0

B

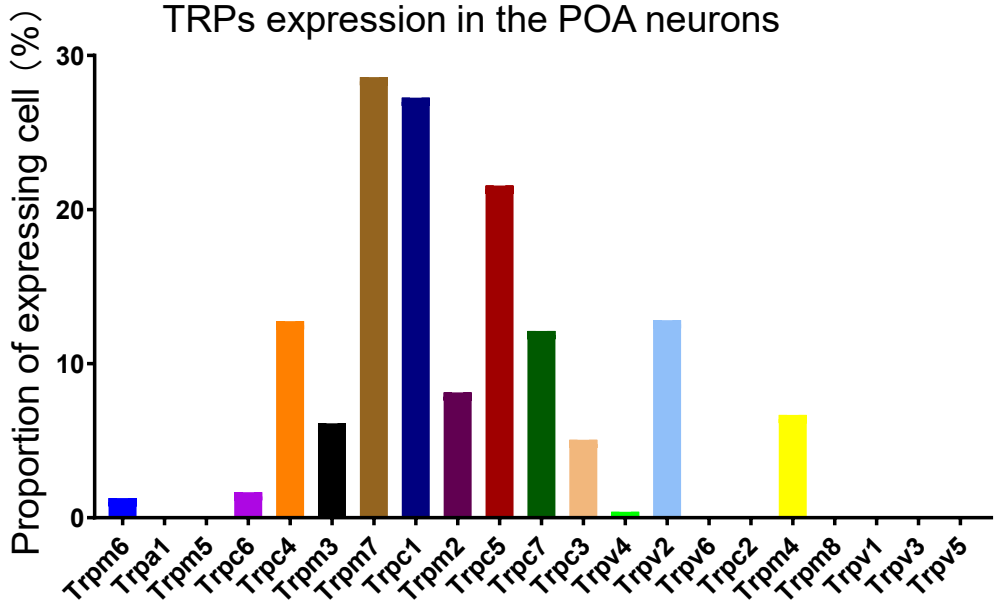

Figure S12. Expression TRP family genes in the POA, Related to Figure 3.

(A) Table showing the TRPs gene expression in different clusters of cells related to temperature sensing and the enrichment ratios. Enrichment ratio of TRPs in WSNs were calculated using the normalized expression counts in different clusters. WSNs, warm-sensitive neurons; silent-TSNs, silent (temperature-sensitive neurons); silent-TINs, silent (temperature-insensitive neurons); CSNs, cold-sensitive neurons; TINs, temperature-insensitive neuron. Enrichment ratio = (counts in WSNs+ silent-TSNs) / (counts in silent-TINs+CSNs+TINs).

(B) Expression ratio of TRP family genes in POA neurons, reanalyzed from scRNA-seq data (GSE113576). The ratios were calculated by dividing "expressed' cells by the total POA neurons sequenced (18553 neurons). We defined a gene as “expressed” when its expression counts were larger than the mean counts of the total 23476 cells.

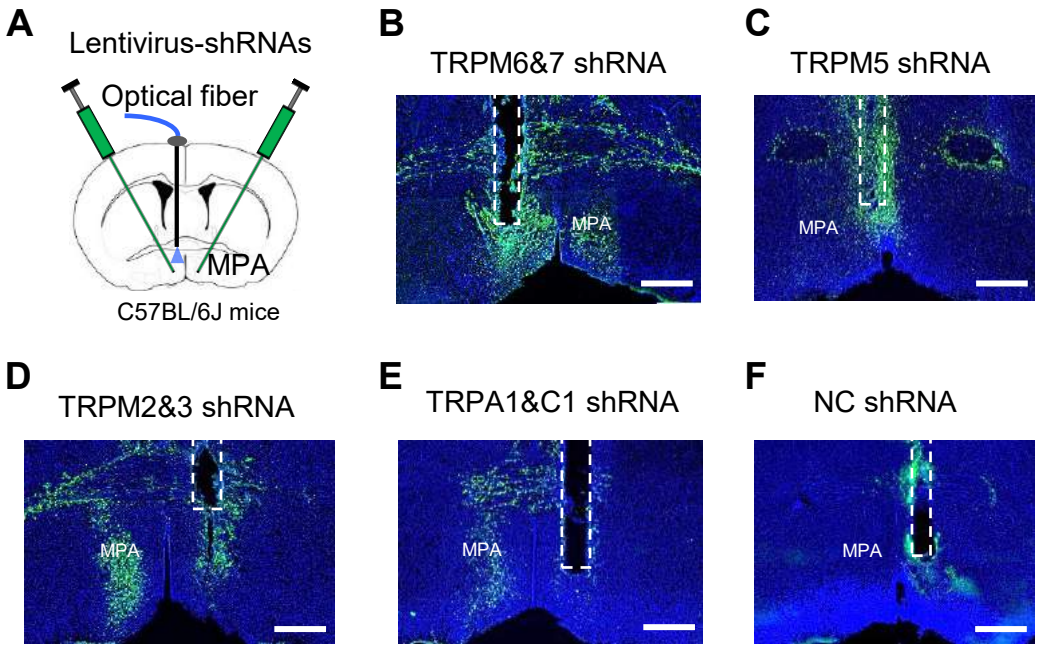

Figure S13. Viral expression of TRP shRNAs, Related to Figure 3.

(A) Schematic of RNAi-mediated TRP knockdowns in the MPA.

(B-F) Representative expression of GFP (green) co-expressed with shRNAs for TRPM6&7 (**B**), TRPM5 (**C**), TRPM2&3 (**D**), TRPA1&TRPC1 (**E**), and NC (negative control, **F**) in the MPA. Scale bars are 0.5 mm.

Figure S14. TRPC4 mRNA in situ, Related to Figure 4.

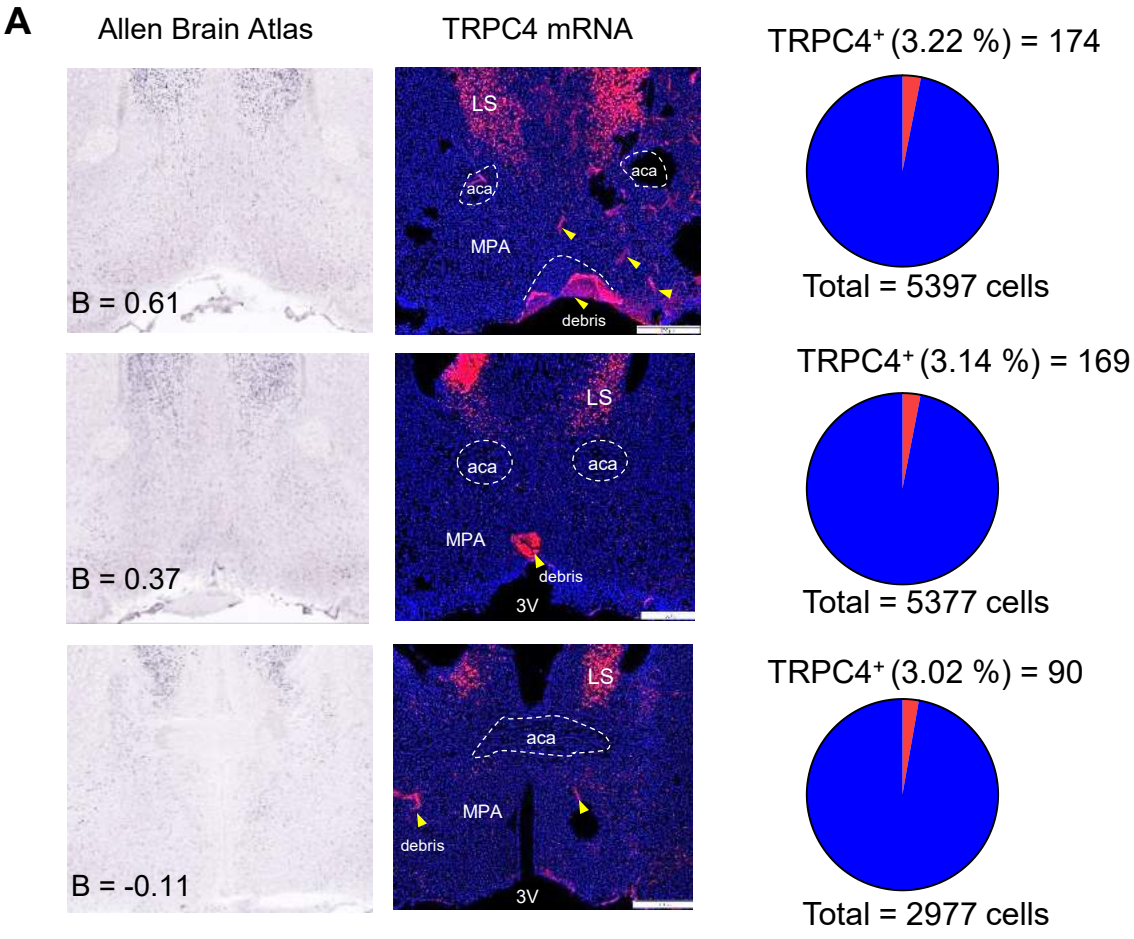

Figure S14. TRPC4 mRNA in situ, Related to Figure 4.

(A) In situ hybridization images show patterns of TRPC4 mRNA expression in the POA. Yellow arrowheads indicate tissue debris with autofluorescence due to fragile sections and harsh treatment during in situ hybridization. Scale bar, 500 μm. For comparison, the left panel are in situ hybridization images downloaded from the Allen Brain Atlas. The right panel show the percentages of TRPC4 positive neurons in the POA. B, Bregma. aca, anterior commissure, anterior part. 3V, 3rd ventricle. MPA, medial preoptic area. LS, lateral septal nucleus.

Figure S15. TRPC4/6 shRNA expression and fever responses in TRPC KD, Related to Figure 5.

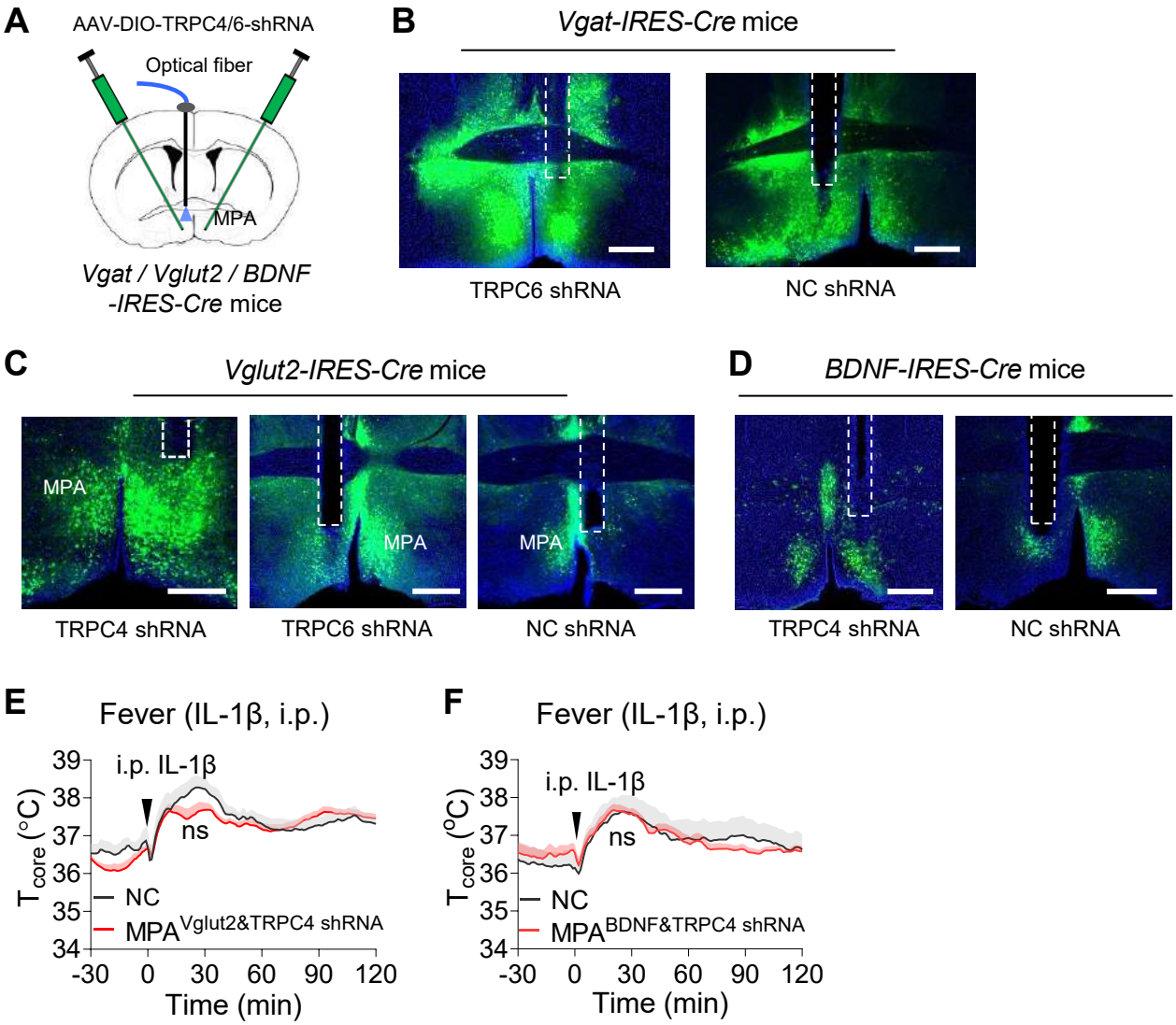

Figure S15. TRPC4/6 shRNA expression and fever responses in TRPC4/6 KD, Related to Figure 5.

(A) Schematic of Cre-dependent TRPC4/C6 shRNA knockdown in the MPA using Vglut2-IRES-Cre, Vgat-IRES-Cre, or BDNF-IRES-Cre mice.

(B-C) Representative expression (green) of TRPC6 and NC (negative control) shRNA virus in MPA^{Vgat} neurons (**B**) and TRPC4, TRPC6, and NC shRNA virus in MPA^{Vglut2} neurons, as indicated (**C**). Scale bars were 500 μm.

(D) Representative expression (green) of TRPC4 shRNA and NC shRNA viruses in MPA^{BDNF} neurons labeled by the GFP co-expressed. Scale bars were 500 μm.

(E) Impact of TRPC4 knockdown in MPA^{Vglut2} neurons on the fever induced by IL-1β injection (i.p.) (n = 7 mice each group; 4-6 weeks post-viral injection).

(F) Impact of TRPC4 knockdown in MPA^{BDNF} neurons on the fever induced by IL-1β injection (i.p.) (TRPC4, n = 8 mice; NC, n = 10 mice; 4-6 weeks post-viral injection).

All data are shown as mean ± SEM, and were analyzed by two-way RM ANOVA in (**E-F**).

Figure S16. TRPC4 thermosensitivity and PLCβ pathway, Related to Figure 6.

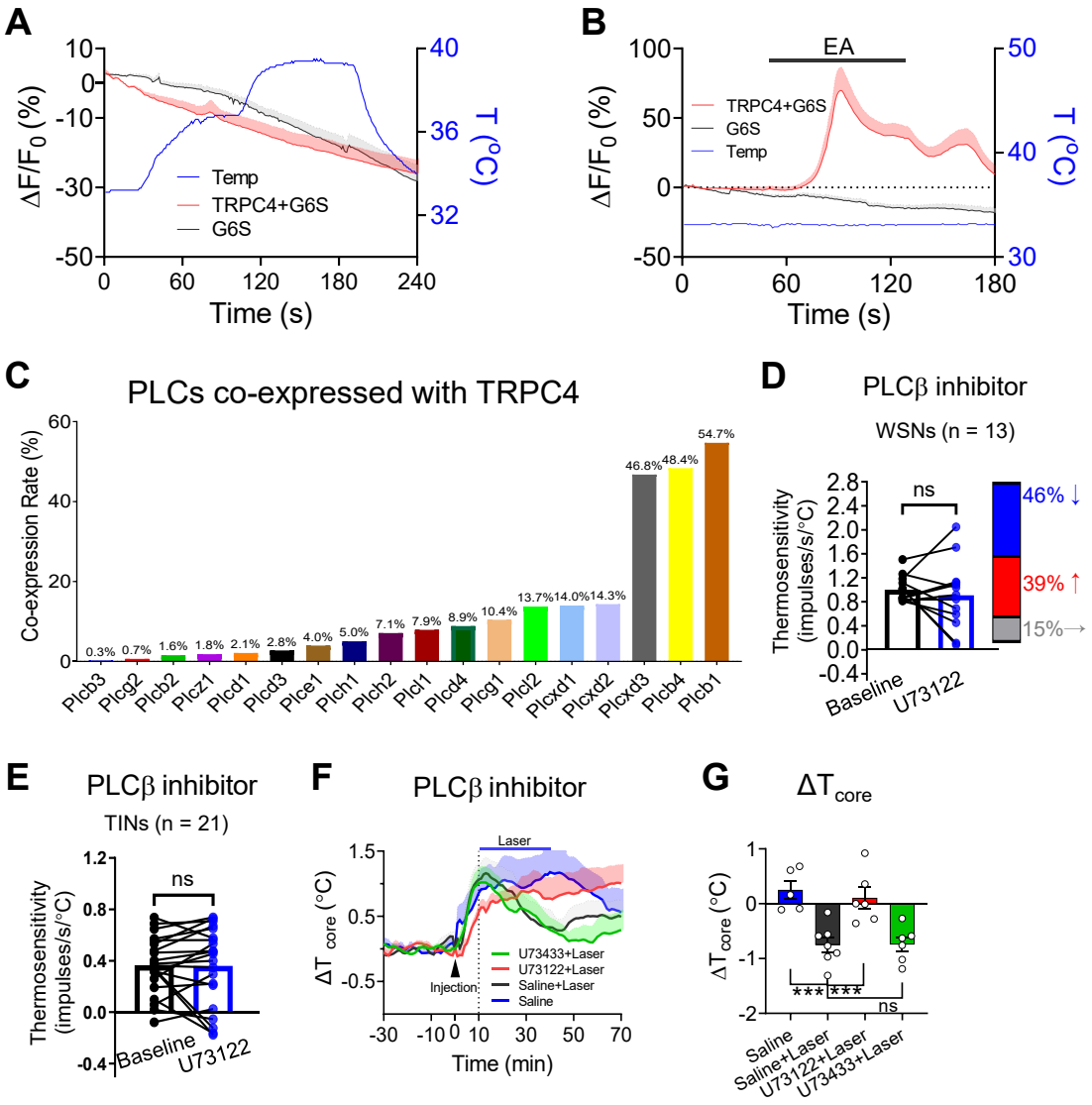

Figure S16. TRPC4's intrinsic thermosensitivity and PLCβ pathway, Related to Figure 6.

(A-B) Calcium dynamics in the HEK293T cells transfected with TRPC4 and GCaMP6s. Cells were treated with either temperature (**A**) or agonist Englerin A (**B**; EA, 100 nM).

(C) PLCs co-expression with TRPC4, reanalyzed from sc-seq data (GSE113576). The ratios were calculated by "co-expressed" cells divided by total TRPC4 cells.

(D-E) Summary of the thermosensitivity of MPA WSNs (**D**) and TINs (**E**) before (black) and after (blue) perfusion with PLCβ inhibitor U73122 (10 μM) (IC_{50} = 0.1-1 μM), recorded in the presence of synaptic transmission blockers (10 μM CNQX, 50 μM AP-5, and 25 μM bicuculline). The percentage of neurons with their sensitivity increased (up arrow), decreased (down arrow), or unchanged (horizontal gray arrow) are indicated in (**D**).

(F-G) Changes of T_{core} by MPA heating after intra-POA microinjection of PLCβ inhibitor U73122 (1 nmol - CSF concentration = ~ 10 μM) (IC_{50} = 0.1-1 μM) or its inactive-analogue U73433 (1 nmol - CSF concentration = ~ 10 μM). Summary is shown in (**G**) (Saline, n = 5 mice; Saline + Laser, n = 7 mice; U73122 + Laser, n = 6 mice; U73433 + Laser, n = 6 mice).

All data are shown as mean ± SEM, and were analyzed by paired t test in (**D-E**), two-way RM ANOVA in (**A, B, F**), and ordinary one-way ANOVA in (**G**).

Figure S17. TRPC4 and TRPC6 blockers on TINs, Related to Figure 6.

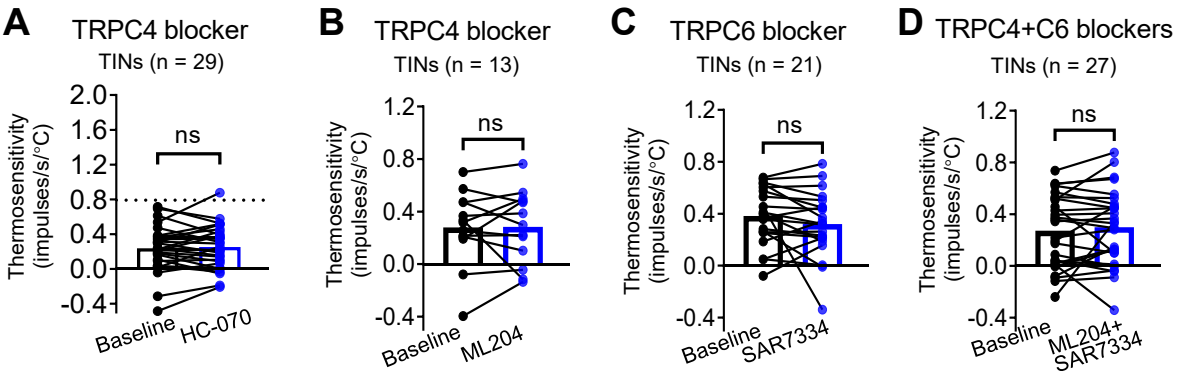

Figure S17. Effects of TRPC4 and TRPC6 blockers on the thermosensitivity of TINs in the MPA, Related to Figure 6.

(A-D) Summary of the thermosensitivity of MPA TINs before (black) and after (blue) perfusion with TRPC4 blocker HC-070 (**A**; 20 nM; IC_{50} = 10-100 nM), ML204 (**B**; 10 μM; IC_{50} = 1-3 μM), TRPC6 blocker SAR7334 (**C**; 100 nM; IC_{50} = 8-10 nM), or 10 μM ML204 & 100 nM SAR7334 (**D**), recorded in the presence of synaptic transmission blockers (10 μM CNQX, 50 μM AP-5, and 25 μM bicuculline).

All data are shown as mean ± SEM, and were analyzed by paired t-test in (**A-D**). ns, not significant.